UNIVERSITY OF CALIFORNIA

Santa Barbara

A Neuroengineering Platform for *Ex Vivo* Analysis of Single-Axon Dynamics of Serotonergic Neurons

A dissertation submitted in partial satisfaction of the

requirements for the degree Doctor of Philosophy

in Psychological & Brain Sciences

by

Melissa T. Hingorani

Committee in charge:

Professor Skirmantas Janusonis, Chair

Professor Benjamin Reese

Professor Christopher Bates

Professor Adele Doyle

December 2022

The dissertation of Melissa T. Hingorani is approved.

_____

Benjamin Reese

_____

Christopher Bates

_____

Adele Doyle

_____

Skirmantas Janusonis, Committee Chair

November 2022

ACKNOWLEDGEMENTS

Words cannot express my gratitude to my advisor and chair of my committee, Dr. Skirmantas Janusonis, for his invaluable feedback, encouragement, and patience. His belief in me kept my spirits and motivation high during my Ph.D. journey. Thank you for helping me discover my love of the serotonin system, for encouraging an innovative mindset, and for emboldening me to pursue my interdisciplinary research interests. I will leave UCSB with confidence in myself as a scientist largely due to his unwavering support.

I also could not have undertaken this journey without my defense committee, Dr. Benjamin Reese, Dr. Adele Doyle, and Dr. Christopher Bates, who generously provided knowledge and expertise.

Thank you to Dr. Jen Smith (BNL) and Dr. Ben Lopez (NRI) for their help navigating complicated logistics and for making my research goals possible.

Many thanks to my team of research assistants who supported me and assisted me while we established our cell culture domain. Adele Viviani, Jenna Sanfilippo, Justin Chiu, Sammi Siu, Hao Li, Allison Vargas: I am eternally grateful to them and will always cherish the memories of doing face masks together during plating day incubation periods.

A special thank you to Justin Haiman, for his perseverance during his cell culture training. I can’t wait to see where he takes this work.

Lastly, I would be remiss in not mentioning and thanking my dad, Sunny Hingorani, and my dog, Meeko, for their emotional support. Thank you, Dad, for the countless times you drove to Goleta to spend time with Meeko so that I could spend extended periods of time in the lab.

VITA OF Melissa T. Hingorani
October 2022

EDUCATION
Bachelor of Science in Psychology; Minor in Biology, University of North Dakota, May 2013 (magna cum laude)

Master of Science in Neuroscience, Trinity College Dublin, June 2014

Doctor of Philosophy in Psychological & Brain Sciences- Neuroscience & Behavior, Bioengineering emphasis, University of California, Santa Barbara, December 2022 (expected)

PROFESSIONAL EMPLOYMENT
2017-2018; 2020-2022: Teaching Assistant, Department of Psychological & Brain Sciences, University of California, Santa Barbara

2018-2022: Graduate Student Researcher, Janusonis Lab, Department of Psychological & Brain Sciences, University of California, Santa Barbara

2022: Graduate Student Assistant for Center for Science & Engineering Partnership – Professional Development Series (CSEP-PDS)

PUBLICATIONS
Melissa Hingorani, Adele M.L. Viviani, Jenna E. Sanfilippo, Skirmantas Janušonis (2022) "High-Resolution Spatiotemporal Analysis of Single Serotonergic Axons in an *In Vitro* System" Front. Neurosci, doi: https://doi.org/10.3389/fnins.2022.994735

Janusonis, S., Mays, K.C., Hingorani, M.T. (2019). "Serotonergic Axons as 3D-Walks." ACS Chemical Neuroscience, doi:10.1021/acschemneuro.8b00667.

"Examining the Effects of Selective Platelet Depletion on Serotonergic Gene Expression"- manuscript in preparation.

AWARDS

University of California, Santa Barbara Graduate Division Dissertation Fellowship, 2022

New Venture Competition finalist and winner of: "People's Choice", "Impact Award", "Best of Fair", 2022

University of California, Santa Barbara Art of Science competition winner; "People's Choice", 2020

ABSTRACT

A Neuroengineering Platform for *Ex Vivo* Analysis of Single-Axon Dynamics of Serotonergic Neurons

by

Melissa T. Hingorani

All neural processes in the human brain take place in a dense matrix of thin fibers (axons) that release serotonin, an ancient neurotransmitter that supports the plasticity of neural tissue and has profound implications for mental health. The self-organization of the serotonergic matrix is not well understood, despite recent advances in experimental and theoretical approaches. Previous work in our laboratory has demonstrated that individual serotonergic axons produce highly stochastic trajectories, fundamental to the construction of regional fiber densities, but further advances in predictive computer simulations require more accurate experimental information. However, visualizing this dynamic behavior *in vivo* is currently extremely difficult. Recent technological advances (e.g., digital holotomography, three-dimensional (3D)-cell culture systems, microphysiological systems) have changed the way complex neuronal systems can be studied and offer promising alternatives to *in vivo* approaches. This research examined single serotonergic axons in culture systems (co-cultures and mono-cultures), by using a set of complementary high-resolution methods: confocal microscopy, holotomography (refractive index-based live imaging), and super-

resolution (STED) microscopy. Several 3D-hydrogel systems were additionally tested. This research shows that serotonergic axon walks in neural tissue may strongly reflect the stochastic geometry of the tissue and it also provides new insights into the morphology and branching properties of serotonergic axons. The proposed experimental platform can support next-generation analyses of the serotonergic matrix, including seamless integration with computational approaches.

TABLE OF CONTENTS

I. Chapter 1: Introduction 1

A. Anatomy of the 5-HT system 2

B. Development 6

C. Diversity of the 5-HT system 7

D. 5-HT axonal projections 11

E. Axon plasticity mediated by mitochondria 16

F. Neurotrophic factors 18

G. Extracellular 5-HT 22

H. Axonal plasticity during regeneration 25

I. Current methods of studying the 5-HT system 28

J. Cell culture geometry 32

II. Specific Aims 37

III. Chapter 2: General Methods 39

A. Animals 39

B. Immunocytochemistry 39

C. Epifluorescence microscopy & confocal 40

D. Holotomography 40

E. Immunohistochemistry and super-resolution microscopy (STED) 45

IV. Chapter 3: 2D-cell cultures 47

A. Cortical glia-brainstem neuron coculture 47

B. Co-culture vs mono-culture 51
C. Development of brainstem monolayers 53
D. Cell culture protocol modifications 53
E. Validating the system 65
F. Identifying 5-HT neurons in vitro 68
V. Chapter 4: Properties of single 5-HT axons 73
A. Co-culture axon dynamics 73
B. Monolayer 74
C. 5HT adhesion/close contact with MAP2+ neurites 75
D. Axon walks 83
E. Axon-axon interactions (lack of same-axon repulsion in brainstem cultures) 87
F. STED 89
G. Discussion 92
VI. Chapter 5: Hydrogels 99
A. Hydrogel overview 99
B. Hydrogel methods 104
C. Main findings in hydrogel tests 110
D. Discussion of hydrogel tests 118
VII. Chapter 6: General Discussion 124
VIII. Chapter 7: Conclusion 139

I. Chapter 1: Introduction

All neural processes in the human brain take place in a dense matrix of thin fibers (axons) that release serotonin (5-hydroxytryptamine, 5-HT, 5HT), yet less than one in a million neurons (~26,000 in the mouse and ~400,000 in humans) in the central nervous system (CNS) produce 5-HT (Baker et al., 1990; Berger et al., 2009; Hornung, 2003; Ishimura et al., 1988). These 5-HT synthesizing fibers are classically referred to as "serotonergic axons," but currently they are more accurately interpreted as axons of a heterogeneous group of neurons that cluster in specific brain regions and are unique in their expression of tryptophan hydroxylase 2 (Tph2), a rate-limiting enzyme in the 5-HT synthesis pathway (Okaty et al., 2019; Ren et al., 2018).

The 5-HT system is functionally complex, and 5-HT modulates essentially all human behavioral processes, exerting its various actions by binding to cell surface receptors that are classified into seven distinct families (5-HT_1 to 5-HT_7) (Berger et al., 2009; Gershon & Tack, 2007). Given how widespread 5-HT action is within the CNS, it is unsurprising that 5-HT neurotransmission has many functions that if disturbed can result in mental health issues, sometimes only later in life. The 5-HT system is widely implicated in neurodivergent conditions (e.g., attention deficit hyperactivity disorder (ADHD), Autism, and obsessive-compulsive disorder (OCD)) and neuropsychiatric disorders such as major depressive disorder (MDD) (Azmitia et al., 2011; Numasawa et al., 2017). Naturally occurring compounds and selective serotonin reuptake inhibitors (SSRIs) are used to specifically

manipulate the serotonergic system in an effort to manage these conditions (Ghaffari Darab et al., 2020).

Neurons that express Tph2, have the ability to synthesize, release, and take up 5-HT (Okaty et al., 2019). The biosynthetic pathway of 5-HT involves two main metabolic steps: the amino acid tryptophan is first hydroxylated to 5-hydroxytryptophan (5-HTP) by Tph2, which is the rate-limiting step (El-Merahbi et al., 2015), and 5-HTP is then decarboxylated by aromatic L-amino acid decarboxylase to form 5-HT (El-Merahbi et al., 2015). 5-HT is packaged into vesicles by the vesicular monoamine transporter (VMAT2) and, after neurons fire and release 5-HT into the synaptic cleft, the serotonin reuptake transporter (SERT, 5-HTT) transports 5-HT back into the neuronal cytoplasm (El-Merahbi et al., 2015). 5-HT can also be degraded by monoamine oxidase (MAO-B), converting it to 5-hydroxyindoleacetic acid (5-HIAA) (El-Merahbi et al., 2015; Sahu et al., 2018). Activation of this set of genes is required for acquisition of 5-HT transmitter identity (Sahu et al., 2018).

*A. **Anatomy of the 5-HT system** Raphe nuclei*

Serotonergic neurons are part of the brainstem reticular formation and have the largest cohesive projective network throughout the CNS (Azmitia, 2001). Serotonergic neurons develop from rostrocaudally discrete progenitor pools that span transcriptionally and anatomically defined hindbrain segments called rhombomeres (r1–r11) and the ‘isthmus’ (sometimes referred to as r0) at the mid–hindbrain junction (Okaty et al., 2019). These neurons from different rhombomeres distribute into different raphe nuclei. Sorting 5-HT neurons into anatomical subdomains has provided the necessary vocabulary for 5-HT

researchers, however, the precise domain boundaries and nomenclature used to describe these neurons continue to be refined (Alonso et al., 2013; Baker et al., 1991; Bang et al., 2012; Hale & Lowry, 2011; Ishimura et al., 1988; Jacobs & Azmitia, 1992; Okaty et al., 2019; Tork, 1990).

Over 50 years ago, Dahlström and Fuxe (1964), defined nine distinct 5-HT neuron clusters or nuclei (B1–B9), starting from the caudal medulla through the pons up to the rostral extent of the system in the midbrain (Dahlstrom & Fuxe, 1964; Okaty et al., 2019). In the 1990's, an updated schema was proposed that categorized 5-HT neuron clusters into two brainstem groups, and further subdivided these groups into nuclei (Jacobs & Azmitia, 1992; Okaty et al., 2019). This schema has since been widely embraced: the rostral 'superior' brainstem group is divided into the dorsal raphe nucleus (DR), the caudal linear nucleus (CLi), the median raphe nucleus (MR), and the B9 nucleus (Jacobs & Azmitia, 1992; Okaty et al., 2019). The caudal 'inferior' brainstem group is divided into the nucleus raphe magnus (RMg), the nucleus raphe pallidus (RPa), the nucleus raphe obscurus (ROb), and the ventrolateral medulla (VLM) (Jacobs & Azmitia, 1992; Okaty et al., 2019). This schema also introduced the area postrema as a fifth serotonergic nucleus with the brainstem group, though examination of 5-HT neurons in this region has been limited (Okaty et al., 2019).

Rhombomere origin relates to the mature anatomy of 5-HT neurons

There have been advances in understanding how rhombomere origin relates to the mature anatomy of 5-HT neurons (Okaty et al., 2019). The first technique involves the development of a genetic fate mapping method to label and manipulate 5-HT neuron cohorts

on the basis of their molecularly defined rhombomeric domain of origin (Okaty et al., 2019). This method revealed the relationships between 5-HT neuron origin (the spatial and molecular coordinates), descendant genetic cell lineage and mature anatomy, as well as the behavioral and physiological functions of these neuronal cohorts (Okaty et al., 2019). The second method involves observing anatomical distribution of rhombomeric gene transcription, visualized by mRNA *in situ* hybridization, over development to infer relationships between rhombomeres and mature 5-HT neuron anatomy (Alonso et al., 2013; Okaty et al., 2019). However, some rhombomeric marker genes are expressed only transiently, making it challenging to explicitly infer mature neuron lineage by this approach when there is migration and intermingling of cells from multiple lineages (Okaty et al., 2019).

Nontraditional synapses

Serotonergic axons typically (70-80%) do not form conventional synapses and can release 5-HT at virtually any segment along their trajectory, based on *in vivo* and *in vitro* observations of their varicosities (dilated axon segments) (Benzekhroufa et al., 2009; Gagnon & Parent, 2014; Oleskevich & Descarries, 1990; Quentin et al., 2018). Serotonergic neurons can also release 5-HT from the soma, dendrites, and growth cones, effectively making their entire membrane surface active (Ivgy-May et al., 1994; Quentin et al., 2018). This does not rule out conventional synapses (Papadopoulos et al., 1987), but the scope of this "wiring" transmission (Agnati & Fuxe, 2014) in 5-HT signaling is currently unknown.

Recently, Sheu et al. (2022) presented evidence that serotonergic axons release 5-HT onto axo-ciliary synapses and activate a novel signaling pathway to the nucleus that is distinct from signaling at the plasma membrane. Like in conventional neurotransmission, axo-ciliary synapses localize and concentrate 5-HT to achieve a specific function (Sheu et al., 2022). *In vitro*, hippocampal neuronal primary cilia readily form contacts with 5-HT axonal varicosities in primary cultures of hippocampal neurons and 5-HT neurons from the raphe nuclei (Sheu et al., 2022). The vesicles of the varicosities were seen within 10-20 nm of the axonal membrane opposing the cilium and occasionally appeared to be docking or fusing with the plasma membrane, suggestive of vesicular release (Sheu et al., 2022).

Co-release

Serotonergic neurons can also co-release other neurotransmitters, such as glutamate and GABA (Okaty et al., 2019; Stamp & Semba, 1995). The classification of glutamatergic-5-HT neurons was facilitated by the identification of the vesicular glutamate transporters, VGLUT1 and VGLUT2 gene paralogue, VGLUT3 (Gras et al., 2002; Okaty et al., 2019). VGLUT3 is expressed by a select group of cells in the rat brain among the DR and MR (roughly 80% of 5-HT neurons in the DR and MR express VGLUT3), though this expression is not limited to 5-HT neurons (i.e., GABAergic and cholinergic neurons also express VGLUT3) and not all DR VGLUT3-expressing neurons produce 5-HT (Okaty et al., 2019). VGLUT3 and SERT are present in 5-HT axonal varicosities of the mouse forebrain, and the co-release of glutamate and 5-HT is suggested to play a critical role in encoding reward- and anxiety-related behaviors (Belmer et al., 2019).

B. Development

In mammals, 5-HT neurons mature early in development. They begin synthesizing 5-HT around embryonic day 11-13 in the mouse and rat brains (Hawthorne et al., 2010; Lidov & Molliver, 1982) and around 5 weeks of gestation in the human brain (Mai JK, 2004; Sundstrom et al., 1993). The development of 5-HT axons begins with the initial growth in well-defined fiber tracts, followed by branching (arborization) and then eventual dispersal of fibers in "terminal fields" (Carrera et al., 2008; Donovan et al., 2019; Jin et al., 2016; Kiyasova & Gaspar, 2011; Lidov & Molliver, 1982; Maddaloni et al., 2017). 5-HT axons in rodents have classically been thought to complete their terminal field development within 1 month after birth (Lidov & Molliver, 1982), but recent studies demonstrate that the establishment of target-specific heterogeneity in 5-HT axons proceeds beyond this time (Maddaloni et al., 2017). For example, while regions like the medial prefrontal cortex (mPFC) had fiber length maintained from post-natal day (PND) 28 to adulthood, the diameter of these fibers (in the mPFC) were significantly reduced in the adult compared to PND 28. An additional example of target specific heterogeneity of 5-HT fibers can be seen in the dorsal hippocampus (HP), where 5-HT fibers became thicker but decreased in total length per volume from PND 28 to adulthood (Maddaloni et al., 2017).

Region-specific fiber behavior during development

Using a transgenic GFP-mouse model, Maddaloni et al. (2017) identified two distinct developmental patterns showing either a progressive or temporary increase in 5-HT fiber length from early post-natal stages up to adulthood, with region-specific timing. Regions

such as the caudate putamen (CPu), basolateral amygdala (BLA), dorsal lateral geniculate nucleus (DLG), and substantia nigra (SN), demonstrated a progressive increase in fiber length, where the total length of 5-HT fibers increased starting from postnatal day (PND) 7 (BLA and SN) or PND 14 (CPu and DLG), followed by a peak at PND 28 and without further change into adulthood (Maddaloni et al., 2017). A temporary increase in fiber length was characterized by two unique temporal trends (Maddaloni et al., 2017). In the mPFC (layer V) and the barrel field of the primary somatosensory cortex (S1BF, layer V), 5-HT innervation peaked at PND 7, decreased up to PND 28 and, limited to the S1BF, increased again in the adult brain (Maddaloni et al., 2017). 5-HT innervation transiently increased up to PND 28 and then appeared pruned in the adult in both the globus pallidus (GP) and dorsal hippocampus (HP) (Maddaloni et al., 2017). Given that the density of serotonergic fibers could be directly linked to 5-HT levels and given the well-established role of 5-HT signaling in brain development, the presence of two distinct region-specific patterns of 5-HT fiber development may account for different developmental roles of 5-HT (Maddaloni et al., 2017; Teissier et al., 2017).

C. Diversity of the 5-HT system

5-HT-producing neurons are heterogeneous—differing in location, morphology, neurotoxin sensitivity, and associated clinical disorders (Jensen et al., 2008). Due to its biomedical significance, rigorous efforts have been made to understand the complexity of the 5-HT system and to identify specific markers that distinguish physiological subtypes of 5-HT neurons (Carhart-Harris & Nutt, 2017; Jensen et al., 2008).

Molecular diversity

A single cell transcriptomic atlas of 5-HT neurons within the dorsal raphe of young adult mice aged 6–10 weeks was recently published (Okaty et al., 2020). This work identified 14 distinct neuronal subtypes within the dorsal raphe, all expressing 5-HT (Okaty et al., 2020). Generally, these subtypes can be split into two groups, those that co-express GABA and those that co-express glutamate (Okaty et al., 2020).

Morphological diversity

Soma

Immunohistochemical studies describe raphe neurons as circular, ovoid, polygonal, triangular, and fusiform (Baker et al., 1990; Michelsen et al., 2008; Michelsen et al., 2007; Rodríguez et al., 2012; Steinbusch et al., 1981). One feature of 5-HT-immunoreactive neurons compared to other neuronal types in the raphe nuclei is their larger cell bodies that can reach 20-50 μm in length (Rodríguez et al., 2012).

Axon

The processes of neurons are specific and distinct for every neuron type (Azmitia, 2001). Uniquely, 5-HT axons innervate the entire neural axis of the human brain (Azmitia, 2001), and they are the only portion of serotonergic neurons that extend outside the raphe region (Adell et al., 2002; Tao-Cheng & Zhou, 1999). The morphological heterogeneity of

5-HT axons results in projections that vary in axon morphologies in different brain regions (Belmer et al., 2019; Gagnon & Parent, 2014).

Many 5-HT axons have prominent swellings, or varicosities, that are typically between 0.5-3 μm in diameter and contain a high concentration of 5-HT molecules (Benzekhroufa et al., 2009; Jacobs & Azmitia, 1992; Janusonis, 2014). 5-HT axons in the adult brain have traditionally been noted to display two different morphologies: D-fibers (originating from the DR) appear thin with fusiform or granular shaped homogenous varicosities, and M-fibers (originating from the MR and less plentiful than D-fibers) show larger and oval-shaped varicosities along thin axons (Bang et al., 2012; Kosofsky & Molliver, 1987; Maddaloni et al., 2017; Mamounas & Molliver, 1988; Tork, 1990; Wilson et al., 1989). The "fine" axons from the DR are characterized by varicosities less than 1 μm in diameter (Mamounas & Molliver, 1988). The "beaded" axons from the MR are characterized by 2-5 μm wide spherical varicosities; the quick physical expansion from a thin axon to a dilated varicosity gives these axons a beaded appearance (Mamounas & Molliver, 1988).

Subcellular varicosity dynamics

Cell culture studies have found that varicosities can form from growth cones through a combination of vesicle trafficking and local recruitment of synaptic proteins along neurites after their advancement (Buchanan et al., 1989; Malkinson & Spira, 2010; Rees et al., 1976), or by splitting of preexisting varicosities (Burry, 1986; Giachello et al., 2012; Grabham et al., 2005; Hatada et al., 1999; Hatada et al., 2000). Varicosities generally host a

heterogenous population of subcellular organelles including dense core vesicles, mitochondria, and endoplasmic reticulum (Giachello et al., 2012; Malkinson et al., 2006). The varicosities of 5-HT axons contain clusters of synaptic vesicles (Tao-Cheng & Zhou, 1999) enforcing their involvement in the release and/or storage of 5-HT (Adell et al., 2002). While 5-HT varicosities may not contain specialized synaptic junctions (Chazal & Ralston, 1987; Descarries et al., 1982), 5-HT can undergo volume or paracrine transmission in the DR (Adell et al., 2002; Bunin et al., 1998).

Functional diversity

Considerable evidence suggest that functional diversity of 5-HT circuits has a molecular and connectivity basis, but the foundation of intrinsic developmental mechanisms guiding the formation of 5-HT sub-systems is uncertain (Barettino et al., 2021). Barettino et al. (2021) have identified that ErbB4 is expressed in a subset of adult DR Pet1+ neurons and coordinates a precise long-range circuit that is ultimately involved in the formation of emotional and social memories. Through an *in vivo* loss-of-function approach using ErbB4$^{f/f;\ Pet1\text{-}Cre;Ai9f/+}$ transgenic mice (ErbB4 conditional knockout mice), in which exon 2 of the Erbb4 gene is excised in 5-HT neurons since early fate specification using the Pet1-Cre-recombinase, this group probed the contribution of the tyrosine kinase receptor ErbB4 to 5-HT circuit formation and function. Results indicated that ErbB4 expression occurring in a subset of 5-HT neurons is necessary for axonal arborization of defined long-range projections to the forebrain, but is dispensable both for 5-HT expression and global excitability in the DR and also for the innervation of other targets of the 5-HT system such

as the posterior periventricular nucleus of the thalamus (PVN) (Barettino et al., 2021). Behavioral testing was used to evaluate whether the connectivity deficits observed upon ErbB4-deficiency in Pet1+ 5-HT neurons impact on brain function, revealing that this deficiency leads to specific behavioral deficits in memory processing that involve aversive or social components (Barettino et al., 2021).

D. 5-HT axonal projections

The functional, morphological, and molecular diversity of 5-HT neurons is well established (Calizo et al., 2011; Fernandez et al., 2016; Gaspar & Lillesaar, 2012; Kiyasova et al., 2011), but the heterogeneity of their axonal projections is not fully understood (Belmer et al., 2019; Okaty et al., 2019). Very little is known about the growth dynamics of single 5-HT axons. The first detailed morphological description of single serotonergic fibers in fixed tissue has become available only recently (Gagnon & Parent, 2014). Based on a relatively small fiber set (N=32 DR axons), this study has suggested that individual 5-HT fibers travel through multiple brain regions, infrequently branching in some of them and producing abundant arborizations in others (Gagnon & Parent, 2014). However, no information is available about the dynamics of branching in serotonergic fibers, as well as the true frequency of these events.

The branching of axons is a fundamental aspect of nervous system development and neuroplasticity (Spillane et al., 2013). The number of branches of each neuron typically influences the number of possible connections with their synaptic targets, and these extensions determine the ability of the CNS to carry out complex cognitive, sensory, and

motor tasks (Azmitia, 2001). The formation of axon branches underlies the development of complex patterns of neuronal connectivity and contributes to both adaptive and maladaptive neuroplasticity following nervous system injury in adults (Gibson & Ma, 2011; Smith & Onifer, 2011; Spillane et al., 2013). A branching point can be unambiguously verified only by examining an individual fiber at high resolution in all three-dimensions (Pratelli et al., 2017). Even when a confocal system with high-power objectives is used, a branching point can be virtually impossible to differentiate from separate fibers that pass each other at sub-micrometer distances (Janusonis et al., 2019).

Forces that act on fibers and influence circuitry

During development and following injury of the nervous system, axons use several distinct pathfinding mechanisms to create ordered neural tracts, including the fasciculation, or bundling of individual axons along common routes, with cell-specific pathfinding patterns (Chédotal & Richards, 2010; Šmít et al., 2017; Voyiadjis et al., 2011). These pathfinding patterns are regulated by molecular cues that mediate interactions between axons and their environment, including other axons, cells, and the extracellular matrix (ECM) (Chédotal & Richards, 2010).

Axon guidance

Axon guidance involves the spatiotemporal interplay between guidance cues and membrane-bound cell-surface receptors located on the growth cone (Liu et al., 2018). Four dominant families of guidance molecules have been identified: ephrins, netrins, slits, and semaphorins (Bellon & Mann, 2018). These proteins direct axons to make particular wiring choices by binding to one or several receptors on the growth cones: Eph receptors, dcc and UnC, Robos, and Neuropilins and Plexins, respectively (Bellon & Mann, 2018).

In order to simplify the long journey across a complex environment by breaking it into sections, growing axons rely on specific intermediate targets, or guidepost cells, that express guidance factors at the right time and place along the axon path (Bellon & Mann, 2018; Minocha et al., 2015). Most known guidepost cells are glial cells (Bellon & Mann, 2018). For example, populations of embryonic astrocytes derived from ventral telencephalic Nkx2.1 progenitors, also known to control the specification of GABAergic interneurons, have been recognized as guidepost cells for axons of the anterior commissure acting via Slit2 secretion (Bellon & Mann, 2018; Minocha et al., 2015).

Formation of long-range axons occurs over multiple stages of morphological maturation, but the intrinsic transcriptional mechanisms that temporally control different stages of axon projection development are largely unknown (Donovan et al., 2019). However, some of the molecular mechanisms that influence 5-HT fibers during early development and beyond have been identified. For example, WNT signaling is required during the initial organization of 5-HT neurons within the raphe nuclei and the initial orientation of axons (Onishi et al., 2014). During the second stage of 5-HT neuron

development, growth associated protein 43 (GAP-43) and a microtubule-associated protein, stable tubule only polypeptide (STOP), can influence the growth of 5-HT axons. STOP is required during this time for stabilization of microtubules and axon elongation (Donovan et al., 2002; Fournet et al., 2010; Katori et al., 2017). GAP-43 is a protein expressed in early development, and has a role in axonal pathfinding, neurotransmitter release, and synaptic plasticity (Donovan et al., 2002). Interestingly, 5-HT axons fail to innervate the cortex and hippocampus in neonatal GAP-43−/− mice (Donovan et al., 2002).

GAP-43 is also a critical regulator of growth cone elaboration, acting through the regulation of the actin filament cytoskeleton, with levels of GAP-43 declining with developmental age (Jacobson et al., 1986; Rodemer et al., 2020). Overexpression of GAP-43 in adult sensory neurons has also been found to promote axon regeneration in the spinal cord, making it a prime example of how regulators of growth cones can undergo developmental downregulation that correlates with decreased regenerative potential (Bomze et al., 2001; Rodemer et al., 2020).

Pet-1 in the brain is a key transcriptional regulator of genes required specifically for the serotonergic neuron phenotype (Liu et al., 2010). Liu et al. (2010) have demonstrated that not only is Pet-1 required after 5-HT neuron generation, but also for multiple steps in 5-HT neuron maturation including axonal innervation to the somatosensory cortex, firing properties, and 5-HT_{1A} and 5-HT_{1B} autoreceptor expression. In addition, LIM homeodomain factor 1b (Lmx1b) is a continuously expressed, terminal selector-type transcription factor in 5-HT neurons (Donovan et al., 2019; Hobert, 2008). Lmx1b controls both the capacity for 5-HT synthesis and reuptake (Zhao et al., 2006), and the formation of long range profusely

arborized projection pathways that enable delivery of the transmitter throughout the CNS (Donovan et al., 2019). Lmx1b-deficient 5-HT neurons fail to generate axonal projections to the forebrain and spinal cord (Donovan et al., 2019).

Once 5-HT axons are properly oriented, they are guided from the midbrain to the forebrain by interactions of Slit proteins and their Robo receptors (Couch et al., 2004; Okaty et al., 2019). Research by Donovan et al. (2019) demonstrated that during postnatal development of forebrain 5-HT axons the Lmx1b→Pet1 regulatory cascade is temporally required for 5-HT arborization and the upregulation of the 5-HT axon arborization gene, protocadherin-αC2, (Pcdh-αC2). Subsequently, Pcdh-αC2 can influence the distribution of serotonergic axons in many target brain areas (Donovan et al., 2019). Among the Pcdh-α genes, αC2 is dominantly expressed in the serotonergic neurons of the raphe nuclei, and the loss of αC2 causes unbalanced distributions (densification and sparsification) of serotonergic axon density in various brain regions, including the hippocampus (Donovan et al., 2019). *While early projections produce predictable trajectories, the processes that lead to the emergence of regional fiber densities(i.e., density of fiber innervation in a terminal field) remain poorly understood.*

Growth cones

Axon extension and regeneration are considered to be processes occurring at the distal tip of the axon and during development, the distal tip often exhibits a clearly defined growth cone (Smith & Gallo, 2018). Serotonergic growth cone filopodia, which allow for sampling the environment and for the formation of axonal branches (Gallo & Letourneau,

2004), are described as fast-moving and dynamic, even when grown on inhibitory substrates (Hawthorne et al., 2011). Compared to other cell types (i.e., cortical neurons), 5-HT neurons display unique resilience and growth cone behavior depending on the extracellular substrate they encounter (Hawthorne et al., 2011). 5-HT neurons maintain a more robust growth cone when grown on the challenging substrate of high levels of aggrecan with low levels of laminin, whereas cortical neurons grown in the same conditions mostly lack growth cones and lose their dynamic ability (Hawthorne et al., 2011). Similarly, in embryonic development, rodent serotonergic neurons exhibit more growth potential on chondroitin sulfate proteoglycans (CSPG) than cortical neurons, which highly fasciculate to avoid contact with the substrate (Hawthorne et al., 2011). In addition, the morphology of postnatal 5-HT growth cones resembles embryonic dorsal root ganglion (DRG) growth cones, which are more resistant to the negative effects of CSPG than adult DRGs (Busch et al., 2009; Hawthorne et al., 2011).

E. Axon plasticity mediated by mitochondria

5-HT axons inherently show a high degree of plasticity, as extensively demonstrated by several studies involving fixed tissue density measures and the implication of abnormal densities of 5-HT fibers in numerous neuropsychiatric disorders (Awasthi et al., 2021; Bauman & Amaral, 2005). The widespread dispersal and early development of 5-HT axons facilitates 5-HT in maintaining and promoting synaptic plasticity.

Mitochondrial dynamics play an important physiological role in the development of the nervous system and in synaptic plasticity beyond development where they maintain an

active role in plasticity within mature neurons (Flippo & Strack, 2017). In development, dendritogenesis, axon outgrowth, and branching are directly affected by the regulated transport, fusion–fission, and anchoring of mitochondria (Rangaraju et al., 2019). In mature neurons, mitochondria contribute to synaptic transmission and plasticity through local ATP supply and Ca^{2+} buffering (Rangaraju et al., 2019). 5-HT exerts a putative trophic-like action by serving as an upstream regulator of mitochondrial biogenesis in neurons (Fanibunda et al., 2019). Mitochondria have been found in almost all serotonin-positive axon terminals in the rat suprachiasmatic nucleus (SCN), and there are at least two types of mitochondria in serotonergic neuronal cell bodies and dendrites: one containing MAO-B on their outer membranes, and the other lacking this enzyme (Arai et al., 2002). In addition, 5-HT_3 and 5-HT_4 receptors are located on the mitochondrial membrane of cardiomyocytes and participate in the regulation of mitochondrial function (Tempio et al., 2020; Wang et al., 2016). Furthermore, recent studies have observed that 5-HT_7 receptor (a receptor highly involved in plasticity) is also located on the mitochondrial membrane in SH-SY5Y cells (Tempio et al., 2020), and that pharmacological simulation of the 5-HT_7 receptor rescues mitochondria dysfunction in female mice from two different models of Rett syndrome (Valenti et al., 2017). The vital importance of mitochondria in the context of neurons underscores the importance of upstream pathways that drive mitochondrial biogenesis and function in neurons (Fanibunda et al., 2019; Mattson et al., 2008; Scholpa et al., 2018).

F. Neurotrophic factors

Neurotrophic factors are regarded as crucial regulatory components in neuronal plasticity and are believed to play an important role in depression pathology (Rafa-Zablocka et al., 2018).

BDNF

Brain-derived neurotrophic factor (BDNF) is a dominant factor in the brain, made "on demand" in response to neuronal activity, with expression regulated by cyclic AMP response element-binding protein (CREB) (Benarroch, 2015; Popova et al., 2017; Rafa-Zablocka et al., 2018). In depression pathology, the downregulation of BDNF is thought to be correlated with depression as its upregulation is frequently observed after chronic treatment with common antidepressants (Rafa-Zablocka et al., 2018). Using mice lacking CREB in their serotonergic neurons, Rafa-Zablocka et al. (2018) demonstrated that the upregulation of BDNF in the hippocampus or PFC after fluoxetine (FLX) administration might be dependent on CREB activation exclusively in serotonergic neurons.

5-HT and BDNF are the main players in the mechanisms of neurogenesis and neuroplasticity (Homberg et al., 2014). Distinctive effects of BDNF on the 5-HT system has been identified *in vitro* (i.e., cell cultures) and *in vivo*. In raphe cell cultures of rat embryos, 18h exposure to BDNF was enough to almost double the number of serotonergic neurons and promote axonal growth (Rumajogee et al., 2002). *In vivo*, chronic administration of BDNF locally into the DR altered the electrophysiological activity of 5-HT neurons (Celada et al., 1996). In addition, BDNF administered into the midbrain or intraventricularly increased the level of 5-HT and its major metabolite 5-HIAA in the rat hippocampus, cortex,

striatum, nucleus accumbens, substantia nigra, and hypothalamus (Siuciak et al., 1996). The 5-HT system is dependent on BDNF for normal development and function, but brain 5-HT also influences BDNF. For example, 5-HT increases gene expression and BDNF protein levels in cultures of embryonic cells of raphe nuclei (Galter & Unsicker, 2000).

GDNF

Glial-derived neurotrophic factor (GDNF) is predominantly found in astrocytes and has been recognized as a necessary factor for the development, protection, and maintenance of dopaminergic (DA) neurons (Popova et al., 2017). GDNF is involved in many physiological processes, as well as in the pathogenesis of a variety of neurological and psychiatric disorders, many of which are associated with the serotonergic system (Popova et al., 2017). Similar to BDNF, GDNF stimulates the growth of 5-HT brain neurons and affects the expression of key genes of the 5-HT-system of the brain (i.e., genes coding Tph2 and 5-HT_{1A} and 5-HT_{2A} receptors) (Popova et al., 2017). The effect of GDNF on the 5-HT system has been verified *in vitro*. For example, in cell culture, GDNF increases the size of cell bodies and the length and number of 5-HT axons (Ducray et al., 2006; Popova et al., 2017). An additional connection between GDNF and the 5-HT system is its ability to respond to antidepressants such as selective serotonin reuptake inhibitors (SSRIs) (Popova et al., 2017). Several studies have demonstrated that GDNF expression and secretion increase after both chronic and single administrations of reuptake inhibitors in both cell cultures (Golan et al., 2011; Hisaoka et al., 2001; Mercier et al., 2004) and the serum of patients with depression after a course of antidepressant therapy (Popova et al., 2017; Zhang et al., 2008).

BDNF/GDNF temporal and regional specificity

Regional specificity of the BDNF and GDNF effects in the brain is linked with the particularities of the microenvironment of different brain structures that affect the functioning of 5-HT neurons (Popova et al., 2017). Such particularities include different densities of 5-HT receptors and interactions between various types of 5-HT receptors or with other types of receptors (Naumenko et al., 2014; Popova et al., 2017). In addition to regional specificity, 5-HT neurons show temporally distinct responses to neurotrophic factors *in vitro.* Galter and Unsicker (1999) studied the regulation of survival and serotonergic markers by neurotrophins and various trophically active cytokines in neurons cultured from the embryonic rat raphe region under extreme conditions (i.e., saturating concentrations) (Galter & Unsicker, 1999). Distinguishing responses to different factors were observed depending on embryonic age and regional origin of 5-HT neurons (Galter & Unsicker, 1999). For example, saturating concentrations (10 ng/mL each) of BDNF augmented numbers of Tph-positive neurons at E16 by a factor of 7, but only 1.5- to 2-fold when cultures were established from day E13 or E14 (Galter & Unsicker, 1999). 5-HT neurons taken at different embryonic ages did not differ in their response to neurotrophin-3 (NT-3) (Galter & Unsicker, 1999). Collectively, these results suggest that responsiveness of serotonergic neurons to BDNF and NT-3 is controlled in a temporally distinct fashion (Galter & Unsicker, 1999). In cultures of rostral serotonergic groups (B4–B9), numbers of Tph-positive neurons decreased in the absence of factors, whereas numbers of Tph-immunoreactive neurons in cultures from caudal serotonergic groups (B1–B3) increased during a 12-day culture period (Galter & Unsicker, 1999). When considering how GDNF is

regionally influenced, a central factor is high heterogeneity of astrocytes, since astrocytes of different brain regions vary considerably in their biochemical characteristics (Popova et al., 2017). Such differences affect their functioning, reactions, and role in different neuropathologies (Montgomery, 1994; Popova et al., 2017).

S100ß

S100*ß* is a highly abundant calcium binding protein in the brain produced and secreted by astroglia (Hagmeyer et al., 2019). S100*ß* is concentrated in astrocytes and other glial cells but it has also been reported in specific neuronal subpopulations (Michetti et al., 2019). S100*ß* plays a key role in the development and plasticity of the 5-HT system, as well as in the cascade of glial changes associated with neuroinflammation (Shapiro et al., 2010). During development, 5-HT and S100*ß* have a reciprocal relationship: through 5-HT_{1A} receptors, 5-HT neurons release S100*ß* (Azmitia et al., 1990; Liu & Lauder, 1992), S100*ß* promotes the development of 5-HT axon terminals (Shapiro et al., 2010) and S100*ß* additionally increases the expression of serotonin transporter, a major regulator of serotonergic neurotransmission (Michetti et al., 2019; Yoon et al., 2013). While S100*ß* levels are critical in the regulation and maintenance of 5-HT axon growth, a lack of S100*ß* does not affect the development of 5-HT neurons *in vivo* as 5-HT projections are normal in S100*ß* -null mice (Nishiyama et al., 2002).

Ethanol exposure has the potential to cause severe damage to the developing 5-HT system (Eriksen & Druse, 2001). In primary cultures of E14 serotonergic neurons, if the glial feeder layer conditioned medium was treated with ethanol, a significant decrease in 5-HT neurons is found (Eriksen & Druse, 2001). Interestingly, S100*ß* concentrations as low as

20 ng/ml could significantly increase the number 5-HT neurons in the ethanol treated cultures. Addition of S100*β* to ethanol-free 5-HT/glia co-cultures results in an increase in 5-HT neurons (29% with 40 ng/ml S100*β* and by 38% with 160 ng/ml S100*β*) (Eriksen & Druse, 2001). *In vitro* cultures of embryonic 5-HT neurons treated with S100*β* (500 ng/ml) show morphological changes in soma shape (i.e., more rounded), an increase in the spatial extent and shape of neuritic arbors, and an increase in primary neurites and terminal neurites (Liu & Lauder, 1992).

G. Extracellular 5-HT

Extracellular concentration of 5-HT in the midbrain raphe nuclei tightly regulates serotonergic transmission via a feedback inhibition through 5-HT_{1A} autoreceptors (Adell et al., 2002). The release of 5-HT could occur in any portion of serotonergic neurons as the presence of vesicles in which 5-HT can be stored and released (by exocytosis) has been demonstrated in cell bodies, dendrites, and axonal varicosities (Adell et al., 2002). Vesicular 5-HT release is action potential and Ca^{2+}-dependent but 5-HT can also be released from a non-vesicular, *p*-chloramphetamine-dependent compartment (Adell et al., 1989; Kuhn et al., 1985) by means of a carrier-mediated mechanism (Adell et al., 2002; Levi & Raiteri, 1993).

Extracellular concentrations of 5-HT in the DR and MR in rats determined from dialysate samples and voltametric methods range between 1 and 10 nM (Adell et al., 2002). The rate of clearance of 5-HT from the extracellular compartment is substantially enhanced in the DR (Bunin et al., 1998) likely due to the high density of uptake sites (Hrdina et al., 1990) that constitute the main mechanism of removal of 5-HT from the extracellular space

(Adell et al., 2002). 5-HT axons show substantial structural plasticity in response to genetically induced changes in 5-HT content (Nazzi et al., 2019). Specifically, clinically relevant variations in 5-HT content can dramatically affect the morphology of 5-HT axons (e.g., decrease in axon diameter) in the lacunar-molecular layer of the hippocampus (Nazzi et al., 2019).

Facilitated growth cone advance has been observed in 5-HT treated cultures, and this advancement is correlated with increased F-actin flow rates (Zhang et al., 2012). When plated on laminin substrates, *Aplysia* bag cell neuronal growth cones treated with 5-HT (10 μM) show increased retrograde actin flow and axon elongation (Zhang et al., 2012). Neurite outgrowth in 5-HT treated cultures had a consistent ~3-fold increase in average neurite outgrowth rate over the course of 6 hours and a ~3.5-fold increase over the course of one hour (Zhang et al., 2012).

5-HT modulates local differences in the expression of cell adhesion molecules on the surface of some interacting cells (Zhu et al., 1994). For example, addition of 5-HT to *Aplysia* cultures (mechanosensory neurons isolated from pleural ganglia and co-cultured either with homologous sensory cells or with identified motor cell L7 from the abdominal ganglion) can make motor neurites more attractive for sensory growth cones, thereby affecting new sensory neuritic growth and synapse formation (Zhu et al., 1994). When 2.5M of 5-HT is added to a co-culture of *Aplysia* neurons, the number of sensory cell branches and varicosities contacting the major axons of the target motor cell L7 increase, and a downregulation of *Aplysia* cell adhesion molecules from the surface of the presynaptic sensory cell is observed (Zhu et al., 1994). In addition, recent research has revealed that 5-

HT varicosities can undergo major transformations as a result of extracellular 5-HT levels, plastic changes (e.g., in learning-related processes), diseased conditions (e.g., in epilepsy), and other states (Adori et al., 2011; Daubert et al., 2010; Migliarini et al., 2013; Upreti et al., 2019).

5-HT levels can be manipulated with various pharmacological agents such as FLX. FLX is an SSRI in that it acts through the inhibition of SERT serotonin uptake that is released by the dendrites and axon terminals of neurons located in brainstem raphe (Lazarevic et al., 2019). The binding of SSRIs on SERT leads to the accumulation of 5-HT in the synaptic cleft, and subsequent greater occupation of 5-HT receptors (5-HTR) and enhanced 5-HTR activity is linked to changes in neuroplasticity that lead to the upregulation of synaptic proteins and denser dendritic spines (Lazarevic et al., 2019). Additionally, FLX promotes structural changes in 5-HT axons. Chronic administration of FLX reduces hippocampal 5-HT axon diameter and density in the ventral and dorsal hippocampus of mice bearing the pan-serotonergic driver *Pet1-Cre* partnered with a Cre-responsive tdTomato allele (Nazzi et al., 2019). Conversely, chronic FLX treatment induces the recovery of the 5-HT circuitry damaged by an ischemic lesion in a post-stroke depression (PSD) mouse model (Zahrai et al., 2020). Three weeks of FLX treatment found a reduction of SERT+ fibers and/or SERT+ varicosity density in the medial prefrontal cortex (mPFC), cingulate gyrus (CG), and prelimbic (PL) regions of stroke-induced PSD mice (Zahrai et al., 2020). The DR nucleus of PSD mice did not show changes in SERT+ process volume or varicosity density, without or with FLX treatment, but instead had the greatest density of SERT+ axons and varicosities intact (Zahrai et al., 2020). In the previously mentioned experiment, SERT+

should label 5-HT fibers. SERT is a convenient marker for serotonergic fibers and has been extensively used in IHC and PET imaging. In IHC analyses of fixed tissue, 5-HT can also be used to visualize serotonergic fibers (Janusonis & Detering, 2019; Slaten et al., 2010). The two molecules (SERT and 5-HT) differ in their size, location, and stability, which may lead to differences in signal intensity (Linley et al., 2013), with implications for post-mortem studies.

H. Axonal plasticity during regeneration

The regenerative potential of the peripheral nervous system (PNS), with regeneration defined here as the regrowth of a severed axon, either from the severed end itself or from a new branch of the same axon generated proximal to the injured end that extends past the site of injury, is a phenomenon that has been observed for almost a century (Cooke et al., 2022; D. B, 1930). It has previously been believed that unlike the PNS, the CNS is an environment non-permissive to all axon regeneration. However, recent studies in the axon regeneration field have found that following injury, both PNS and CNS neurons can revert to a developmental phenotype in order to promote axon regeneration (Cooke et al., 2022). Importantly, it has been observed that serotonin and norepinephrine expressing neurons within the CNS are able to regenerate their axons unaided (Cooke et al., 2022).

There is increasing evidence for spontaneous serotonergic axon regrowth within the CNS following chemical or physical insults (Cooke et al., 2022). Initial fixed tissue studies in the mammalian forebrain have showed robust recovery of 5-HT axon density following chemical lesioning with amphetamines as assessed using antibody staining against 5-HT

(Cooke et al., 2022; Mamounas et al., 2000; Molliver et al., 1990; Ohearn et al., 1988; Wilson & Molliver, 1994). A subsequent investigation also used antibody staining against 5-HT to demonstrate regrowth of 5-HT axons in otherwise non-permissive environments, including the subventricular zone and areas adjacent to a glial scar following a thermal injury—an act not replicated by callosal fibers within the same cortical region (Hawthorne et al., 2011). Other studies studying recovery from spinal cord injury in rodents found that surviving 5-HT axons exhibit significant compensatory sprouting extending beyond the site of injury (Camand et al., 2004; Cooke et al., 2022; Hayashi et al., 2010; Holmes et al., 2005; Inman & Steward, 2003).

However, since fixed tissue only displays a single moment in time, the recovery seen in these experiments may not be a result of genuine regeneration, defined as growth originating from damaged axons, but rather the collateral sprouting of surviving axons (Cooke et al., 2022). To address the concern that these axons may be emptying and replenishing with 5-HT following injury rather than retracting and regenerating, researchers have used long-term *in vivo* imaging (two photon microscopy) in transgenic mice expressing eGFP selectively in 5-HT neurons (Cooke et al., 2022; Jin et al., 2016). Jin et al. (2016) investigated the regrowth of 5-HT axons in physical injury models in which mice received a stab wound to the somatosensory cortex that transected serotonergic axons running along their anterior to posterior trajectory. Over the course of 12 weeks following injury, 5-HT axons traversed the glial scar and recovered regional axon density identical to mice that received a sham surgery. In addition, axon regrowth directly from the severed ends of the cut-axons was observed. The same transgenic mouse model was also used to examine

regeneration of 5-HT axons following a controlled cortical impact (CCI) to induce traumatic brain injury (Cooke et al., 2022; Kajstura et al., 2018). These mice received standardized impacts to the surface of the cortex and due to the extensive nature of the injury, axon regeneration was measured in the fixed tissue both anterior and posterior to the site (Kajstura et al., 2018). A week after injury, 5-HT axon density was decreased only posterior (distal) to the CCI injury (Kajstura et al., 2018). Yet, a month after injury, the density of serotonergic axons anterior (proximal) to the injury is largely recovered despite the large crater created by the impact injury, which remains devoid of axons (Kajstura et al., 2018). This research indicates robust axon regeneration by 5-HT neurons in the context of a more extensive injury is possible (Cooke et al., 2022; Kajstura et al., 2018).

5-HT axons are unique for several reasons, but the particulars of what makes them capable of regrowth following injury is unknown. The intrinsic ability of 5-HT neurons to support these impressively long axonal fibers may provide them with the mechanistic framework to rebuild and repair themselves following axonal damage (Cooke et al., 2022). However, even shorter projecting serotonergic axons are capable of regrowth while other very long axons, such as corticospinal tract (CST) axons, are unable to regrow following injury. An additional 5-HT neuron-specific condition that may aid in their capacity to regrow is that they are volume transmitting axons (Cooke et al., 2022). Since their signaling is not as spatially or temporally constrained as synapse-based signaling, regrowth restores pre-lesion function without having to reform each of the precise connections of the previously injured axon (Cooke et al., 2022). Lastly, it remains unclear if regeneration is specific to certain or all 5-HT neuron subtypes.

I. Current methods of studying the 5-HT system *Density measures*

Essentially all studies investigating the serotonergic matrix in mental disorders and other associated conditions have focused on fiber densities rather than single fibers (Janusonis & Detering, 2019). For example, though not supported by brain imaging, one study using SERT-immunohistochemistry (IHC) has found a dramatic increase in the density of serotonergic fibers in some cerebral cortical areas of young ASD brains, examined post-mortem (Azmitia et al., 2011). Individuals with MDD have reduced SERT-binding in some regions (Cumming et al., 2016; Gryglewski et al., 2014), with post-mortem studies implying that this result is associated with possibly age-dependent changes in serotonergic fiber density (Rajkowska et al., 2017). These findings are supported by evidence that experimentally altered fiber densities in mice can result in depressive-like behaviors (Chen et al., 2017). In addition, prolonged exposure to high amplitude sound (acoustic trauma) alters the density of 5-HT fibers in adults, demonstrating plasticity in serotonergic projections to the inferior colliculus (IC) (Keesom et al., 2018; Papesh & Hurley, 2016). Furthermore, since social isolation influences behavior partially through the alteration of neuromodulatory systems, such as the 5-HT system, Keesom et al. (2018) demonstrated a sex-specific effect of social experience on serotonergic fiber density, with social isolation decreasing fiber density in the IC of females, but not males.

5-HT primary cell culture

The ability to produce *in vitro* 2D-cultures of neuronal cells has been fundamental in advancing understanding of *in vivo* cell behaviors such as migration, growth, and mechanics (Duval et al., 2017). In addition, while serotonergic axons are typically studied regarding their collective and regionally specific densities, 2D-cell culture permits observation of single axon behavioral dynamics. Furthermore, the use of primary cells rather than immortalized cell lines, renders this model to be physiologically relevant, as primary neurons have gene and protein expression profiles that more closely resemble those of differentiated cells *in vivo* (Daub et al., 2009; Motti et al., 2018; Nolan, 2007).

Some of the earliest *in vitro* cell culture work with primary 5-HT neurons demonstrated that primary 5-HT neurons can respond to a wide variety of target neurons with a wide developmental window (Azmitia & Whitaker-Azmitia, 1987). The combination of diverse target cells and extended time frames used *in vitro* could be illustrative of the expansive distribution of 5-HT fibers *in vivo* in the vertebrate brain (Azmitia, 1978; Azmitia & Gannon, 1986; Azmitia & Whitaker-Azmitia, 1987). Fiber outgrowth from fetal neurons in culture occurs within hours of plating (Azmitia & Whitaker-Azmitia, 1987; Banker & Cowan, 1977; Dichter, 1978; Letourneau, 1982; Pettmann et al., 1979; Yavin & Yavin, 1974). Primary raphe cultures show 5-HT-immunoreactive neurons are capable of synthesizing and storing 5-HT within hours of dissociation and plating, with fine varicose fibers seen after 1 day *in vitro* (DIV1) and sprawling 5-HT fibers by DIV21 (Azmitia & Whitaker-Azmitia, 1987). In addition, E14 rat raphe cultures have been found to contain roughly 1% serotonergic neurons after 24 hours in culture, stained with Tph and 5-HT

antibodies (Galter & Unsicker, 1999). These same cultures showed 5-HT neurons consistently immunoreactive for the neurotrophin receptors trkB and trkC, though other trkB- and trkC-positive, non-5-HT cells were also present (Galter & Unsicker, 1999). Raphe cultures also contained a small number (less than 1%) of tyrosine hydroxylase (TH)-immunoreactive (IR) catecholaminergic neurons (Galter & Unsicker, 1999).

Organotypic slice culture

Dudok et al. (2009) studied the effect of 5-HT and 5-HT pharmacological compounds on the outgrowth of serotonergic projections using organotypic slice co- cultures of hippocampus and dorsal raphe nuclei. Within 7 days *ex vivo*, several 5-HT neurites were found to have grown into a hippocampal slice (Dudok et al., 2009). The authors then successfully utilized this co-culture model to examine the chronic application of 5-HT pharmacological compounds previously known to affect the outgrowth of 5-HT neurites from the DR using a 5-HT_{1A} receptor agonist, a 5-HT_2 receptor agonist, and FLX (Dudok et al., 2009; Kondoh et al., 2004; Zhou et al., 2006).

Complicated dynamics such as transient hyper-innervation, or large fluctuations in innervation over the course of a few days (Damato et al., 1987; Fujimiya et al., 1986) make modeling the complexities of the serotonin system *ex vivo* challenging (Dudok et al., 2009). For example, regional differences *in vivo* of 5-HT innervation in the hippocampus were not reproduced *ex vivo* (Dudok et al., 2009) and other studies have observed that fewer synapses form in slice culture than *in vivo* (Papp et al., 1995). Papp et al. (1995) demonstrated that raphe-hippocampal serotonergic afferents from rats are unable to form synaptic contacts

with their normal targets *in vitro*, if explanted one to three days postnatally. In addition, the *in vivo* connectivity of the 5-HT system appears to depend largely on non-synaptic release, a trait difficult to replicate in *ex vivo* systems such as organotypic slice culture (Dudok et al., 2009). Slice culture was additionally implemented in the evaluation of FFN246 (fluorescent false neurotransmitter-246) to assess specific labeling of 5-HT neurons of the dorsal raphe nucleus (Henke et al., 2018). While it is a reduced model, slice co-culture is still sufficient to examine the most rudimentary principles that direct 5-HT neurite outgrowth and connectivity (Dudok et al., 2009; Papp et al., 1995).

Disease modeling with human 5-HT neurons

Innovation in induced pluripotent stem cell (iPSC) and transdifferentiation technologies for deriving neurons from adult humans has facilitated the study of disease-relevant cellular phenotypes *in vitro* (Vadodaria et al., 2018). Thus, human 5-HT neurons can now be generated. Vadodaria et al. (2016) successfully generated human serotonergic neurons *in vitro* using primary human dermal fibroblasts established from skin biopsies from healthy donors. Overexpression of *NKX2.2, FEV, GATA2*, *S4F,* and *LMX1* along with the neuronal transcription factors *ASCL1* and *NGN2*, induced serotonergic transdifferentiation with high efficiency (Vadodaria et al., 2016). Induced serotonergic neurons (iSNs) expressed key markers of serotonergic neurons, fired action potentials, and released serotonin in the culture medium, which could be moderated by treatment with SSRIs (Vadodaria et al., 2016).

In addition to iSNs, iPSC-derived serotonergic neurons also share many defining properties of serotonergic neurons and offer promising methods to study human serotonergic neurons *in vitro* (Vadodaria et al., 2016). For example, iPSC-to-neuron differentiation captures the developmental sequence of patterning to produce serotonergic neurons with subtype identity, with the possibility that transdifferentiated serotonergic neurons could be made to adopt region-specific serotonergic identities (Vadodaria et al., 2018). However, iPSC-derived serotonergic neurons may not be mature enough for studying adult raphe-related phenotypes (Vadodaria et al., 2018). Ultimately, *in vitro*-generated human serotonergic neurons signify a first step in exploring the utility of patient-derived serotonergic neurons for studying psychiatric disorders in the future (Cao et al., 2017; Lu et al., 2016; Vadodaria et al., 2018).

J. Cell culture geometry

Many cell behaviors are significantly influenced by cell culture geometry, though it remains unclear which culture geometry is appropriate for probing a specific cell function and mimicking native microenvironments (Smithmyer et al., 2019). *In vitro* cell culture systems have largely facilitated studies on the mechanisms underlying the formation, function and pathology of tissues and organs (Kapałczyńska et al., 2018; Yamada & Cukierman, 2007). The advantages of 2D-cultures are typically associated with simple and low-cost upkeep of the cell culture and with the performance of functional tests (see **Table 1** for overview of 2D vs 3D culture) (Kapałczyńska et al., 2018).

Both 2D and 3D-cell culture systems are an indispensable tool in exposing fundamental biophysical and biomolecular mechanisms of cells and how these cells function in disease (Duval et al., 2017). However, contemporary work has demonstrated that cells often exhibit unnatural behavior when excised from native 3D-tissues and confined to a 2D-monolayer (Tibbitt & Anseth, 2009). 2D-culture confines cells to a planar environment and restricts the more complex morphologies observed *in vivo* (Tibbitt & Anseth, 2009). In 2D-cultures, neurons are constrained to extend their processes in the plane but when cultured within ECM-mimicking hydrogels, the same cells can extend processes isotopically in three dimensions and even form neurospheres (Tibbitt & Anseth, 2009). The cellular microenvironment is known to contribute to the spatially and temporally complex signaling domain that directs cell phenotype (Tibbitt & Anseth, 2009). For example, human breast epithelial cells develop like tumor cells when cultured in two-dimensions but revert to normal growth behavior when cultured in 3D-analogs of their native microenvironment (Petersen et al., 1992; Tibbitt & Anseth, 2009). As a result, it has become imperative to identify 3D-scaffolds that can recapitulate the essential aspects of the native cellular microenvironment in artificial cell systems (Tibbitt & Anseth, 2009).

Hydrogels

The term *hydrogel* describes 3D-network structures obtained from a class of natural and/or synthetic polymers that can absorb and retain considerable amounts of water due to their hydrophilic nature (Catoira et al., 2019). Hydrogels are swollen 3D viscoelastic polymeric networks which have similar physical properties to natural tissue (Catoira et al.,

2019). The hydrogel matrix is formed by crosslinking polymers with covalent bonds or noncovalent interactions and their structure can then be designed to suit the final application (Catoira et al., 2019). Hydrogels are considered unique viscoelastic materials because they possess two independently tunable mechanical properties: the elastic modulus (Young's modulus) and viscous modulus (Okay, 2010). Their mechanical strength depends on the crosslink density; however, the stronger the gel the less it can absorb water (Catoira et al., 2019). The main limitation of hydrogel-based scaffolds is the actual interaction between cells and the hydrogel matrix, as viscoelastic properties largely influence cell phenotype and fate (Aswathy et al., 2020; Lee & Kim, 2018). At the most modest deconstruction, hydrogels typically promote cell function when produced from natural materials and can be permissive to cell function when made from synthetic materials, though both can capture numerous characteristics of the architecture and mechanics of the native cellular environment (Saha et al., 2007; Tibbitt & Anseth, 2009). Most commonly used with stem cells, 3D-hydrogels capture numerous characteristics of the architecture and mechanics of the native cellular environment (Saha et al., 2007; Talebian et al., 2019; Tibbitt & Anseth, 2009), but there is a pressing need for more representative depictions of different cell types and activities in various hydrogel systems (Gyles et al., 2017). 3D-systems more closely resemble *in vivo* environments, offering a more reliable method to examine physiologically relevant neuron dynamics. However, much is still unknown about the variations in specific cell type dynamics in 2D-culture versus 3D-culture (e.g., the feasibility of using primary serotonergic neurons in hydrogel systems). Thus, 3D-culture systems, especially those developed for primary serotonergic neurons, can be considered high-risk/high-reward systems. This project

provides a novel perspective of the behavioral dynamics of individual serotonergic axons in cell culture models of various geometries.

	2D	3D	References
Quality	High reproducibility, performance, long-term-culture	Worse performance and reproducibility, difficult to interpret and carry out	(Hickman et al., 2014)
***In vivo* representation**	Does not mimic natural structure of tissue	*In vivo* tissues and organs are in 3D form	(Griffith & Swartz, 2006)
Cell characteristics	Altered morphology and way of division; loss of diverse phenotype and polarity	Preserved morphology and way of division, diverse phenotype, and polarity	(Kilian et al., 2010; Mseka et al., 2007; Yamada & Cukierman, 2007)
Cell interactions	Deprived of cell-cell and cell-extracellular environment interactions, no *in vivo*-like microenvironments and typically no "niches"	Proper interactions of cell-cell and cell-extracellular environment, environmental "niches" are created	(Bissell et al., 2003; Cawkill & Eaglestone, 2007; Engler et al., 2006; Gilbert et al., 2010; Lee et al., 2008)
Access to essential compounds	Unlimited access to oxygen, nutrients, metabolites and signaling molecules	Variable access to oxygen, nutrients, metabolites and signaling molecules (same as *in vivo*)	(Breslin & O'Driscoll, 2013; Frieboes et al., 2006)
Molecular mechanisms	Changes in gene expression, mRNA splicing, topology, and biochemistry of cells	Expression of genes, splicing, topology, and biochemistry of cells as *in vivo*	(Berthiaume et al., 1996; Birgersdotter et al., 2005; Fuchs et al., 2004; Gomez-Lechon et al., 1998; Li et al., 2006)
Cost of maintaining a culture	Cheap, commercially available tests and the media	More expensive, more time-consuming, fewer commercially available tests	(Aggarwal et al., 2009; Krishnamurthy & Nor, 2013; Sodunke et al., 2007; Weiswald et al., 2015)

Table 1 Comparison of 2D and 3D cell culture methods. (Adapted from (Kapałczyńska et al., 2018).

II. Specific Aims

The proposed research will contribute to the identification of compatible systems to examine brain dysfunction at the single-neuron level and aid in the development of computational predictive models of serotonergic fiber dynamics and self-organization.

Specific Aim 1: Previous work in our laboratory has shown that the self-organization of 5-HT fibers depends in part on the spatiotemporal structure of their individual trajectories. Understanding this structure may allow precise mathematical modeling, but the success of this effort crucially depends on a reliable 2D-*in vitro* model to collect experimental data that is required to validate the general structure of a model and to constrain the values of its parameters. Primary cell cultures of brainstem neurons are demanding in their sensitivity to plating and incubation conditions and are currently used by a small number of laboratories (as compared to the more common cortical neuron cultures). This aim sought to **develop and optimize a reliable 2D-*in vitro* experimental platform to examine the dynamics of single serotonergic axons.**

Specific Aim 2: The 2D-*in vitro* model developed in Specific Aim 1 was analyzed with several techniques, including **high-resolution confocal microscopy, holotomography, and super resolution microscopy (STED) to examine the short-term dynamics of primary brainstem neurons in culture.** In particular, **we collected the first holotomographic recordings of primary brainstem neurons.**

Specific Aim 3: Three-dimensional *ex vivo* systems allow unique access to the processes that underly the dynamics and self-organization of serotonergic fibers. We performed preliminary tests to explore the compatibility of various **3D-platforms** for primary brainstem neurons by transitioning from 2D- to 3D-culture with a **2.5D**-culture system and by examining two complementary 3D hydrogel architectures. These **tunable hydrogels** were based on xeno-free materials, alginate scaffolds (that have been shown to be biocompatible in other tissue systems) and novel polymer chemistries. **Testing the use of primary brainstem neurons in these hydrogel systems provides a foundation for future analyses of serotonergic axons in extracellular environments with controllable physical characteristics that cannot be achieved *in vivo* and can potentially revolutionize the current understanding of the self-organization of the brain serotonergic matrix.**

III. Chapter 2: General Methods

A. Animals

Timed-pregnant female Sprague-Dawley rats (embryonic day 13-15 (E13-15)) and C57BL/6 mice (E13-15) were ordered from Charles River and were maintained singly housed with free access to food and water. For all cell culture work, postnatal day 0.5-2 (P0.5-2) rat and mouse pups were used, and for imaging in fixed brain preparations, E17 C57BL/6 mice were used. All procedures have been approved by the UCSB Institutional Animal Care and Use Committee.

B. Immunocytochemistry

Cultures were fixed by aspirating the culture medium and immediately adding phosphate-buffered 4% paraformaldehyde (PFA) for 10 minutes. They were rinsed in 0.1 M phosphate-buffered saline (PBS) and either processed immediately or stored for a few days at 4°C. All immunocytochemical procedures were done at room temperature on a shaker. Cultures were rinsed in PBS, blocked for 15 minutes in 2% normal donkey serum (NDS) in PBS, incubated in goat anti-5-HT IgG (1:1000; ImmunoStar # 20079) and rabbit anti-MAP2 IgG (1:1000; Abcam #32454) with 2% NDS and 0.3% Triton X-100 (TX) in PBS for 1 hour, rinsed 3 times in PBS (5 minutes each), incubated in Cy3-conjugated donkey anti-goat IgG (1:500; ImmunoResearch #705-165-147) and AlexaFluor 488-conjugated donkey anti-rabbit IgG (1:1000; ThermoFisher #A-21206) with 2% NDS in PBS for 30 minutes, and rinsed 3 times (5 minutes each) with PBS. After a quick (5-10 seconds) rinse in water (to remove

salts), the coverslip with the cells was carefully detached from the bottom of the plate and mounted on a glass slide with ProLong Gold Antifade Mountant containing DAPI (ThermoFisher #P36941). The cells were imaged at least 24 hours after mounting to allow curing to the optimal refractive index.

C. Epifluorescence microscopy & confocal

Live cells were routinely examined using an Olympus CKX-41, an inverted microscope with a color digital camera. Phase contrast/epifluorescence imaging of fixed preparations was performed on an AxioVision Z1 system in three channels (Cy3, GFP, and DAPI), using a 10× objective (NA 0.45) and a 40× oil objective (NA 1.30). Confocal imaging of fixed preparations was performed in three channels (Cy3, AlexaFluor 488, DAPI) on the Leica SP8 resonant scanning confocal system, primarily using a 63× oil objective (NA 1.40) with the xy-resolution of 59 nm/pixel and the z-resolution of 300 nm/optical section. Typical z-stacks consisted of 30-100 optical sections. The confocal microscopy figures show maximum-intensity projections.

D. Holotomography

Holotomography

Quantifying physical properties of biological material contributes to a better understanding of the dynamics of living matter (Schürmann et al., 2016)). Quantitative phase microscopy techniques, such as digital holographic microscopy (abbreviated as DHM;

DHTM; HTM; or HT), enables the quantification of single-cell Refractive Indices (RI) and Refractive Index Gradients (RIG), which hold important information about cell function, as well as subcellular structures (Schürmann et al., 2016; Yakimovich et al., 2018). HTM is a recent technological breakthrough in the field of experimental biology. It is non-invasive, non-phototoxic, and has unique multiplexing capabilities that allows for observing multiple biological objects and phenomena simultaneously, including complex cellular dynamics such as organellar rotations that involve many subcellular structures (Sandoz et al., 2019). In particular, HTM provides the specificity and spatiotemporal resolution necessary to understand the dynamics of serotonergic fibers.

The RI of a medium is defined as the ratio between the speed of light in vacuum and the speed of light in that medium (Doyeon Kim et al., 2018; Nanolive). The RI of a single cell is a highly valuable biophysical property which has been measured and studied since the 1950s (Liu et al., 2016). The RI can be used to determine or correlate with other cell biophysical parameters such as dry mass, wet mass, protein concentration, elasticity, and conductivity, as well as to study certain metabolic activities including cell division and infection (Liu et al., 2016). Due to advanced optical imaging techniques (e.g., digital holotomography), 3D RI maps of single cells are now obtainable, which show the RI distribution in the entire cell. Although 3D RI tomography does not provide molecular specificity in general, some objects with distinct RI values, such as lipid droplets (Kim et al., 2016) and artificially introduced gold nanoparticles (D. Kim et al., 2018; Sung et al., 2018), can be specified and quantified (Doyeon Kim et al., 2018). **Table 2** shows typical refractive index values of various cell organelles (Liu et al., 2016).

Organelles/intracellular matter	Refractive Index
Cytosol	1.360 – 1.390
Nucleus	1.355 – 1.365
Nucleolus	1.375 – 1.385
Mitochondria	1.400 – 1.420
Lysosome	1.600

Table 2 Typical refractive index values for various organelles in a cell (From Liu et al., 2015).

RIG pertains to RI and *spatial* information. Based on the RI change across a volume (i.e., how the RI varies in the proximity of a pixel), the RI gradient (RIG) can be computed across a whole cell (**Figures 1B** & **C**) (Yakimovich et al., 2018). RIG measured by HTM not only provides accurate, noninvasive readouts of cell volume, but it also serves as an indicator for the granularity, or *internal complexity*, of cell structures (Yakimovich et al., 2018). In a study demonstrating that HTM is suitable for observing virus-infected cells, Yakimovich et al. (2018) confirmed that specific RIG signatures indicate virus-induced cytopathic effects (CPEs) (**Figure 1A**). Interestingly, the RIG values of vaccinia virus

(VACV-GFP) infected cells gradually increased as the infection progressed, reaching threefold at 8 hours post-infection compared to the RIG prior to infection (Yakimovich et al., 2018). The applications of using RIG extend beyond viral CPEs to areas such as bacteria identification and early-stage cancer diagnosis.

Nanolive 3D-Cell Explorer

Live cultures were removed from the incubator and immediately imaged with the 3D-Cell Explorer CX-F (firmware 1.5.70; Nanolive SA, Switzerland) equipped with a 60× objective and a CMOS camera with 1024×1024 pixels. The laser used for tomography was 520 nm at an output power of 0.1 mW. The imaging conditions matched the incubation conditions (5% CO_2 at 37°C). The z-stacks contained around 95 sections and were imaged around every 7 seconds. The 4D-recordings were reviewed and analyzed in STEVE 1.6 (the native software of the system). Time-lapse z-projections were generated in ImageJ with a Nanolive macro.

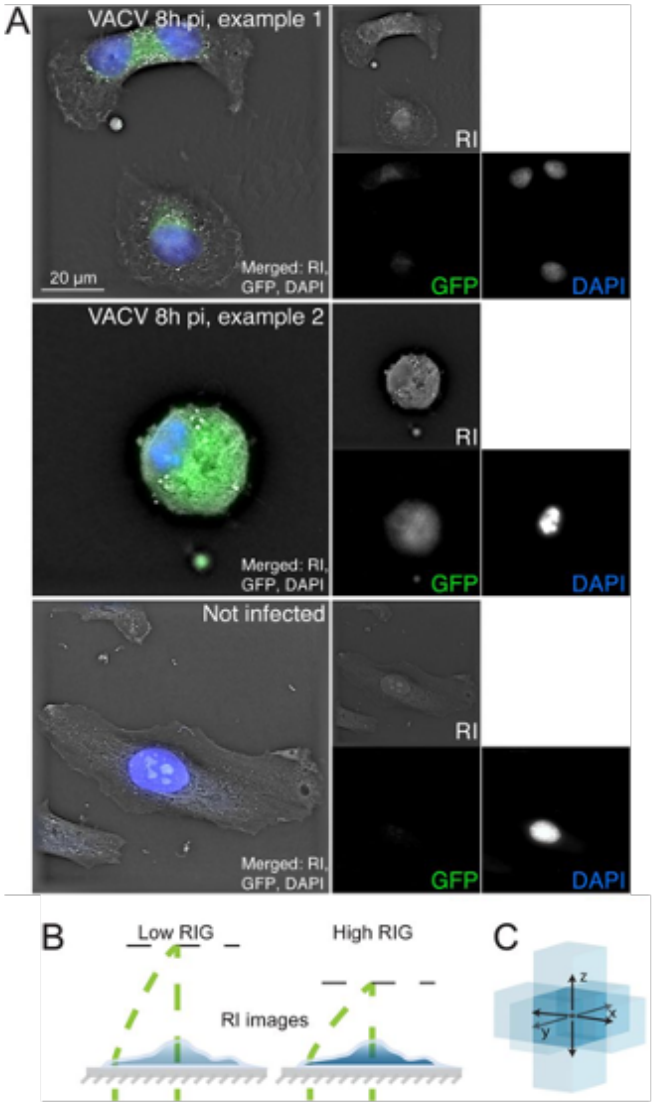

Figure 1 (A) Infected HeLa cells [VACV-GFP]. Cells are fixed 8 h postinfection (pi) with PFA, and recorded RI, nuclear DAPI stain, and GFP intensity was examined *by correlative DHTM and fluorescence microscopy and compared the infected cells to noninfected cells.* The top panels depict a VACV-GFP-infected cell in early infection stage. The middle panels depict a rounding cell, indicating late-stage VACV infection. The bottom panel depicts an uninfected cell. At 8 h pi, all cells inoculated with VACV-GFP were infected based on their GFP intensity and DAPI staining of cell nuclei, whereas the GFP intensity of the uninfected cells was in the range of the background. **(B)** Schematic illustrations of RI computation. A cell can be thought of as a gradient index microlens, changing its optical properties depending on biochemical activities. **(C)** RIG is derived from RI and represents a voxel-based measurement of the difference of the refractive index in 3D space. The RIG value of the voxel in the middle is represented as a middle blue box, which is calculated based on the difference to the light blue voxels in the 3D neighborhood. Note that the reference beam (curved green dashed line) does not pass through the sample. RI is based on changes between the beam (straight green dashed line) and the reference beam. (From Yakimovich et al., 2018.)

E. Immunohistochemistry and super-resolution microscopy (STED)

A timed-pregnant C57BL/6 dam (Charles River) was euthanized with CO_2 at embryonic day 17 (E17). The embryos were removed from the uterus, immediately decapitated, and their brains were dissected and immersion-fixed in 4% PFA overnight at 4°C. They were cryoprotected in phosphate-buffered 30% sucrose for 2 days and embedded in 20% gelatin (type A; FisherScientific #G8-500). The gelatin block was trimmed around the brain, immersed in formalin with 20% sucrose for 3 hours, rinsed in PBS, and sectioned on a freezing microtome at 40 μm thickness. Selected sections were rinsed in PBS, blocked in 2% normal goat serum (NGS) in PBS for 30 minutes, and incubated in rabbit anti-5-HT IgG (1:500; ImmunoStar #20080) with 2% NDS and 0.3% TX in PBS for 2 days on a shaker at 4°C. They were rinsed 3 times in PBS (10 minutes each), incubated in STAR-RED-conjugated goat anti-rabbit IgG (1:200, Abberior #STRED-1002) for 90 minutes, rinsed 3 times in PBS (10 minutes each), mounted on coverslips (to minimize the objective-section distance and improve imaging depth), and allowed to air-dry. The coverslips were mounted on glass slides with ProLong Gold Antifade Mountant (without DAPI; ThermoFisher #P36930). The sections were imaged at least 24 hours after mounting to allow curing to the optimal refractive index. They were imaged on the Abberior STED (Stimulated Emission Depletion) microscope using a 60× oil objective (NA 1.4), the excitation line of 640 nm, and the depletion line of 775 nm. The voxel dimensions were 30×30×100 nm^3. Double-label immunohistochemistry for 5-HT and MAP2 (with AlexaFluor 594-conjugated donkey anti-goat IgG and AlexaFluor 647-conjugated donkey anti-rabbit IgG) was also attempted but

yielded virtually no improvement over regular confocal imaging, likely due to suboptimal properties of the AlexaFluor dyes in the used STED configuration.

IV. Chapter 3: 2D-cell cultures *Cortical glia-brainstem neuron coculture*

The procedures were based on the protocol developed in Dr. David Sulzer's laboratory (Columbia University) (Staal et al., 2007). In the first step, a monolayer of glial cells (primarily astrocytes) was produced. Rat pups (Sprague-Dawley, Charles River, postnatal days (PD) 1-3) were anesthetized on ice, decapitated, and their cerebral cortex was dissected under a stereoscope with fine surgical tools. The collected tissue (from around 2 pups) was placed in Dulbecco's phosphate buffered saline (DPBS; Sigma-Aldrich # D1408) on ice and cut into small (around 1 mm^3) pieces. The pieces were immediately transferred into a glia-specific papain solution effused with carbogen (95% O_2 and 5% CO_2) to dissociate the cells. The papain solution was composed of papain (20 Units/mL; Worthington Biochemical Corporation #LS003126), 1 mM cysteine (from cysteine water, described below), 1× H&B concentrate (described below), and 0.001% phenol red (all concentrations are final). The cysteine water contained 1.25 mM L-cysteine and 1.9 mM $CaCl_2$. The 5× H&B concentrate contained 116 mM NaCl, 5.4 mM KCl, 26 mM $NaHCO_3$, 2 mM $NaH_2PO_2 \cdot H_2O$, 1 mM $MgSO_4$, 0.5 mM EDTA, and 25 mM glucose. Following cell dissociation, cells were washed, gently triturated with GSM (described below), and counted. Cells were diluted to a density of 1,000,000-1,500,000 cells/mL and plated at around 80,000 cells per culture dish. The 35 mm-culture dishes with a bottom glass coverslip (No. 1.5) were pre-coated with poly-D-lysine (Mattek #P35GC-1.5-14-C) and further coated with laminin (at 10 µg/mL: Sigma-Aldrich #CC095). The glia-specific medium (GSM) was

composed of Minimum Essential Medium Eagle (MEM) (180 mL; Sigma-Aldrich #M2279), fetal bovine serum (not heat-inactivated, 20 mL; ThermoFisher # 26140087), glucose (1.5 mL of a 45% solution; Sigma-Aldrich # G8769), insulin (40 µL of 25 mg/mL [0.02 M HCl]; Sigma-Aldrich #I5500), glutamine (0.5 mL of a 200 mM solution; Sigma-Aldrich #G2150), and penicillin-streptomycin (0.24 mL of a solution containing 10,000 Units/mL penicillin and 10 mg/mL streptomycin; Sigma-Aldrich #P0781). When the glia (feeder) layer became 70% confluent (3-5 days after plating), 5-fluoro-2'-deoxyuridine (FDU) was added to inhibit non-neuronal cell proliferation. The FDU stock solution was prepared by adding 15 mL of a uridine solution (16.5 mg/mL; Sigma-Aldrich #U3003) to 100 mg of FDU (FDU; Sigma-Aldrich # F0503). Before use, it was diluted by adding 0.2 mL of the stock to 1.8 mL MEM, and 20 µL of the diluted solution was added to each dish with 2 mL of the glia-specific medium.

In the second step (around 7-14 days after the initial plating), midbrain neurons were added to the culture. Mouse pups (C57BL/6, Charles River, PD 1-2) were anesthetized on ice, decapitated, and their midbrain at the level of the rostral raphe nuclei was dissected under a stereoscope with fine surgical tools. The collected tissue (from 5-7 pups) was placed in PBS on ice and cut into small (around 1 mm^3) pieces. The pieces were immediately transferred into a neuron-specific papain solution effused with carbogen to dissociate the cells. The papain solution was composed of papain (20 Units/mL), 1 mM L-cysteine (from cysteine water), 1× H&B concentrate, 3.75 mN HCl, 0.5 mM kynurenic acid (from a 0.5 M solution [in 1 N NaOH]; Sigma-Aldrich #K3375), and phenol red (0.001%) (all concentrations are final). Following cell dissociation, cells were washed, triturated with

cNSM (described below), and counted. Cells were diluted to a density of 1,000,000 cells/mL and plated at around 60,000-80,000 cells per dish. Cells were plated in slide rings (Thomas Scientific # 6705R12) on glia monolayers to ensure neurons adhere to the coverslips and do not get washed away. The midbrain neuron-specific medium (cNSM) was composed of MEM (94 mL), Dulbecco's Modified Eagle's Medium (low glucose) (80 mL; Sigma-Aldrich #D5546), heat-inactivated fetal bovine serum (2 mL; ThermoFisher #A3840301), glucose (1.5 mL of a 45% solution), glutamine (0.5 mL of a 200 mM solution), bovine serum albumin (fraction V) (0.5 g; Sigma-Aldrich # A4503), Ham's F-12 nutrient mixture (20 mL; Sigma-Aldrich # N4888), catalase in an aqueous solution (0.1 mL; Sigma-Aldrich # C3155), kynurenic acid (200 µL of a 0.5 M solution), HCl (50 µL of a 5 N solution), and the di Porzio concentrate (2 mL). The di Porzio concentrate (di Porzio et al., 1980; Casper et al., 1991) was composed of 6.25 µg/mL progesterone (Sigma-Aldrich #P0130), 4 µg/mL corticosterone (Sigma-Aldrich #C2505), 2.5 mg/mL insulin, 0.52 µg/mL Na_2SeO_3 (Sigma-Aldrich #214485), 2 µg/mL 3,3',5-triiodo-L-thyronine sodium salt (Sigma-Aldrich #T2752), 0.5 mg/mL superoxide dismutase (Sigma-Aldrich #S7571), 0.24 mg/mL putrescine dihydrochloride (Sigma-Aldrich #P7505), and 10 mg/mL apo-transferrin (Sigma Aldrich #T1428) in Hanks' Balanced Salt Solution (HBSS) (ThermoFisher #14170120). The neuron-specific medium was additionally pre-conditioned for 24 hours in either confluent glia cultures (in the original culture dishes) or T225 flasks containing glial cell monolayers **(Table 3).** Two hours after plating, the slide rings were removed, and glial-derived neurotrophic factor (GDNF) was added at the final concentration of 10 ng/mL (Sigma-Aldrich #GF322) to protect cultures from cell death and support neurite outgrowth. One day

after cell plating, FDU was added to inhibit non-neuronal cell proliferation at the final concentration of 6.7 µg/mL. The cultures were imaged immediately or maintained healthy for up to 4-6 weeks.

All cell culture solutions were sterile filtered (with the pore size of 0.22 µm) before use. The cultures were incubated in a Thermo Scientific Forma Series II water-jacketed incubator at 5% CO_2 and 37°C. Further details about the preparation of the used reagents are available in Staal et al. (2007).

Glia-specific medium (GSM)	**Midbrain neuron-specific medium (cNSM)**	**Neuron-specific medium (mNSM)**

• MEM (180 mL)
• FBS (not heat-inactivated (20 mL)
• glucose (1.5 mL of a 45% solution)
• insulin (40 µL of 25 mg/mL [0.02 M HCl]
• glutamine (0.5 mL of a 200 mM solution)
• penicillin-streptomycin (0.24 mL of a solution containing 10,000 Units/mL penicillin and 10 mg/mL streptomycin)
	• MEM (94 mL)
	• DMEM (low glucose) (80 mL)
	• heat-inactivated FBS (2 mL)
	• glucose (1.5 mL of a 45% solution)
	• glutamine (0.5 mL of a 200 mM solution)
	• bovine serum albumin (fraction V) (0.5g)
	• Ham's F-12 nutrient mixture (20 mL)
	• catalase in an aqueous solution (0.1 mL)
	• kynurenic acid (200 µL of a 0.5 M solution)
	• HCl (50 µL of a 5 N solution)
	• di Porzio concentrate (2 mL).
	  • 6.25 µg/mL progesterone
	  • 4 µg/mL corticosterone
	  • 2.5 mg/mL insulin
	  • 0.52 µg/mL Na_2SeO_3
	  • 2 µg/mL 3,3',5-triiodo-L-thyronine sodium salt
	  • 0.5 mg/mL superoxide dismutase
	  • 0.24 mg/mL putrescine dihydrochloride
	  • 10 mg/mL apo-transferrin in HBSS
		• 95% Gibco Neurobasal Plus Medium
		• 2% Gibco B-27 Plus
		• 2% GlutaMAX
		• 0.1-0.5% penicillin-streptomycin

Table 3 All primary culture media formulations used.

B. Co-culture vs mono-culture

Co-culture models as opposed to mono-cultures are typically considered advantageous due to the adhesion-related and nutritional benefits. However, the optimal development of biomimetic *in vitro* and *ex vivo* models is dependent on cell type and/or brain regions being modeled. For example, the viability and axon growth of mouse motor neurons (MNs) is notably enhanced when co-cultured with Schwann cells (SCs) compared to MN mono-cultures consisting of a thin layer of Matrigel (Hyung et al., 2015). Interestingly, in the MN mono-cultures, 96% of neurons failed to survive whereas the MN-SC co-cultures resulted in essentially no cell death for up to DIV21 (Hyung et al., 2015). In addition, *in vitro* gut models can be enhanced by incorporating co-culturing methods such as including an epithelial monolayer in combination with tissue derived primary cells, resulting in the promotion of *in vivo* resembling mucus and villus-like structures (Zhang et al., 2021). In addition, Kidambi et al. (2008) assessed neuronal responses to levels of saturated free fatty acids (FFAs), specifically the accumulation of reactive oxygen species (ROS), in mono-cultures versus co-cultures. In co-culture, since both the astrocytes and the neuronal cells were on the same surface, in direct contact, and in the same culture media, elevation in the ROS levels was observed earlier (i.e., faster elevation of ROS levels) than in the monoculture system. In addition, they found that using patterned co-culture systems as opposed to random co-culture systems resulted in neuronal responses to FFAs that was more representative of what would be expected *in vivo*, and therefore, a better *in vitro* model of neuronal metabolism (Kidambi et al., 2008).

The role of astrocytes for maintaining neuronal homeostasis both *in vivo* and *in vitro* is well established (Pozzi et al., 2017). Subsequently, co-cultures involving neurons and astrocytes has become conventional as cell-cell communication between primary neurons and astrocytes is crucial for the development, repair, and metabolism of neuronal systems (Feng & Walsh, 2001; Kidambi et al., 2008). These co-culture systems allow for the neuronal responses that may be mediated by the astrocytes *in vivo* (Kidambi et al., 2008). Co-cultures of neurons and astrocytes have been employed to study the pathogenesis of neurodegenerative disease and neuronal metabolism, though most of these models use trans-well, conditioned media, or random co-cultures (Chen et al., 2001; Desagher et al., 1996; Kidambi et al., 2008; Park et al., 2001). However, a number of neuronal-astrocyte co-culture models involve cell lines rather than primary neurons due to the difficulties involved in attaching primary cells onto synthetic surfaces (Kidambi et al., 2008).

Transitioning from co-culture to mono-culture

Previous research has found that astrocytes can significantly influence the behavior of CNS neurons *in vitro* and these glial-neuronal interactions are moderated by glial cell surface properties which make for optimal adherent substrates for axonal growth (Noble et al., 1984). Since these adherence interactions may account for many observations of neuronal behavior, the use of an astrocytic monolayer in 2D-cultures is biologically relevant (Noble et al., 1984). Despite the physiological relevance and nutritional benefits of providing an astrocytic feeder layer in culture, live imaging is a crucial component of the current research. Our live recordings using the holotomography microscope resulted in

motile glia, moving at a pace which resulted in torn axons. Therefore, to examine the properties of single axons with live imaging, mono-cultures were also used.

C. Development of brainstem monolayers

These cultures consisted only of a neuronal layer, with no glial layer. The midbrain tissue was dissected from mouse pups as described above. After dissociation, cells were washed, gently triturated with cNSM, and counted. We found that in this step cNSM could be replaced with mNSM (described below) with 1% heat-inactivated fetal bovine serum. Cells were diluted to a density of 1,000,000-1,500,000 cells/mL and plated at around 50,000-100,000 cells per culture dish. Lighter trituration resulted in denser but healthy cultures. The neuron-specific medium (mNSM) consisted of 95% Gibco Neurobasal Plus Medium (ThermoFisher #A3582901), 2% Gibco B-27 Plus Supplement (ThermoFisher #17504044), 2% GlutaMAX (ThermoFisher # 35050061), and 0.5% penicillin-streptomycin (all concentrations are final). The addition of GDNF and FDU, as well as the other procedures, were the same as in the co-cultures. The cultures were imaged immediately or maintained healthy for up to 4-6 weeks.

D. Cell culture protocol modifications

The propagation and culturing of animal cells for diverse cell-based assays are fundamental to biomedical and pre-clinical research (Baust et al., 2017). Unfortunately, a lack of adherence to best tissue culture practices has been costly due to flawed data and

irreproducible results (Baust et al., 2017; Freedman, Cockburn, et al., 2015; Freedman, Gibson, et al., 2015; Reid, 2011). Efforts to reduce environmental or methodological variabilities are often lacking, and whether these variabilities could have any effects on the experiments is commonly discounted or ignored ("Refresh cell culture," 2021). The environmental conditions used in mammalian cell culture are routinely underreported in biomedical studies ("Refresh cell culture," 2021). Particularly, regardless of the cells used (i.e., human or non-human cell lines, primary cells, or stem cells), the pH of the media and the level of atmospheric oxygen in the culture chamber are rarely specified in the literature ("Refresh cell culture," 2021). Moreover, only about 40% of biomedical studies report the level of carbon dioxide and the temperature in the culture chamber, yet it has long been known that the levels of oxygen and carbon dioxide in the environment of cells alter their physiology. Indeed, and as an aside, the 2019 Nobel Prize in Physiology or Medicine recognized work that unveiled how cells sense and adapt to the availability of oxygen ("An award to oxygen sensing," 2019; "Refresh cell culture," 2021). Given the significance of the cell culture environment, all factors used in the protocol are next discussed.

Media

Different culturing considerations – such as media composition or cell density – lead to altered experimental results (Pozzi et al., 2017). The cell culture medium is a complex mixture of nutrients and growth factors that along with the physical environment can either support or inhibit cell viability (Baust et al., 2017). Nutritional requirements differ with

different cell types and functions, as do optimal pH and osmolality (Baust et al., 2017). As cell growth proceeds from initial seeding to confluence, different cells will utilize amino acids and other components at different rates (Baust et al., 2017). Optimal cell culture media allows for the necessary regulation of ammonia, free radicals, heavy metal toxicity, pH shifts, fluctuations in osmolality, nutrient depletion, and chemical and biological contaminants (Baust et al., 2017).

Animal serum

Medias supplemented with serums, most often from fetal bovine (FBS) origin, are commonly used for neuronal cultures (Pozzi et al., 2017). Unfortunately, not only are animal serums prone to batch to batch variability, but the chemical composition of animal serums such as FBS are not fully defined and include factors not present in the brain (Arigony et al., 2013; Pozzi et al., 2017; Zheng et al., 2006). Due to these limitations of animal serums, the use of chemically defined, serum-free medium is often recommended for studies that require absolute control of the environment (Kivell et al., 2000; Pozzi et al., 2017). Most often used, and now utilized in our own mono-culture protocol, is B-27™ Plus Neuronal Culture System (Gibco™ A3653401) (Neurobasal™ Plus Medium (Gibco™ A3582901) with B-27™ Supplement (Gibco™ 17504044)) (including the modification of adding glycoproteins) which was designed to support long-term neuronal survival in E18 and P0 neuronal cultures consisting of less than 10% glial cells (Pozzi et al., 2017). While we utilize only 1% animal serum during the trituration stage, even protocols stating to use serum free media still utilize serums, but during the coating stage. For example, following poly-D-

lysine incubation at room temperature for 5 min, coverslips get pre-treated with 10% FCS for a minimum of 2 hours to assist cell attachment (Kivell et al., 2000).

Media for primary neuron cultures

Research that utilizes primary neurons most commonly use hippocampal or cortical neurons with protocols that have already been well developed. For example, various methods for obtaining successful cultures of primary hippocampal neurons exist, with all of them involving astrocytes: directly plating dissociated neurons on a glial feeder layer (as used in our initial approach) (Ivenshitz & Segal, 2010), neurons plated on a coverslip that is suspended above a glial feeder layer (Kaech & Banker, 2006), and culturing neurons in astrocyte conditioned medium (ACM). Pozzi et al. (2017) examined the use of primary hippocampal neurons in the previously noted media conditions. ACM-based cultures gave the best results for all tested criteria (i.e., growth cone size and shape, neuronal outgrowth and branching, network activity and synchronization, maturation, and long-term survival) (Pozzi et al., 2017). Interestingly, Neurobasal/B27 cultures were comparable to ACM for young cultures at 1 day(s) *in vitro* (DIV1), but not for culturing times longer than DIV7 (Pozzi et al., 2017).

Media for primary brainstem neurons

Only a handful of publications involving primary brainstem neurons exist. Masuko et al. (1986) utilized primary brainstem neurons from postnatal mice and rats investigating noradrenergic neurons from the locus coeruleus where they observed processes with varicosities and flattened growth cones after DIV7. They found these neurons survived best

when cultured on a feeder layer of brainstem-derived glia, and these cells precisely resembled cells of the locus coeruleus *in vivo* (Masuko et al., 1986). However, Masuko et al. (1986) did not utilize specific neuronal markers so unequivocal identification of neuronal cells is not possible (Kivell et al., 2000). The culture medium utilized included MEM containing L-glutamine, glucose, $NaHCO_3$, L-ascorbic acid, penicillin, streptomycin, 10% FBS, and 10% heat-inactivated horse serum (Masuko et al., 1986); this composition means 20% of the culture medium was not chemically defined. Ternaux and Portalier (1993) prepared a media formulation most similar to the media incorporated in our initial co-culture protocol (Staal et al., 2007). Ternaux and Portalier (1993) worked with primary brainstem cultures using media containing DMEM/F-12 supplemented with human transferrin, insulin, putrescine, sodium selenite, progesterone, estradiol, D-glucose, L-glutamate, penicillin, streptomycin or gentallin, as well as 3% fetal calf serum (FCS), though some cultures were made without FCS.

In cultures of primary brainstem neurons from postnatal rats, Kivell et al. (2000) used Neurobasal™-A medium containing 2% B27 supplement, 0.25 mM L-glutamine, 0.25 mM GlutaMAX, penicillin G, and streptomycin sulphate. However, neurons in these cultures were reported to be stable for only DIV9 (Kivell et al., 2000).

Monolayer development

The initial modifications of our co-culture protocol stemmed from experiencing live-imaging challenges in co-culture conditions as well as a need for simplification. Before mono-cultures were established, the initial step in simplifying the co-culture protocol

involved testing if a condensed media formulation could supplement the GSM used in the co-culture protocol (**Figures 2C**, **D**).

At this time, GSM was still used as the trituration media, but the feeding media consisted of mNSM. When plating, media used during trituration comprises 5% of the final media volume in each dish. Glia monolayers with mNSM at DIV7 (**Figure 2D**) appeared healthy with active growth cones and though not confirmed with immunocytochemistry visually appeared to have a higher population of neurons at DIV7 than glia cultured with GSM (**Figure 2C**). The cortical growth cone in **Figures 2E** and **F** resembles the 5-HT growth cone seen in **Figure 11C**. We also tested plating neurons on a floating glass coverslip suspended over a glial feeder layer (**Figures 2A**, **B**). Following success using the condensed media formulation, mNSM, in place of GSM, the next stage in simplification used the same glia dishes for co-culture and replaced cNSM with mNSM. cNSM was still used as brainstem neuron trituration media, which makes up 5% of total volume in final cell culture dish (**Figures 2G**, **H**).

As demonstrated in the development of our culture system, the requirements to have healthy cultures of cortical neurons are less strenuous compared to obtaining healthy neuronal cultures that include serotonergic neurons. For example, even when culturing glia for the utilized co-culture methods (Staal et al., 2007), cortical neurons were robust despite the glia-specific media and papain solutions used (**Figures 3A**, **B**).

We assessed substrate preferences using glia monolayers with either laminin substrate (Sigma, CC095-1MG-M) or poly-D-lysine-laminin substrate (Sigma, 127-2.5) on dishes (MatTek, P35GC-1.5-10-C) already precoated by the manufacturer with poly-D-

lysine. (**Figures 3C**, **D**). Results showed minimal variation, though a higher number of neuron-appearing cells were visible in the poly-D-lysine-laminin substrate.

When establishing neuron monolayers, cNSM was initially used during trituration but cNSM was replaced with mNSM *(Pen/Strep concentration can vary from 0.1% – 0.5%)* for feeding. When comparing nonconditioned cNSM (i.e., not glia conditioned) versus mNSM, both result in visually healthy cultures (**Figures 3E**, **F**). Most recently, the neuronal mono-culture protocol was further simplified by replacing cNSM during the trituration stage with mNSM and 1% FBS (**Figures 3G**, **H**).

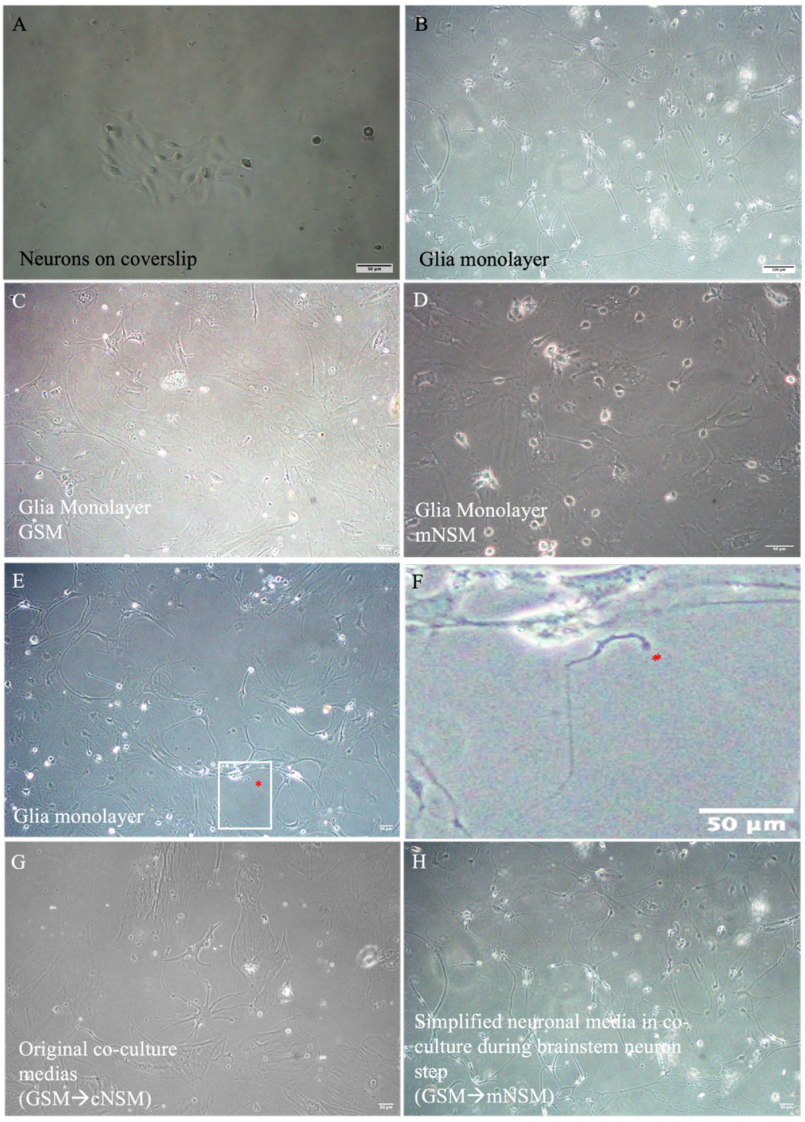

Figure 2 (A, B) Floating coverslip method. **(A)** DIV5 Neurons on coverslip above DIV14 glia monolayer Scale bar = 50 µm. **(B)** DIV14 glia monolayer. Scale bar = 100 µm. **(C)** DIV7 glia monolayer with original GSM. **(D)** DIV7 glia monolayer with mNSM. Scale bar = 50 µm. **(E, F)** DIV9 glia monolayer with mNSM. Red asterisk shows growth cone. Scale bar = 50 µm. Original Co-culture and simplified media co-culture of DIV15 cortical glia and DIV4 brainstem neurons. **(G)** "Classic co-culture". Glia were cultured with glia specific media GSM. At DIV11, primary brainstem neurons were cultured on top of the glia layer in cNSM media that was preconditioned (added to glia cultures at least 24 hours before neurons are added). **(H)** In this co-culture method, glia were cultured with glia specific media GSM. At DIV11, primary brainstem neurons were cultured on top of the glia layer in mNSM that was preconditioned (added to glia cultures at least 24 hours before neurons are added). Scale bar = 50 µm.

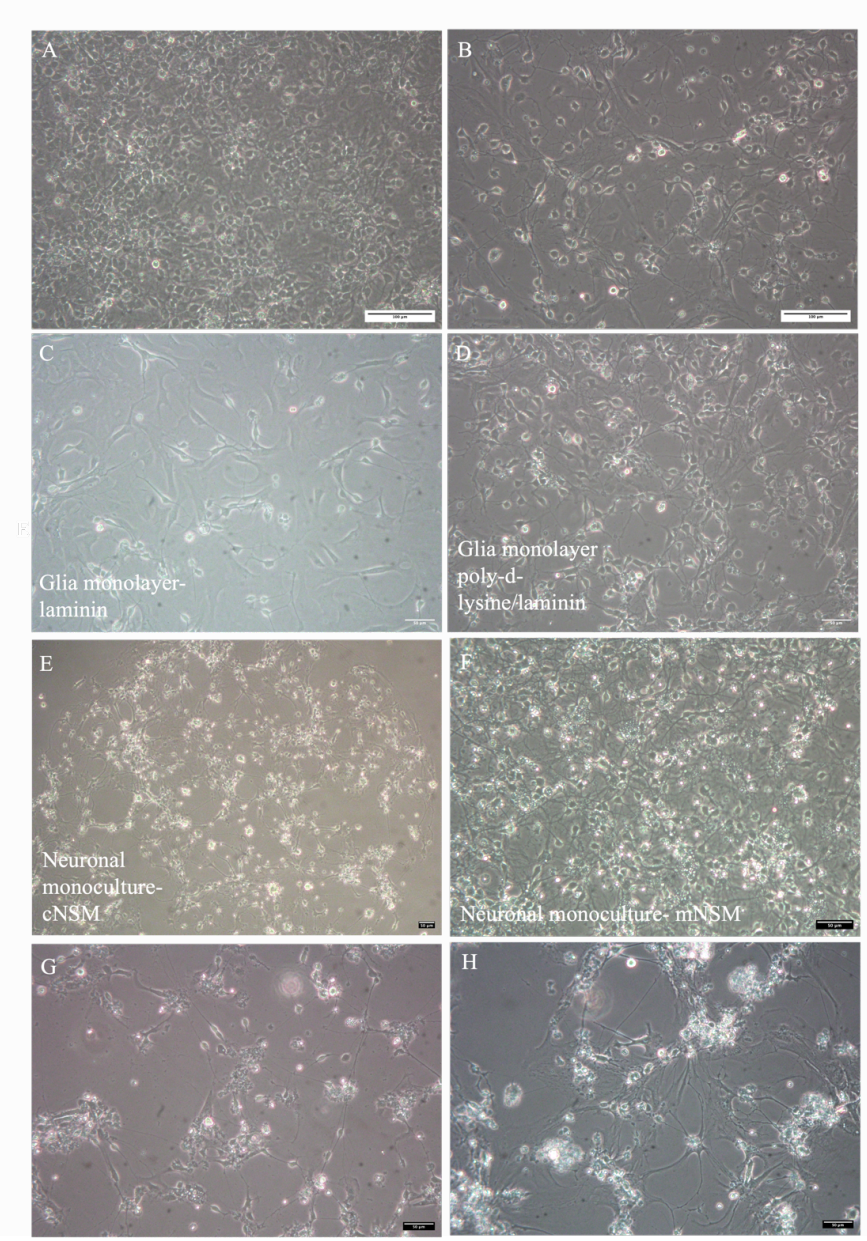

Figure 3 (A, B) Two examples of cortical glia monolayers (DIV3) with high population of neuron-appearing cells. Scale bar = 100 µm. **(B)** DIV2 glia monolayer with laminin substrate (Sigma, CC095-1MG-M). **(C)** DIV2 glia monolayer on poly-D-lysine-laminin substrate (Sigma, 127-2.5). All cell culture dishes (MatTek, P35GC-1.5-10-C) are precoated by manufacturer with poly-D-lysine. Scale bar = 50 µm. **(E)** DIV3 brainstem neurons cultured with cNSM. **(F)** DIV4 brainstem neurons cultured with simplified NB media. Scale bar = 50 µm**. (G, H)** Neuronal monolayers with simplified protocol: replacing cNSM trituration media with simplified mNSM + 1%FBS media. **(G)** DIV2 brainstem neurons. **(H)** DIV6 brainstem neurons. Scale bar = 50 µm.

We also examined our methods for glia population control. FDU (used in our current system) and ara-C are both mitotic inhibitors that prevent the proliferation of non-neuronal cells. When raphe monolayers have been previously attempted, ara-C added at the time of initial plating resulted in poor survival in raphe monolayers, but not in raphe/hippocampal or raphe/spinal cord co-cultures (Azmitia & Whitaker-Azmitia, 1987). Previous raphe primary culture work shows that when grown alone, raphe cells do not survive well after DIV6 (Azmitia & Whitaker-Azmitia, 1987). When FDU was not added to confluent glia monolayers, a visible increase in neuron-appearing cells was observed (**Figures 4A**, **B**).

CultureOne™supplement (ThermoFisher A3320201) is a serum-free supplement designed to improve the differentiation of neural stem cells (NSCs) to neurons. When added at DIV0 (the time of initial cell plating), it can fully suppress both astrocytes and oligodendrocytes with no harmful effects on neurons. We tested the use of CultureOne™supplement per the manufacturer's directions during initial tests to develop primary brainstem cultures sans feeder layer. Rather than use FDU to inhibit proliferation of non-neuronal cells, we used CultureOne™supplement. Results did not yield successful cultures (they were sparse with many cells not differentiated). Due to the urgency to get satisfactory cultures, CultureOne™supplement tests did not continue further.

We additionally tested plating techniques. During cell plating, glass microscope rings (Thomas Scientific, 6705R12) are used to plate dissociated neurons above the glia monolayers/wells to prevent cells from floating away and to encourage neuron adhesion in the well. When developing the neuronal mono-culture protocol, two technical methods were tested. The first, "no ring", resembled the method used for plating glia, where dissociated

cortical cells were added to a well, left in an incubator for 2 hours, rinsed 2x with MEM, and cold fed appropriate media. To minimize disturbance as neurons are more susceptible to environmental turbulence than glia, dissociated brainstem neurons were plated, incubated for 2 hours, and then warm mNSM was slow dripped into the dish (**Figure 4C**). In the "ring" condition, dissociated neurons were added in an identical manner to neuron addition in the co-culture protocol, sans glia feeder layer (**Figure 4D**). Instead, a microscope ring was inserted above a well in a media-filled dish, and dissociated neurons were added in a circular motion, the dish then was incubated for 2 hours, and the glass ring was removed with forceps.

Both methods yielded successful results with more noticeable spherical clusters of cells in the no-ring condition. This could be due to cells needing additional support to adhere to the substrate, thus relying on neighboring cells to act as an additional anchor.

Surface

An alternative method of obtaining surfaces with relatively low stiffness to resemble *in vivo* conditions involves utilizing the geometrical properties of pillars of or other topographical structures made of stiff materials that ultimately affect the effective shear modulus (Sharaf et al., 2022). In addition, the response of cells to smooth surfaces is different than when they are on diverse textures (Liberio et al., 2014; Saltzman, 2000). Rough surfaces are advantageous for cell attachment (Deligianni et al., 2001). This advantage is utilized in the development of osteoimplants (Deligianni et al., 2001; Liberio et al., 2014; Palin et al., 2005; Strauss et al., 2013).

A frequent observation found in our primary brainstem cultures was that neurons tended to adhere near the vertical edge of the wells. This could be due to the meeting of two surfaces (the vertical edge between the plastic dish and the glass coverslip), enhancing adhesion. To present a mechanically rough surface, we cultured neurons on laminin-coated dishes that were scratched with fine point forceps prior to cell plating.

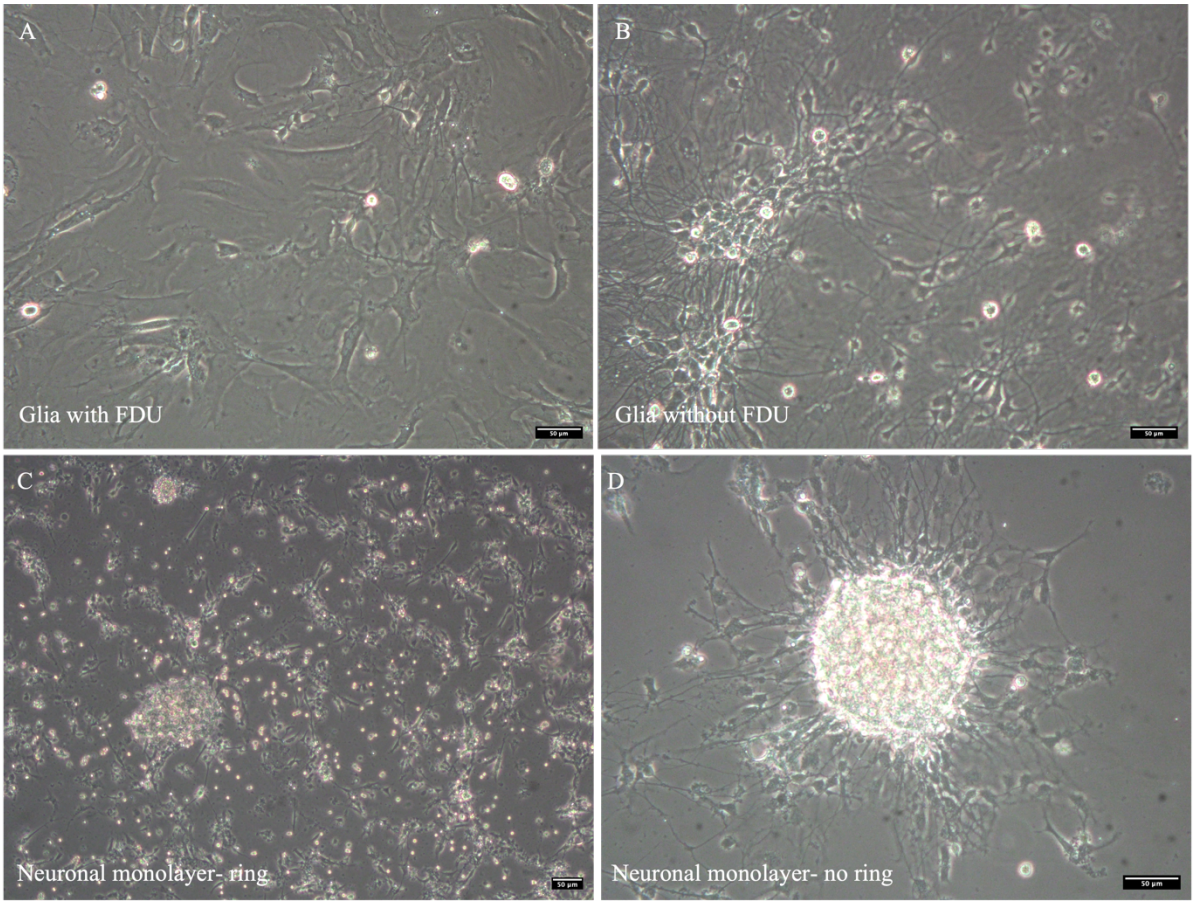

Figure 4 (A) DIV5 Glia monolayer with FDU addition at 70% confluency (~DIV3). **(B)** DIV5 Glia monolayer *without* FDU addition. **(C)** DIV1 brainstem neurons plated sans microscope ring (Thomas Scientific, 6705R12). **(D)** DIV1 brainstem neurons plated with ring. Scale bar = 50 µm.

E. Validating the system

Morphology

5-HT cell bodies found in our simplified monolayer method display the large cell body and cell-shape variety (i.e., fusiform, triangular, etc.) previously described in the literature (Baker et al., 1990; Michelsen et al., 2008; Michelsen et al., 2007; Rodríguez et al., 2012; Steinbusch et al., 1981) (**Figures 5A-C**). Recent studies have demonstrated that at birth, 5-HT fibers present thick and dot-shaped enlargements with few and often barely detectable connections (Damato et al., 1987; Maddaloni et al., 2017). Successively, thin connecting segments were detectable and fibers gradually became smoother and more uniform along their length up to PND 28, and additional intrinsic rearrangements resulted in the acquisition of the morphology observed in the adult (Maddaloni et al., 2017). Similarly, our brainstem monolayers display 5-HT axonal morphologies with both thin segmented fibers and smooth and uniform fibers visible (**Figure 5D**, **E**).

In addition, our primary brainstem cultures show varicosities, as are expected in 5-HT axons (**Figures 5F**, **G**). Further validation of the physiological relevance of our primary brainstem culture system is demonstrated by the extensive branching of 5-HT axons (**Figure 5H**). 5-HT neurons have been reported to produce a considerable number of axonal branches, which are widely distributed in the DR (recurrent axons), periaqueductal gray and reticular formation (Adell et al., 2002; Li et al., 2001). The plasticity (e.g., their ability to grow and regress) of these neurites is believed to be the biological basis for cognitive functions such as learning and memory (Azmitia, 2001).

The first cultured serotonergic neurons were midbrain raphe explants from newborn rats, where they survived until DIV16 (Halgren & Varon, 1972). Since this initial study, dissociated raphe cells have been reported to survive in culture until DIV21 and by DIV3-5, display many fiber bundles (Azmitia & Whitaker-Azmitia, 1987). Similarly, we have dissociated raphe cells viable in culture to DIV31 and beyond (**Figures 24I**, **J**) Prior literature has showed that varicosities can be seen as early as DIV1 and become numerous after DIV5 (Azmitia & Whitaker-Azmitia, 1987). 5-HT-immunoreactive cells show fine wispy processes covering the soma and dendrites at DIV1, with extensive dendritic branching evident by DIV3-5 (Azmitia & Whitaker-Azmitia, 1987). 5-HT growth cones are immunoreactive in culture as early as 18h after plating, with growth cones appearing bulbous with numerous filopodia (Azmitia & Whitaker-Azmitia, 1987). Single 5-HT cells were reported to have more than one growth cone, with these processes extending over collagen and poly-D-lysine substrates and *encircling* non-stained cells in their path (Azmitia & Whitaker-Azmitia, 1987). Such observations of multiple growth cones are consistent with our own observations (**Figure 5I**).

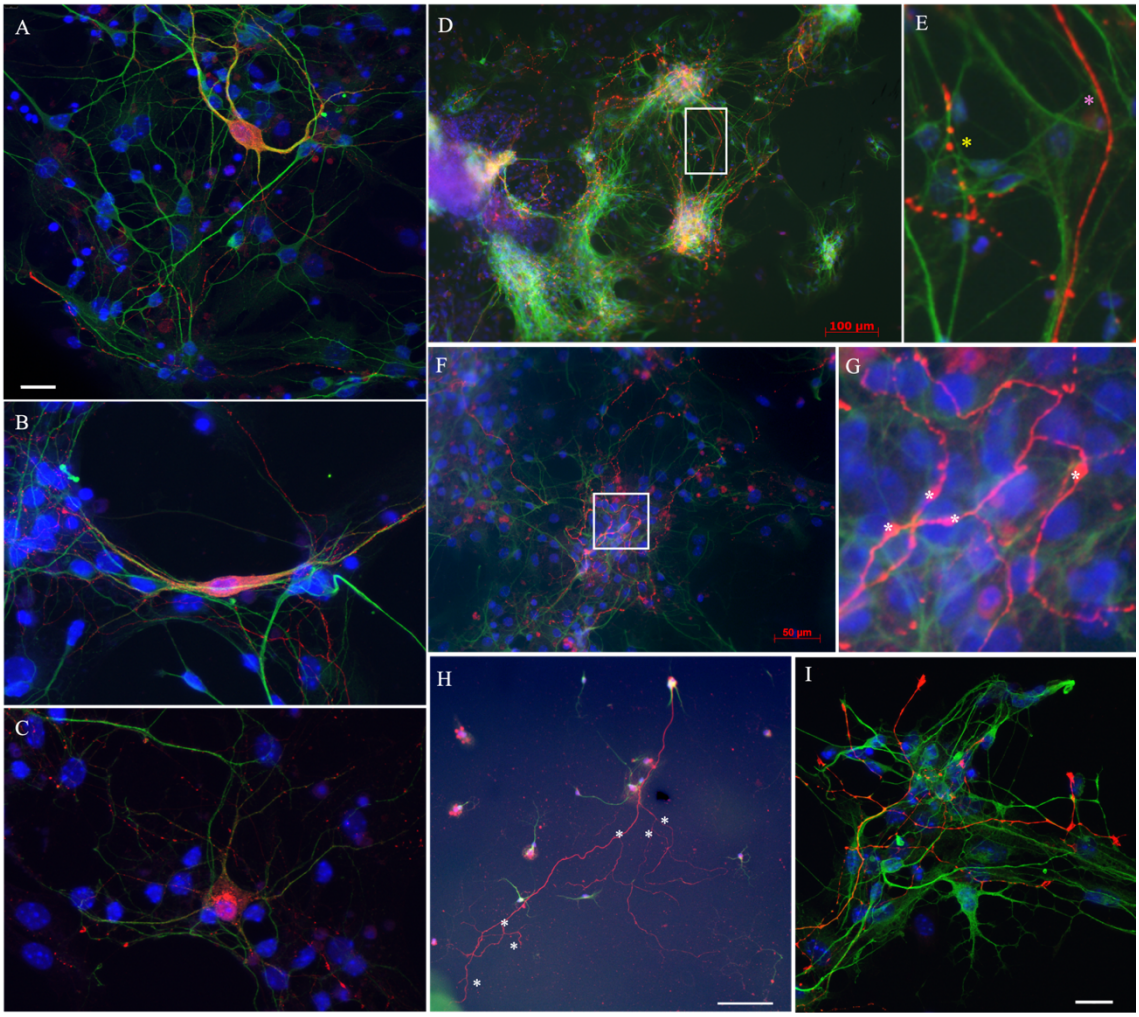

Figure 5 Serotonergic cell bodies found in our *in vitro* model at DIV4 display expected large size and various morphologies. **(A)**, **(B)** display fusiform cell bodies. **(C)** represents a polygonal cell body. (5-HT red; MAP2 green; DAPI blue) DAPI. Scale bar for **(A-C)** = 20 µm. **(D, E)** 5-HT (red) fibers presenting both dot-shaped enlargements (yellow asterisk) and smooth and more uniform fibers (pink asterisk) in our DIV3 brainstem neuronal cultures. (MAP2 green; DAPI blue). Scale bar = 100 µm. **(F**, **G)** 5-HT (red) varicosities (denoted with white asterisks) in DIV5 cultures of primary brainstem neurons. (MAP2 green; DAPI blue). Scale bar = 50µm. **(H)** A 5-HT (red) fiber has several branching points (white asterisks) in DIV5 cultures of primary brainstem neurons. (MAP2-green; DAPI-blue). Scale bar = 100 µm. **(I)** Multiple 5-HT + (red) growth cones in DIV5 cultures of primary brainstem neurons. (MAP2-green; DAPI-blue). Scale bar = 20 µm.

F. Identifying 5-HT neurons in vitro

Cell-specific markers in culture

There is extensive variation in morphogenesis of identified transmitter systems in culture. For example, aggregate cultures of dopaminergic neurons after DIV4 (Levitt et al., 1976) and explant cultures of locus coeruleus neurons after DIV8-14 contain glyoxylic acid-induced fluorescent cells with fine fibers (Dreyfus et al., 1979; Schlumpf et al., 1977) whereas dissociated mesencephalic cultures do not have fluorescent cell bodies or axonal varicosities for up to 3 weeks in culture (Azmitia & Whitaker-Azmitia, 1987; Prochiantz et al., 1979). Consistent with variations in *in vivo* temporal patterns in the developing rodent brain (Lidov & Molliver, 1982; Olson & Seiger, 1972), serotonergic neurons cultured *in vitro* have been reported to mature at a more advanced rate than catecholinergic neurons (Azmitia & Whitaker-Azmitia, 1987). We observed 5-HT immunoreactivity by DIV2**.**

Several methods can be used to identify living serotonergic neurons in culture (Jacobs & Azmitia, 1992). Serotonergic neurons and their processes have distinct morphological features such as varicosities (dilated axon portions) of a certain shape and size, as well as fine, "wispy" processes that may emerge from the cell body and neurites (Azmitia & Whitaker-Azmitia, 1987; Benzekhroufa et al., 2009). Serotonergic dendrites have been observed to be spiny compared to non-5-HT neurons of the DR *in vitro* (Li et al., 2001). Without other cell-specific identifiers, morphology is not a reliable parameter.

Mouse transgenic models are also available in which fluorophores are expressed under a serotonin-specific promoter. Our laboratory has used an inducible Cre/loxP estrogen receptor (ER) transgenic mouse line in which Cre-recombinase is expressed under the

promoter of the Tph2 gene. This line (JAX: Tg (Tph2-icre/ERT2)6Gloss/J) can be crossed with a Cre-reporter line (e.g., JAX: B6.129(Cg)-Gt (ROSA)26Sor$^{tm4(ACTB-tdTomato,-EGFP)Luo}$/J) to produce offspring in which serotonergic neurons carry a fluorescent tag. Work with this line was halted due to colony complications but preliminary viability testing with 4-hydroxytamoxifen (4-OHT) indicated that it did not affect cell viability.

Our laboratory is currently testing Tph2-ChR2-YFP BAC transgenic mice (JAX: B6; SJL-Tg (Tph2-COP4*H134R/EYFP)5Gfng/J (Stock# 014555). This line consistently expresses EYFP under the promoter of the Tph2 gene and allows for easy identification of 5-HT neurons.

A highly efficient approach has recently been introduced which is based on fluorescent false neurotransmitters (FFNs) (Henke et al., 2018). Serotonin transporter (SERT)-specific, non-cytotoxic FFNs (e.g., FFN246) can be taken up by serotonergic neurons as “false serotonin” and reveal the identity of these cells (Henke et al., 2018). We obtained FFNs from the Sames lab (Columbia University) and performed initial tests to determine if FFN246 can identify serotonergic neurons in brainstem monolayer cultures using holotomography (**Figure 6**).

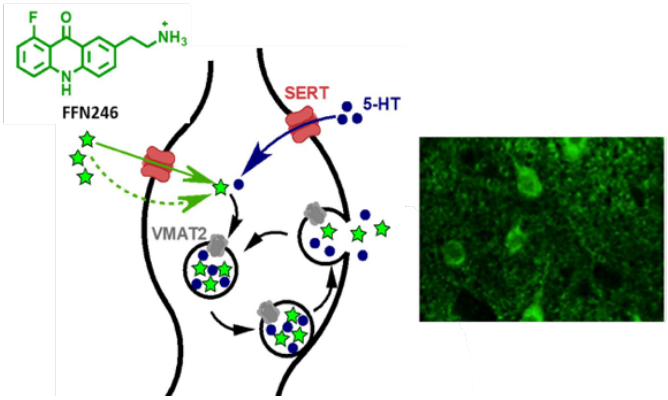

Figure 6 FFN246 can be taken up by SERT and the vesicular monoamine transporter (VMAT), allowing visualizing of live serotonergic cells (From Henke et al., 2018).

FFN methods

Brainstem monolayers were prepared in an identical manner as previously described for the 2D mono-culture system (Chapter 3, section C). The initial test with FFN246 involved adding 20 µM, 40 µM, or 80 µM of FFN246 to DIV5 primary midbrain cultures and examining for signaling with the Olympus CKX-41, inverted microscope. FFN246 was added to the cell culture dishes at the recommended concentration *(*20 µM) and left in the incubator (5% CO_2 at 37°C) for 30 minutes prior to HTM recording. The detection of FFN246 with HTM was evaluated following immunocytochemistry for 5-HT and MAP2 which revealed extensive axonal networks.

FFN findings

Due to the specific excitation emission wavelength required for FFN246 visualization (excitation/emission (nm): 392/427), we used confocal microscopy to image a

dish with and FFN concentration of 40 μM. Transporting the cell culture dishes from their place of incubation to the confocal microscope in a different building introduced sudden stress and mechanical disruption to the living cells due to the distance between these two locations. All concentrations used in the initial FFN were then tested in the cell culture incubation room with the Olympus CKX-41 inverted microscope, using a suboptimal filter, which indicated slight fluorescence. FFN246 also was tested in HTM, where slight axonal fluorescence was observed. (**Figures 7A-D**). In addition, an axon with an active growth cone was visible (**Figures 7E**, **F**).

To validate these observations of FFN246 with HTM, we performed immunocytochemistry following the HTM recording where the FFN246+ dish revealed extensive axonal networks (**Figure 9A**). Ultimately, only cultures of exceptionally high density (lightly triturated and minimally dissociated) revealed slight FFN positivity.

In summary, we performed the first test of FFN246 (Henke et al., 2018) compatibility with primary brainstem neurons and holotomography. In initial tests by the developing research groups (Sames Lab & Sulzer Lab), FFN246 has successfully labeled 5-HT neurons in DR mouse brain slices but was not previously found to significantly label axonal projections (Henke et al., 2018). Our results indicate that FFN246 can be somewhat effective in the identification of 5-HT axons, but further work is required to achieve optimal imaging conditions. In the future, FFN246 can help to identify 5-HT neurons and axons in wild-type mouse preparations as well in cultures obtained from other species (including iPSC-derived human 5-HT neurons). Further tests with FFN246 could include longer pre-

imaging incubation periods, as well as re-examination of higher concentrations (i.e., 40 µM and 80 µM).

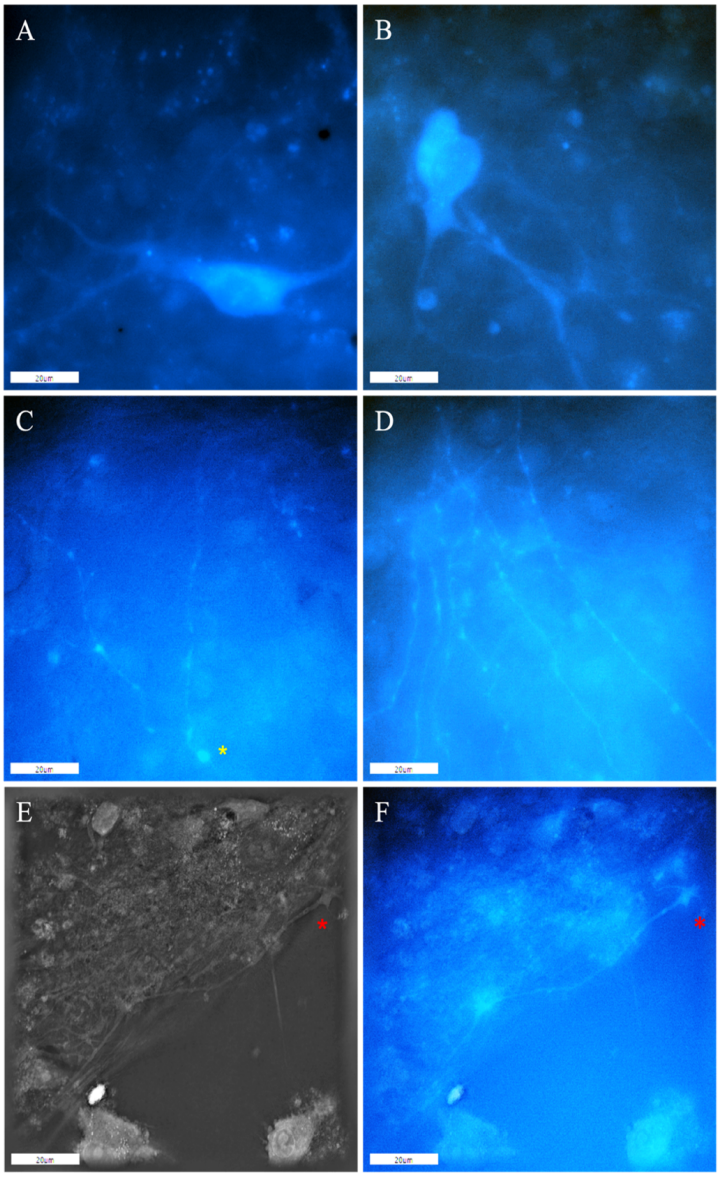

Figure 7 FFN246 positive cell bodies **(A**, **B)** and axons **(C, D)** imaged with the Nanolive 3D Cell Explorer. **(C)** Yellow asterisk marks possible 5-HT axonal varicosity before axon fork. **(E, F)** Still shots of primary brainstem neurons using the Nanolive 3D Cell Explorer. **(E)** Standard HTM image view of an axon and growth cone (denoted by red asterisk) moving along the edge of other cells. **(F)** Fluorescent view of FFN246 (excitation and emission spectra 392/427 nm) positive axon with growth cone, imaged using Nanolive's DAPI channel. Scale bar = 20 µm.

V. Chapter 4: Properties of single 5-HT axons

All methods were identical to those described in Chapter 2 and Chapter 3.

A. Co-culture axon dynamics

The original co-culture model yielded healthy brainstem cultures with 5-HT neurons (**Figures 8A-B**) of various morphologies such as triangular (**Figure 8A**) and fusiform (**Figure 8B**). 5-HT axons tended to adhere to astrocytes (**Figures 8C-F**). Live imaging of an axon with widths of ~1 μm on top of another cell is challenging and makes discerning segments of separate but overlapping axons unmanageable in unlabeled cells. In addition, live imaging revealed that when an axon attached to an astrocyte, considerable glia movement added strong tension forces to delicate axons that had part of its axon adhered to the motile glia, and another portion of its axon adhered to a different substrate (i.e., occasionally another astrocyte). Relatedly, immunocytochemistry often revealed that isolated and broken 5-HT+ axon fragments could be found scattered around a cell culture dish, often times a notable distance from a 5-HT+ cell body. Also, immunocytochemistry often revealed that 5-HT+ axons that were no longer adhered to astrocyte surfaces and were often broken and fragmented, a notable distance from 5-HT+ neuron bodies.

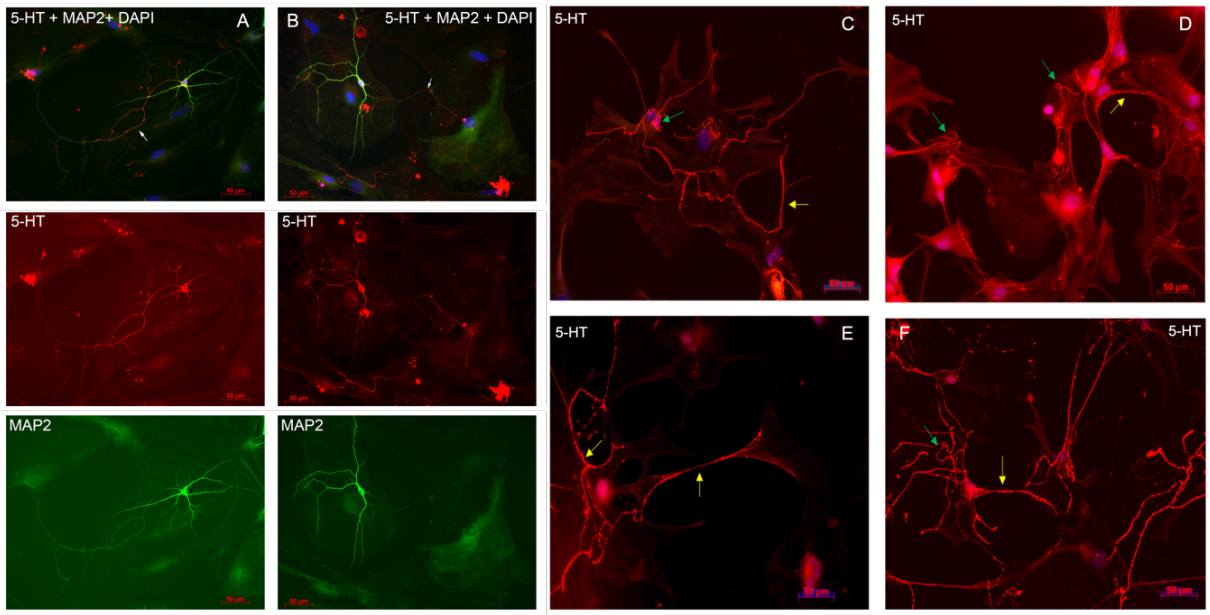

Figure 8 Original co-culture method using cortical glial cells from P-0.5-P3 Sprague Dawley rats and brainstem tissue from P0.5-P2 C57BL/6 mice. **(A**, **B)** Serotonergic somata and dendrites (MAP2 green; DAPI blue) and serotonergic axons (5HT, red). **(C-F)** Serotonergic fibers (red) produce stochastic-like trajectories on the surface of astrocytes. These paths are characterized by a high degree of tortuosity (twists and turns; green arrows). In contrast, fibers move with extreme precision near the edges of astrocytes, adhering to their membranes (yellow arrows). Scale bar = 50µm.

B. Monolayer

Midbrain serotonergic neurons grown in primary cultures were strongly immunoreactive for 5-HT and had normal morphology (**Figure 9**). Their somata were round (typically, around 20 µm in diameter) or fusiform (extending up to 50 µm in length) and immunoreactive for MAP2. They typically had long, 5-HT-immunoreactive axons distinguished from other neurites (*e.g.*, dendrites) by the characteristic varicosity-like profiles and the absence of MAP2-immunoreactivity. Serotonergic neurons appeared normal at various plating densities. Many axons were observed extending from a cluster of raphe

neurons that had not been fully dissociated (**Figure 9A**), as well as from sparsely distributed single neurons (**Figures 9B-C**).

C. 5HT adhesion/close contact with MAP2+ neurites

High-resolution confocal imaging revealed that many serotonergic axons were in contact with MAP2-positive neurites (*e.g.*, putative dendrites) of non-serotonergic neurons (**Figure 10**). Some serotonergic axons appeared to wind around these neurites (**Figure 10A**) and some simply advanced along them in the same imaging plane (**Figure 10B**). These neurite contacts appeared to be functionally important for axon extension, as was evidenced by instances in which one axon branch remained on the neurite but the other lost its contact (**Figure 10C**). In some cases, the detached branch increased its caliber dramatically (at least two-fold), likely due to its multiple active (growth cone-like) zones in the terminal segment. The appearance of these branches in fixed preparations suggested that they were attempting to find the next attachment point (**Figure 10C**). Serotonergic axons were also found sliding along other serotonergic axons, with no apparent repulsion, but these instances were considerably less frequent (**Figure 10E**).

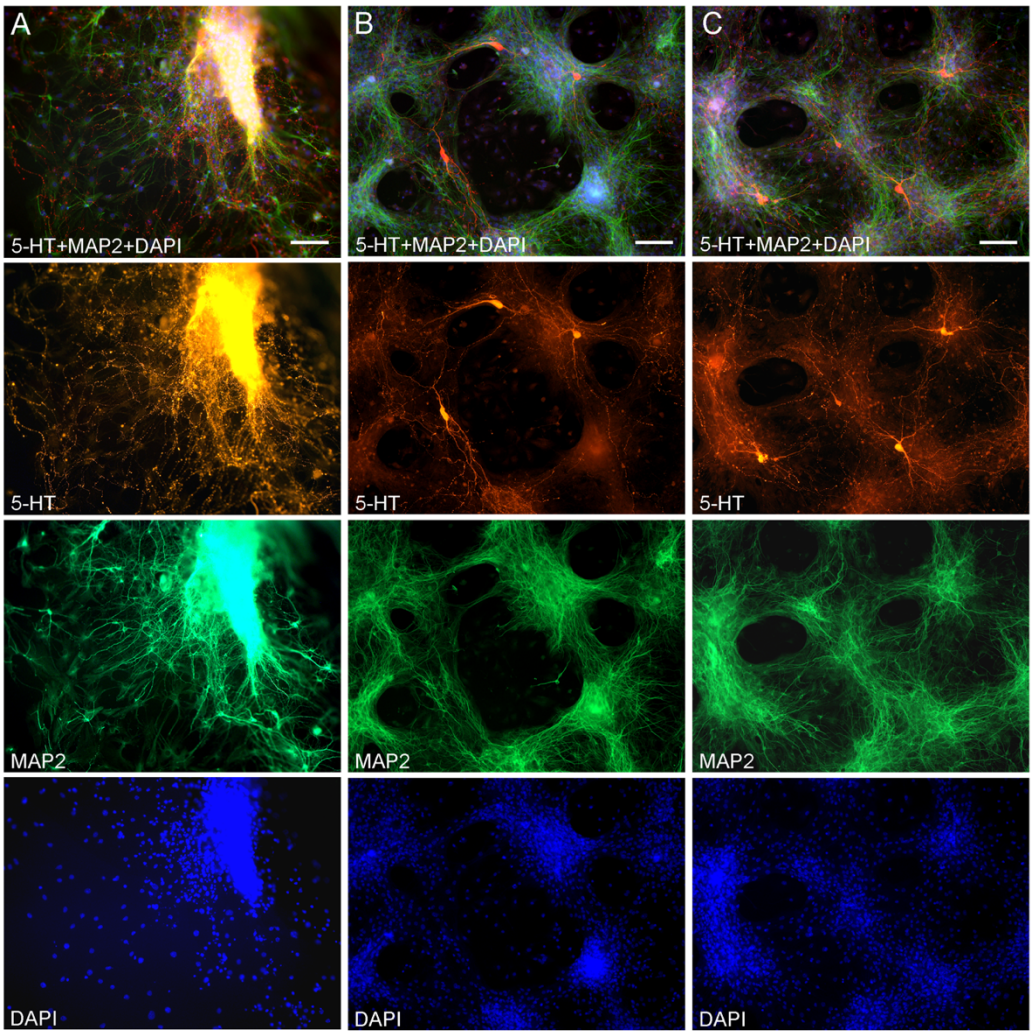

Figure 9 Primary midbrain cultures (all monolayers at DIV5), visualized with immunocytochemistry for 5-HT (red) and MAP2 (green) and imaged with epifluorescence microscopy. Cell nuclei are stained blue (DAPI). **(A)** A tissue piece from the midbrain raphe region, the cells of which have not been fully dissociated. Long serotonergic axons with varicosities emerge from the tissue, suggesting that the culture protocol can also be used in organotypic preparations. **(B** and **C)** Typical dissociated serotonergic neurons, with morphological features (round or fusiform somata) and neurites virtually indistinguishable from those in intact neural tissue. Scale bar =100 µm. (From Hingorani et al., 2022).

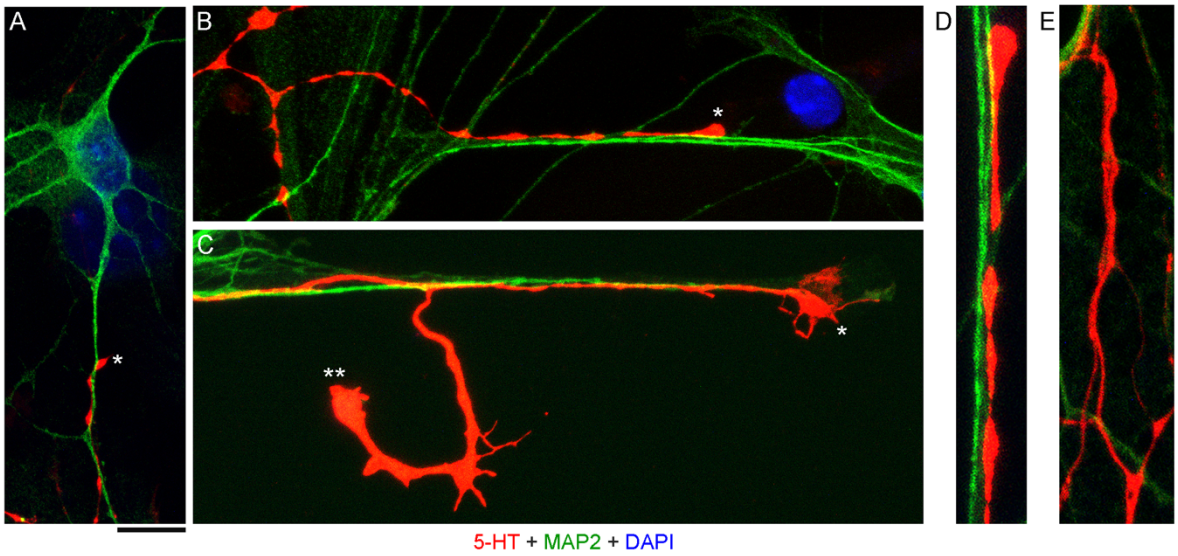

Figure 10 Primary midbrain cultures, visualized with immunocytochemistry for 5-HT (red) and MAP2 (green) and imaged with high-resolution confocal microscopy. Cell nuclei are stained blue (DAPI). **(A)** A serotonergic axon (5-HT+/MAP2-, asterisk) that advances along a dendrite of a non-serotonergic neuron (5-HT-/MAP2+). **(B)** Another serotonergic axon (5-HT+/MAP2-, asterisk) that advances along a 5-HT-/MAP2+ neurite. **(C)** A serotonergic axon (5-HT+/MAP-, asterisk) that advances to the end of a 5-HT/MAP2+ neurite and produces a branch that has lost contact with the neurite (double asterisk). Note the much larger caliber of the branch, as well as multiple growth cone-like zones, perhaps in search of the next attachment point. **(D)** A typical contact between a serotonergic axon (5-HT+/MAP2-) and a 5-HT-/MAP2+ neurite (an enlarged part of **B**). **(E)** Contacts between two serotonergic axons (5-HT+/MAP2-) are less frequent but also occur, with no apparent repulsion between the axons. **A**, **B**, **D**, and **E**: monolayers at DIV4; **C**: neuron-glia co-culture at DIV3. Scale bar (shared by all panels) = 10 µm in **A**, **B** and **C**; 5 µm in D and **E**. (From Hingorani et al., 2022).

To investigate the nature of contacts between serotonergic axons and MAP-positive neurites, we examined axons that were advancing along a neurite but were not in close apposition to it (**Figure 11A**). It revealed discrete adhesion structures, composed of a strongly 5-HT-postive “foot” (directly in contact with the neurite) and an extremely thin

(nanoscale) membrane tether anchoring it to the main axon (**Figures 11B-C**). These structures were located close to the growth cone but outside its active zone. Putative adhesion sites were also detected on neurites where the axon was no longer present. In some instances, these sites were strongly elongated (**Figure 11D**), suggesting that the contacting axon membrane was flattened, perhaps to reflect the width of the neurite.

The presence of 5-HT-positive adhesion sites raises the question of whether they can be mistaken for varicosities in brain tissue. Image analysis suggests subtle transitions between actual axon varicosities (connected with continuous cell membrane) and residual adhesion sites (with no membrane continuity), which may be difficult to tell apart in fixed tissue visualized with immunohistochemistry (**Figure 12**). This situation is further complicated by the observation that serotonergic axons themselves can have segments with no detectable 5-HT-immunoreactivity, interspersed among segments with strong 5-HT-immunoreactivity (**Figure 12A**). This phenomenon may be due to sharply delineated accumulation of 5-HT in specific segments (with no change in the fiber caliber) or to an extremely small caliber of the interconnecting segments (which physically cannot contain many 5-HT molecules).

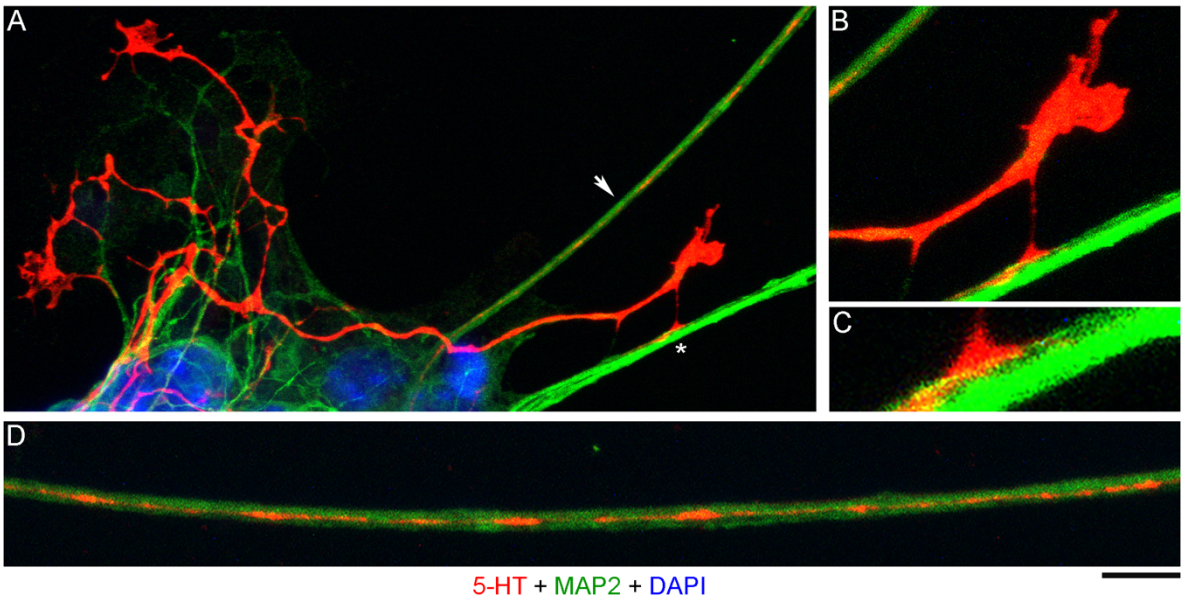

Figure 11 A primary midbrain culture (neuron-glia co-culture at DIV3, visualized with immunocytochemistry for 5-HT (red) and MAP2 (green) and imaged with high-resolution confocal microscopy. Cell nuclei are stained blue (DAPI). **(A)** A serotonergic axon (5-HT+/MAP2) that advances along a 5-HT-/MAP2+ neurite and reveals its adhesion sites (one site is marked with an asterisk). **(B)** An enlarged view of the growth cone region in **A**. **(C)** A further enlarged view of the adhesion site marked with an asterisk in A. **(D)** Relatively regularly spaced putative adhesion sites (5-HT+/MAP2-) on a 5-HT-/MAP2+ neurite (an enlarged part of **A**, arrow). Scale bar (shared by all panels) = 10 µm in **A**; 5 µm in B and D; 2 µm in **C**. (From Hingorani et al., 2022).

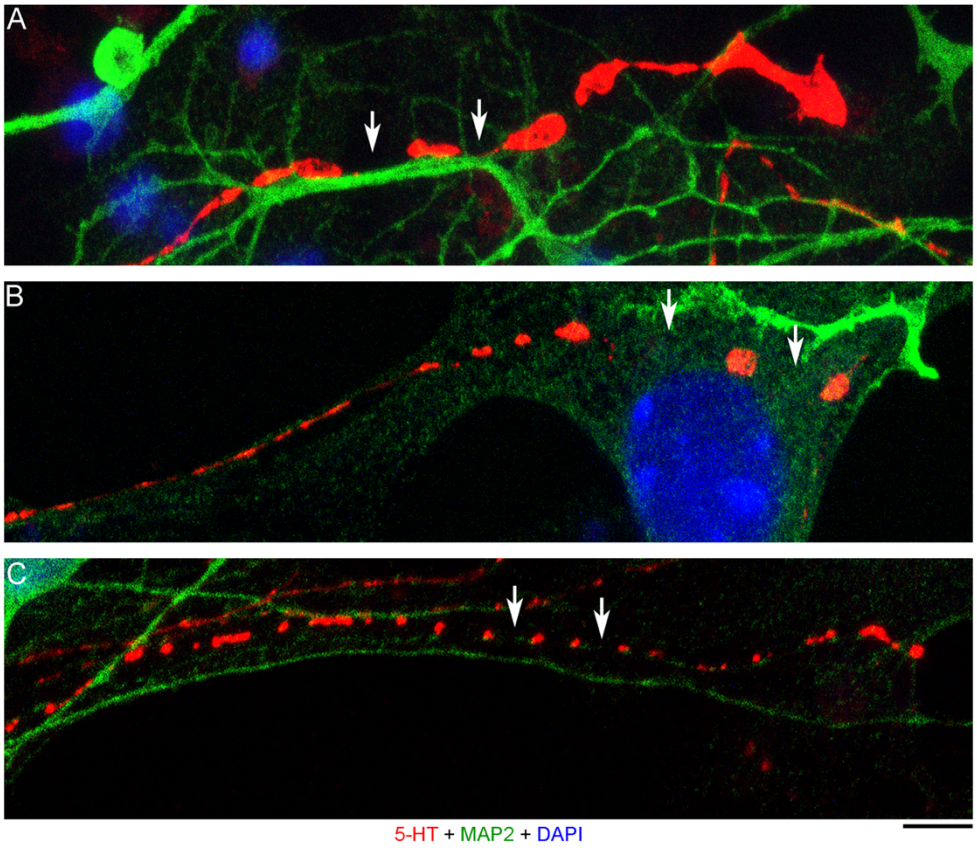

Figure 12 Primary midbrain cultures (all monolayers at DIV4), visualized with immunocytochemistry for 5-HT (red) and MAP2 (green) and imaged with high-resolution confocal microscopy. **(A)** The growth-cone region of a serotonergic axon (5-HT+/MAP2-) that shows wide gaps in 5-HT-immunoreactivity (arrows). These gaps may be due to nanoscale-caliber bridges between intensely labeled segments or actual interruptions in fiber continuity. The presence of normal-caliber segments virtually devoid of 5-HT also cannot be ruled out. **(B)** A serotonergic axon or a series of its adhesion sites (5-HT+/MAP2-) that transitions from a thin, nearly continuous trace to a much thicker trace with large gaps (arrows) between circular 5-HT+ regions. **(C)** A serotonergic axon or a series of its adhesion sites (5-HT+/MAP2-) that shows circular 5-HT+ regions (around 1 µm in diameter) spaced at around 4 µm (arrows). Scale bar (shared by all panels) = 5 µm. (From Hingorani et al., 2022).

To distinguish between these possibilities, we immunostained cultures for 5-HT and axon markers (Tau-1 or neurofilaments) (**Figure 13**). No detectable immunoreactivity for the two axon markers was found in neurites with strongly alternating 5-HT-positive and 5-

HT-negative segments, thus not allowing direct comparison of the signals. However, similar patterns of Tau-1-immunoreactivity were present in other (non-serotonergic) neurites (**Figure 13A**), suggesting that the absence of 5-HT-immunoreactivity in some fiber segments was likely caused by an actual variability of the axon diameter. It is further supported by the observation that 5-HT tends to accumulate in well-defined puncta (with the *apparent* diameter of around 300 nm in confocal imaging) and that segments with no puncta remain identifiable in neurites with a constant caliber (**Figure 13A**). In contrast, a gradual transition to extremely thin segments (that can no longer accommodate a single 5-HT-positive punctum) was observed in some growing serotonergic axons (**Figure 13B**). This inference is consistent with studies in which serotonergic axons have been visualized with green fluorescent protein (GFP or EGFP), as opposed to 5-HT (Benzekhroufa et al., 2009; Maddaloni et al., 2017).

It is possible that some distal axon segments can become detached from the main axon, due to the highly dynamic active zones extending beyond the growth cone (*e.g.*, **Figure 10C**). Since these zones can be accompanied by rapid fluctuations of the axon diameter, distal segments may become disconnected in stochastic events. Such terminal "shedding" would not be detrimental to neural tissue because serotonergic axons exhibit robust growth and naturally regenerate, even in the adult mammalian brain (Jin et al., 2016).

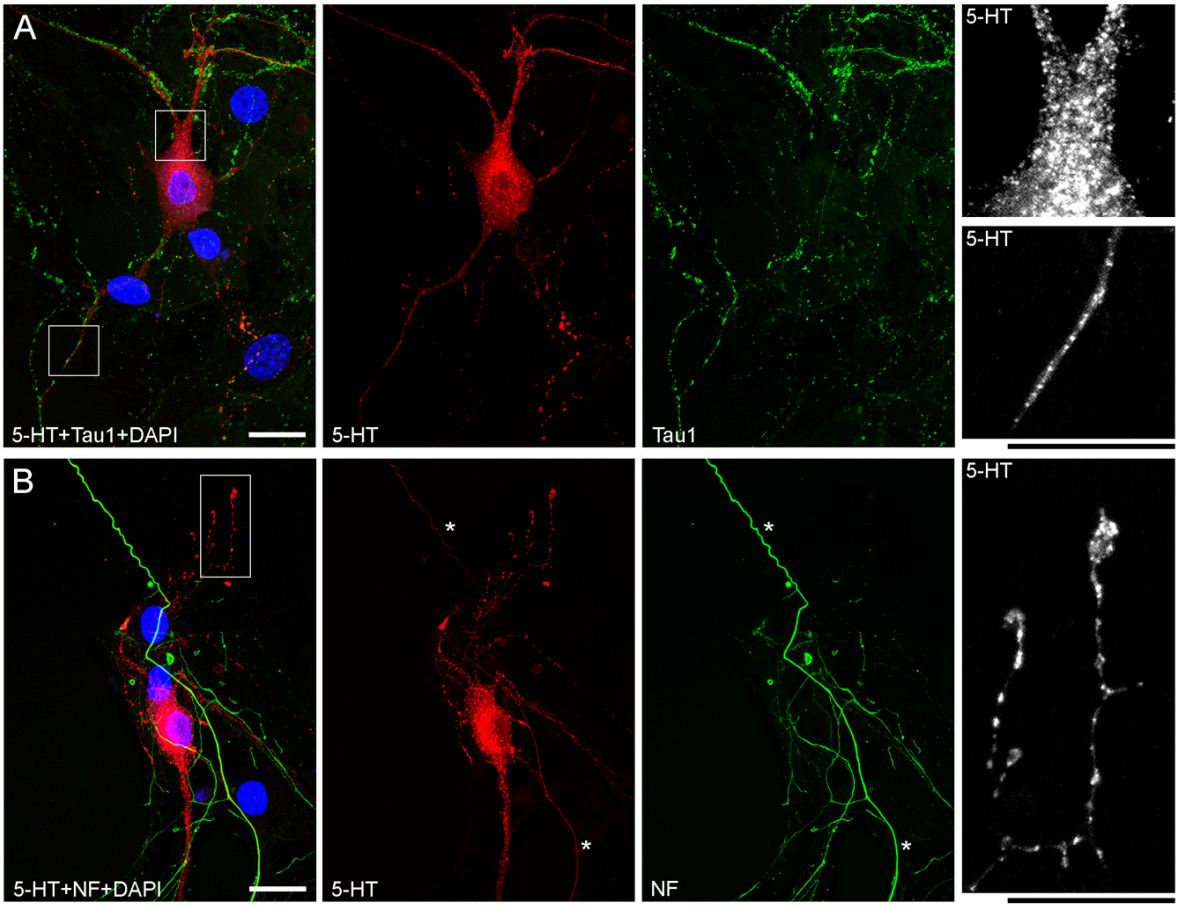

Figure 13 Primary midbrain cultures (both monolayers at DIV13, visualized with immunocytochemistry for 5-HT (red) and either Tau-1 or neurofilaments (green) and imaged with high-resolution confocal microscopy. **(A)** There is no overlap between the 5-HT and Tau-1 signals, but both serotonergic (5-HT+/Tau-1-) and non-serotonergic (5-HT-/Tau-1+) axons have segments with alternating signal intensities. It suggests that in serotonergic axons this property cannot be explained solely by 5-HT accumulation. In serotonergic neurons, the 5-HT signal tends to accumulate in puncta, but segments with no puncta are still detectable in neurites with a constant caliber (insets, with the corresponding regions marked with the rectangles in the merged image). **(B)** Generally, there is no overlap between the 5-HT and neurofilament signals (NF), but some strongly NF-positive and weakly 5-HT-positive axons with continuous 5-HT-immunoreactivity are present (asterisks). In some serotonergic axons with growth cones, gradually narrowing axon segments are clearly visible (inset, with the corresponding region marked with the rectangle in the merged image). Scale bars = 20 µm. (From Hingorani et al., 2022).

D. Axon walks

To understand the dynamics of these processes, midbrain cultures were examined with time-lapse 3D-holotomography (label-free, refractive index-based imaging). Highly dynamic, discrete contact events between growth-cone protrusions and neurites were recorded (**Figure 14**). Some of these contacts may eventually become adhesion sites (**Figure 15)**. As the axon continues to advance along the surface, its spatial position retains a considerable degree of flexibility. The axon can stay closely adhered to the surface (*e.g.*, **Figure 10B**) but it can also be displaced away from the surface, while still anchored to it by thin membrane tethers (*e.g.*, **Figure 11B**). Live imaging suggests that these tethers can extend by around 10 μm (the diameter of a small neuron) in around 10 minutes, with the attachment points firmly fixed (**Figure 15**). Such physical flexibility is important to accommodate unavoidable lateral shifts of the axon, as its leading end clambers from neurite to neurite (**Figure 16**). Perhaps in response to tension forces, axon segments can become flat and assume a corkscrew-like configuration, even far away from the growth cone and naturally flat lamellipodia (**Figure 15 inset**).

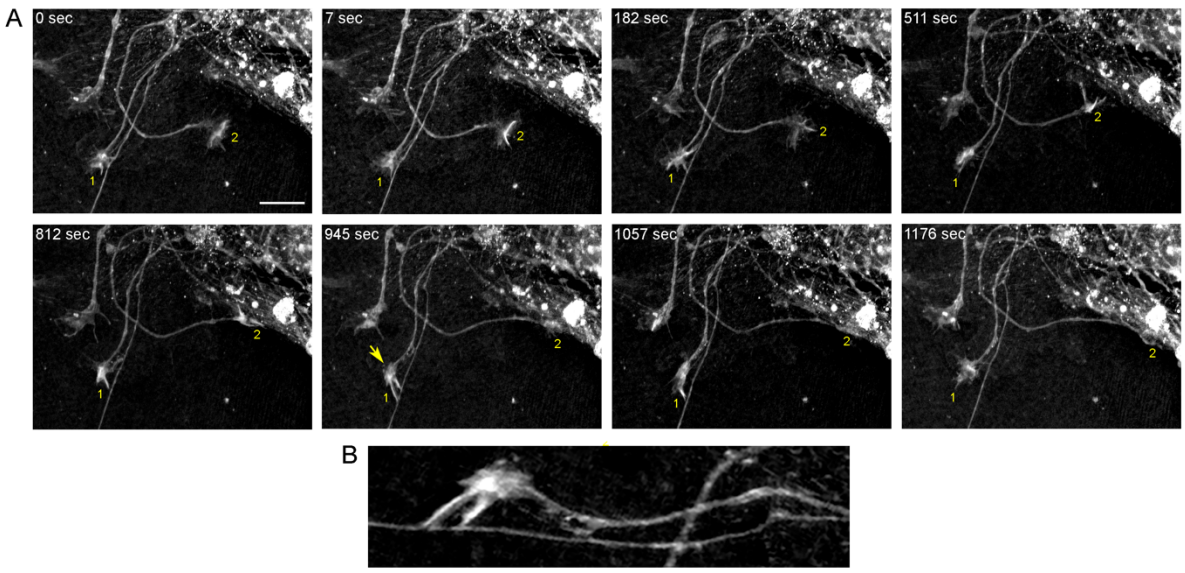

Figure 14 The dynamics of two growth cones (GC; labeled 1 and 2) in a primary midbrain culture (monolayer at DIV5), visualized with time-lapse holotomography. **(A)** GC 1 attempts to move along a neurite by producing protrusions that come in contact with the neurite at well-defined points (arrow, enlarged in **B**). The distance between adjacent points is similar to that between the discrete 5-HT+ regions in **Figure 4**. GC 2 detects a substrate (around t = 511 sec) and rapidly advances along its edge. To emphasize key transitions, time points are not evenly spaced. This imaging supports the interpretation of the dynamics that may underly the confocal microscopy data, but the recorded axons are not labeled and may not be serotonergic. Scale bar = 10 µm. (From Hingorani et al., 2022).

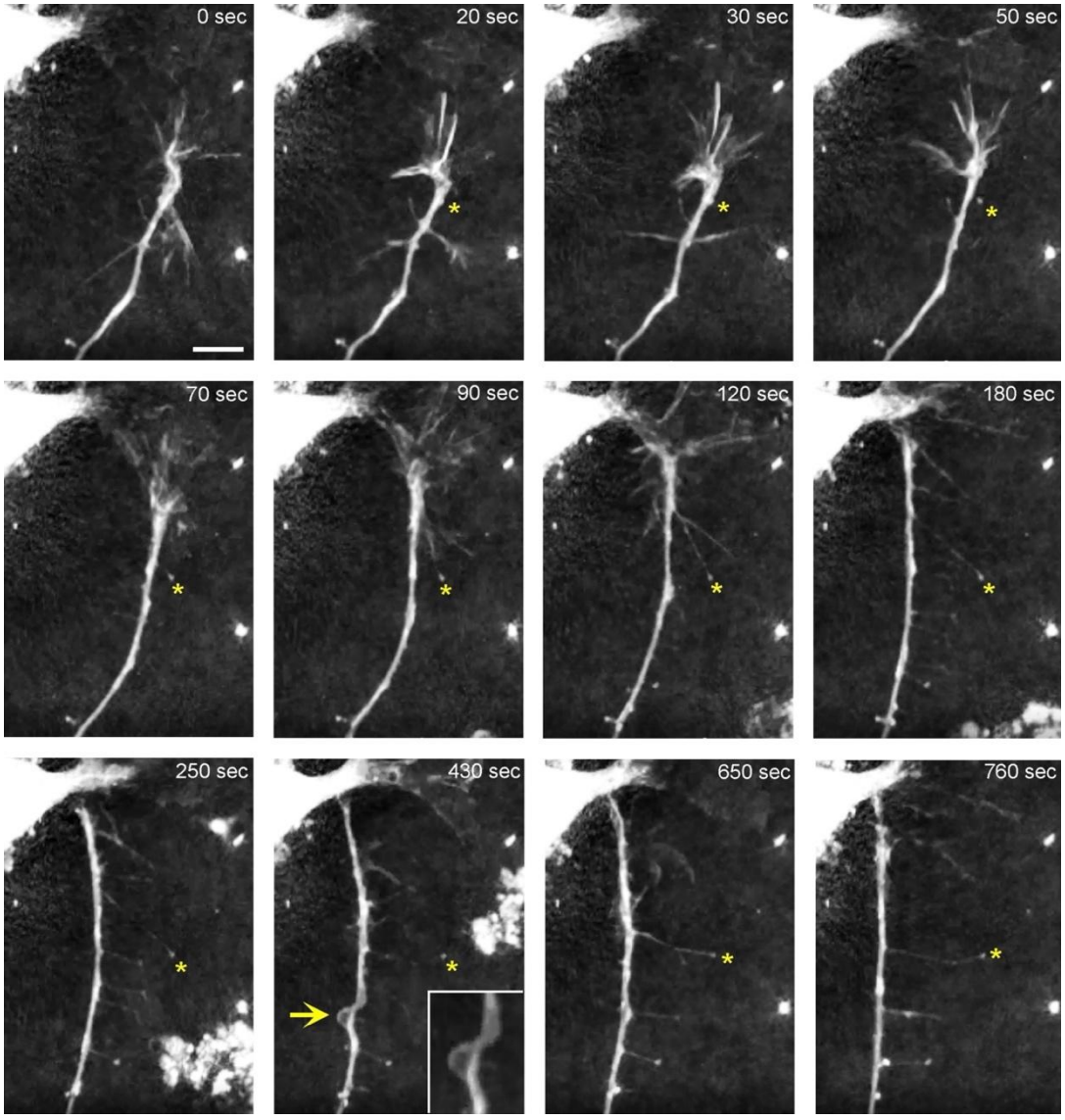

Figure 15 The dynamics of a growth-cone region in a primary midbrain culture (monolayer at DIV1), visualized with time-lapse holotomography. As the growth cone finds its next attachment target and pulls the axon to the left, its adhesion sites are revealed (one such site is marked with an asterisk). The spacing between the adhesion sites is around 2-6 μm, and the nanoscale tethers connecting them to the main axon can be stretched to as long as 10 μm (to accommodate axon shifts). This spatial configuration closely resembles that shown in **Figure 11**. The arrow points to an axon segment that appears flat and twisted in a corkscrew-like fashion. To emphasize key transitions, time points are not evenly spaced. This imaging supports the interpretation of the dynamics that may underly the confocal microscopy data, but the recorded axons are not labeled and may not be serotonergic. Scale bar = 5 μm. (From Hingorani et al., 2022).

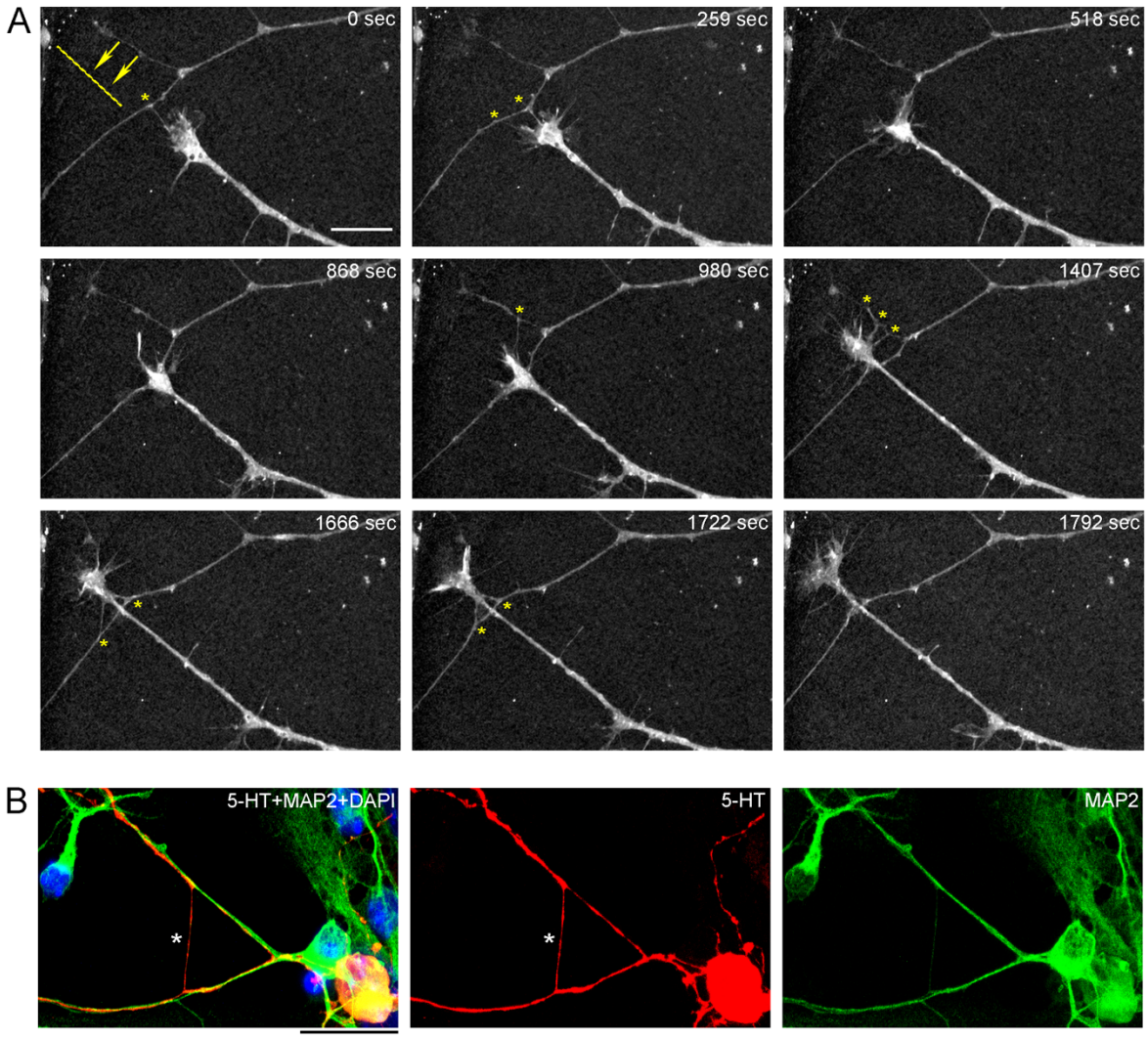

Figure 16 (A) The dynamics of a growth-cone region in a primary midbrain culture (monolayer at DIV5), visualized with time-lapse holotomography. A transition from one neurite branch to another is shown (some key adhesion points are marked with asterisks). The arrows with the dashed line indicate the spatial shift of the top branch, as the growing axon generates sufficient force to line it up with its current growth axis. To emphasize key transitions, time points are not evenly spaced. This imaging supports the interpretation of the dynamics that may underly the confocal microscopy data, but the recorded axons are not labeled and may not be serotonergic. Scale bar = 10 µm. **(B)** A similar transition (asterisk) in a primary midbrain culture (monolayer at DIV2), visualized with immunocytochemistry for 5-HT (red) and MAP2 (green) and imaged with high-resolution confocal microscopy. Cell nuclei are stained blue (DAPI). Scale bar = 20 µm. (From Hingorani et al., 2022).

E. Axon-axon interactions (lack of same-axon repulsion in brainstem cultures)

In the developing nervous system, there are a number of mechanisms, including differential adhesion, chemotropism, and repulsion, that allow growth cones to find, recognize, and synapse with their correct compeer (Goodman & Shatz, 1993). Axon-axon interactions are critical for pre-target axon sorting that facilitates topographic map formation (Bellon & Mann, 2018). Guidance cues can facilitate axon-axon interactions. For example, the repulsive molecule Draxin facilitates the bundling of commissural axons by forming a tripartite complex with Netrin-1 and DCC to create a bridge between axons and promote fasciculation (Bellon & Mann, 2018; Liu et al., 2018). While the current work does not examine the influence of guidance cues *in vitro*, the axon-axon interactions and growth cone-axon biophysical properties can be examined.

Axon zippering

Newly growing axons may fasciculate, or bundle together or with previously grown axons, which helps them to move along a common path (Šmít et al., 2017). Individual axons can later defasciculate or detach from the bundle to reach their specific target. It is generally thought that the growth cone controls axon bundling by latching on to the shaft of a neighboring axon and then moving along it (Šmít et al., 2017). However, this viewpoint does not consider possible dynamic adjustments in the adhesion of the shafts behind the growth cone (Šmít et al., 2017).

Very recently, in an *ex vivo* model using olfactory epithelium explants, Šmít et al. (2017) observed that axons dynamically interact with each other along their shafts, leading

to zippering and unzippering behavior that regulates their fasciculation (Šmít et al., 2017). Growing axons formed progressively larger bundles without direct involvement from the growth cones (Šmít et al., 2017). Instead, the shafts of the axons stuck together in a way that resembles fastening a zipper (Šmít et al., 2017). Šmít et al. (2017) then manipulated the 'axon zippers' and observed that zippering arises from a competition between two forces: the contact force that causes two axons to adhere to each other (which favors zippering) and the mechanical tension that arises from internal or external pulls on the axon (which favors unzippering). HTM recordings of our primary brainstem cultures display axon-axon interactions that resemble axon zippering (**Figures 17A-D**). We do not imply that serotonergic fibers participate in the formation of major axon tracts in the developing brain, but we also note that serotonergic axon involvement in dynamic fasciculation/defasciculation (i.e., "hitchhiking") is unknown.

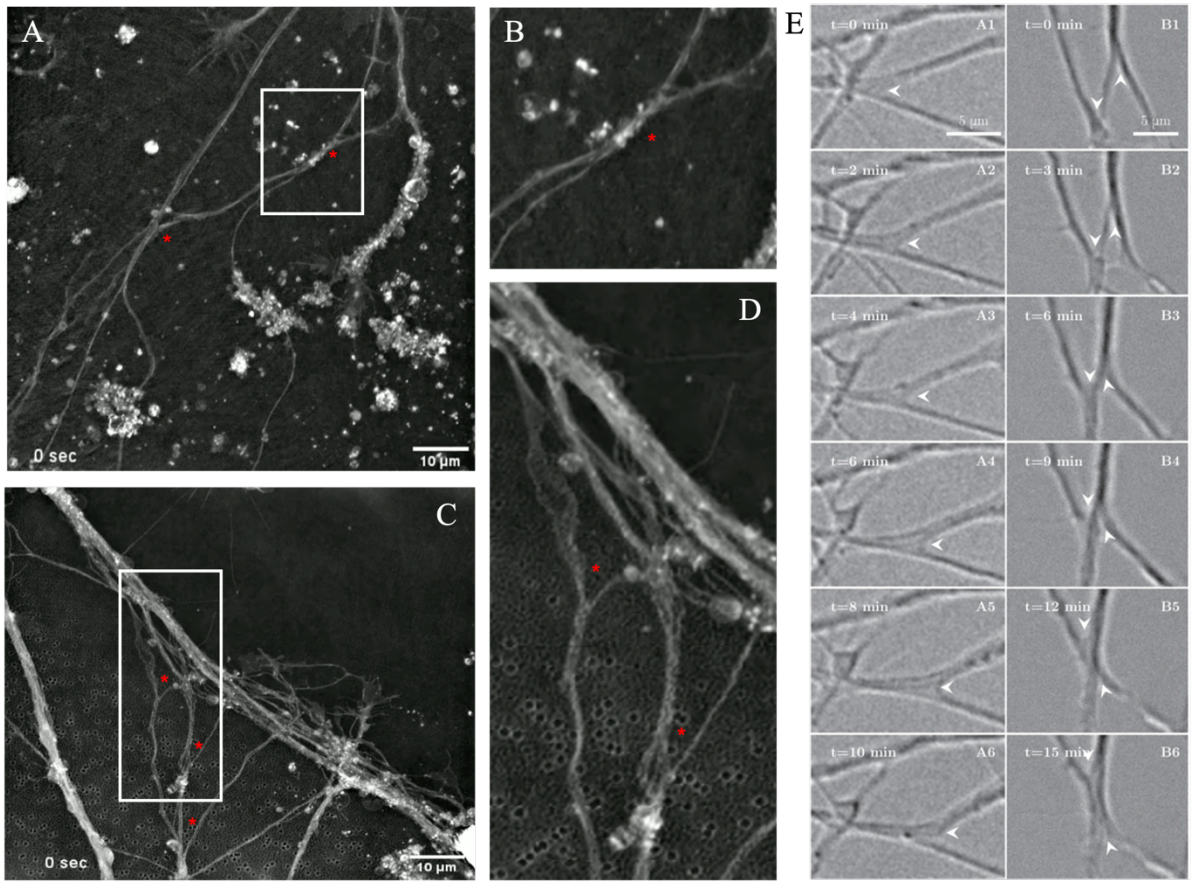

Figure 17 Axon zippering occurring between DIV3-5 **(A-D)** primary brainstem cultures (monolayers) visualized with time-lapse holotomography, red asterisks denote some regions displaying axon zippering **(A-D)**. Scale bar = 10 µm. **(E)** High-magnification images of individual axon zippers and their evolution in time. Scale bar = 5 µm. (From Šmít et al., 2017.)

F. STED

The environment in the culture dish does not accurately reflect the brain environment. The differences include tissue dimensionality (2D vs. 3D), cell packing, viscoelasticity, and

many other factors. To verify some of our findings, super-resolution (STED) microscopy was used to examine single serotonergic axons in the mouse brain at embryonic day 17 (**Figure 18**). This developmental age is convenient because at this time the serotonergic neurons have somata with a mature size and morphology, but their axons only begin to spread in the telencephalon (Lidov and Molliver, 1982; Janušonis et al., 2004). Due to this sparse distribution, single axons and their growth cones can be easily captured in natural brain tissue. In the embryonic telencephalon, growth cone protrusions that closely resemble those in culture (*e.g.*, **Figure 11**) were detected. In particular, some of them appeared to have a "foot" and a tether (**Figure 18 inset**). In addition, unambiguously flattened membrane segments were detected (with the ratio of approximately 5:1), with an apparent cork-screw rotation (**Figure 19**). This suggests that serotonergic axons can be ribbon-like (or human hand-like, to better approximate the ratio) as they travel through neural tissue. Since these profiles were also observed in culture (**Figures 11D**, **11B**, **15**), they may not be induced by dense tissue packing.

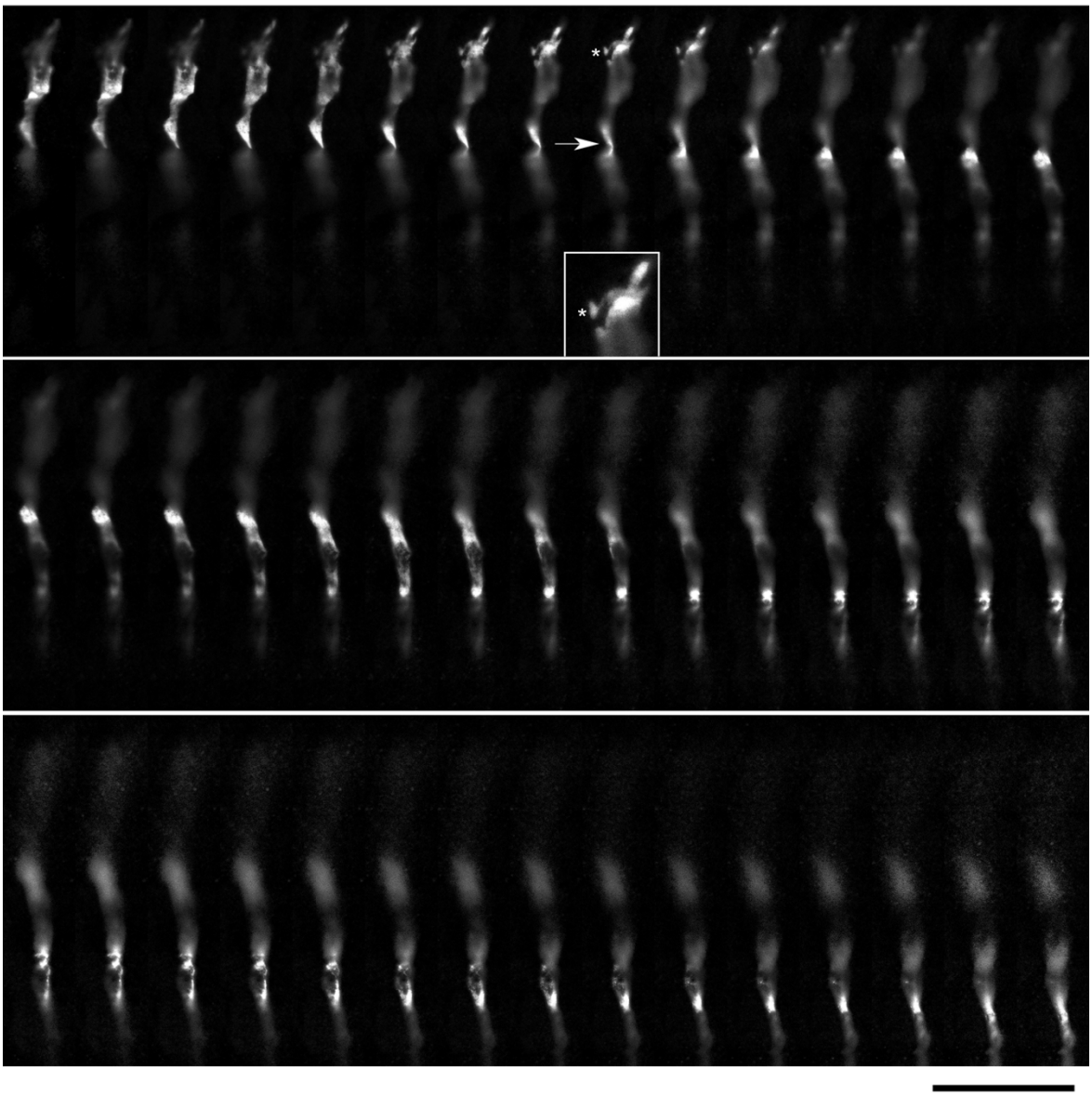

Figure 18 A super-resolution microscopy (STED) z-series of a single serotonergic (5-HT+) axon in the sectioned cortical plate of a mouse embryo at E17. Note the growth cone protrusions similar to those in culture (e.g., **Figures 11B** and **20D**; asterisks, inset) and a potentially flat membrane region (arrow, further analyzed in **Figure 15**). The sequential optical sections are evenly separated by 100 µm. Scale bar = 20 µm. (From Hingorani et al., 2022).

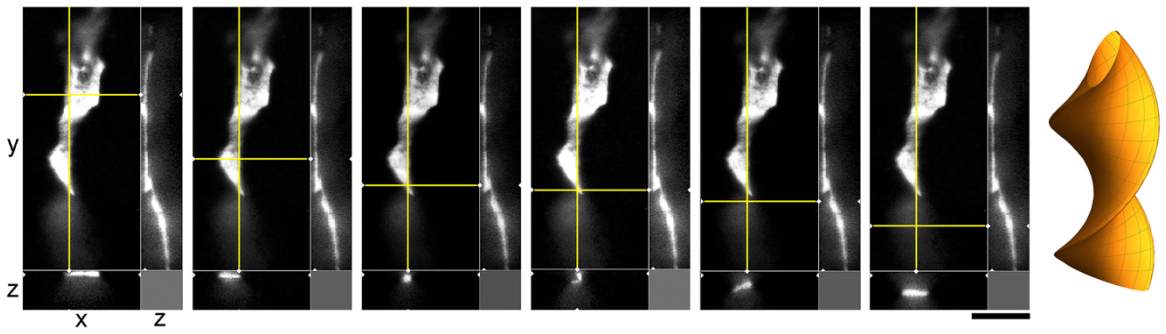

Figure 19 A super-resolution microscopy (STED) images of a single serotonergic (5-HT+) axon in the sectioned cortical plate of a mouse embryo at E17. The axon is shown in all three dimensions, with a fixed yz-plane (at a constant x; the vertical yellow line) and a series of xz-planes (with six different y values; the horizontal yellow line). At the shown levels, the axon is flat (ribbon-like) and appears to rotate. This hypothetical cork-screw configuration is shown in the diagram on the right. Scale bar = 5 µm. (From Hingorani et al., 2022).

G. Discussion

Realistic modeling of serotonergic axons requires experimental information about their branching patterns. At a minimum, it should include the frequency of branching, the typical branching angles, and the trajectory information retained by each of the two branches. This information should ideally be described probabilistically (*e.g.*, the "wait time" between two branching events might be captured by the exponential distribution with a given intensity λ, the branching angles can be described by a directional probability distribution, and the "memory" of the branches can be reflected in the underlying increment covariance structure). Serotonergic axon ramification is often referred to in descriptive density studies, but this process is essentially inferred, with no reliable information at the level of single axons. In brain tissue, these axons can be extremely dense, to the extent that even high-resolution 3D-imaging can be insufficient to distinguish true branching points from axons that cross at sub-

micrometer distances (Janušonis et al., 2019). Serotonergic neurons in culture tended to produce branching events that could be detected unambiguously (**Figure 20**). Locally, they appeared to be rather stereotypic. The two branches of an axon split at wide angles (typically, 90°-180°), which achieved their immediate separation (**Figure 20**). In sparse cultures, both branches can reorient themselves parallel to the original trajectory and thus cannot be treated as independent of their parent trajectory or of each other. Over longer distances, they are likely to completely decorrelate, as they advance through the stochastically distributed attachment surfaces.

This research is the first high-resolution analysis of single serotonergic axons *in vitro*. A key advantage of cell cultures is that long axons can be imaged uninterrupted from the soma to the terminal point, including branching points along the trajectory. In contrast, brain tissue is extremely densely packed, with extracellular distances often well below 100 nm (Hrabetova et al., 2018). This compressed environment may conceal the inherent properties of axons (*e.g.*, their caliber dynamics), as well as their contacts with other cells. Also, only relatively short axon segments can be visualized uninterrupted in sectioned brain tissue because their random walk-like trajectories stay within the section volume only for distances comparable to the width of the section (typically, 40-50 μm) (Janušonis et al., 2019). In brain tissue, reliable identification of branching events in serotonergic axons is currently possible only in relatively sparse regions and with sub-micrometer 3D-imaging, since serotonergic axons routinely cross at distances near the limit of optical resolution (Janušonis et al., 2019). Therefore, the true extent of branching or ramification in serotonergic axons remains unknown, even though these processes are often used to explain regional density differences.

We show that serotonergic axons can be ribbon-like (with the width-thickness ratio of around 5:1) and can also rotate along their axis, perhaps producing periodic point-like constrictions (**Figures 18**, **19**). This morphology is likely induced by tension forces due to axon extension, but it also increases the surface-to-volume ratio and may facilitate 5-HT release. It is less likely to be related to tissue packing because it was also observed in sparse cultures (**Figure 15**). Interestingly, these profiles were noted in early studies (see **Figure 5** in the original paper of Aitken and Tork, 1988), where they were interpreted as "sinuous fibers" with "translucent varicosities" (because of their higher light intensity, likely due to the shorter light path in the flat region). It highlights the limited understanding of what serotonergic "varicosities" are, despite their importance in neuroanatomical and functional studies (*e.g.*, they have been used to classify serotonergic axons into the D- and M-classes (Kosofsky and Molliver, 1987), a system still referred to in some current analyses). Since early descriptions, based on 2D-microscopy, they have been assumed to be dilated segments of axons, but very few studies have performed their high-resolution analyses in the 3D space.

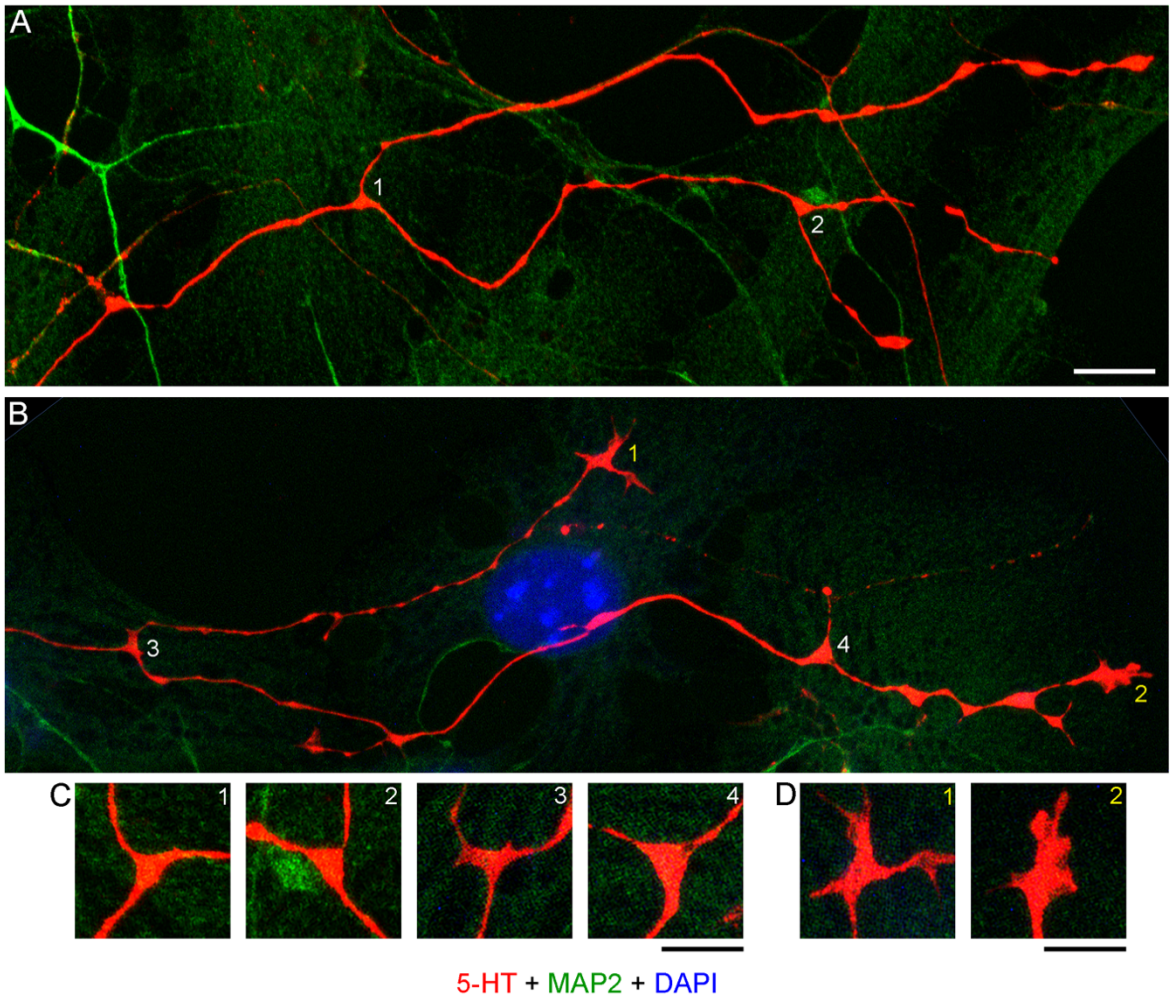

Figure 20 A primary midbrain culture (monolayer at DIV4), visualized with immunocytochemistry for 5-HT (red) and MAP2 (green) and imaged with high-resolution confocal microscopy. Cell nuclei are stained blue (DAPI). **(A** and **B)** Four branching regions (white 1-4) and two growth cones (yellow 1-2) and are shown. Note that the two branches in **(B)** differ in their morphologies. **(C)** An enlarged view of the branching points. The branching regions have a triangular shape, and the branches diverge at large angles (around 90°-180°). **(D)** An enlarged view of the growth cones. Note the similarity of the second growth cone to that in a sectioned mouse brain (**Figure 19**). Scale bars = 10 µm in **A** and **B**, 5 µm in **C** and **D**. (From Hingorani et al., 2022).

The emerging picture of varicosity-like segments (VLSs) is considerably more complex. First, some VLSs may indeed be dilated, ovoid-shaped segments (Maddaloni et al., 2017). This is supported by our findings that demonstrate that the caliber of the same axon can vary considerably over short distances (*e.g.*, **Figure 10C**). Second, a sequence of VLSs may not indicate significant changes in axon morphology but may reflect a ribbon-like segment that periodically exposes its flat surface versus its edge, effectively creating a "blinking" effect in 2D-imaging. Third, some VLSs may not be continuous axons but rather 5-HT-positive "footprints," former adhesion sites left by axons. Our study clearly demonstrates this possibility *in vitro*, but additional studies are needed in brain tissue to prove the absence of membrane bridges between adjacent VLSs (*e.g.*, using other markers and/or super-resolution microscopy). As more experimental information becomes available, VLSs may provide important insights into axonal *dynamics* in *fixed* brain tissue. These observations are generally consistent with recent findings in other systems, where VLSs and other morphological features have been shown to reflect the current, local state of an axon rather than its identity (Liu and Nakamura, 2006; Andersson et al., 2020; Sun et al., 2022). Our analysis sheds new light on the dispersal of serotonergic axons. It has recently been shown that this process is aided by *Pcdh-αC2* that is expressed in serotonergic neurons and can mediate axonal self-avoidance, preventing axon "clumping" (Katori et al., 2009; Chen et al., 2017; Katori et al., 2017). However, our previous modeling has shown that "clumping" is unlikely if axons perform random walks with no interaction (based on the von Mises-Fisher stepwise walk with a high concentration parameter (κ) or fractional Brownian motion with a high Hurst index (*H*)) (Janušonis and Detering, 2019; Janušonis et al., 2020). In this

context, branching points can be disruptive because they can create sister trajectories that travel in close proximity, at least initially. *In vitro* results demonstrate that the sister branches of serotonergic axons tend to separate at very large angles, which efficiently prevents clustering. In the brain, each of the branches is likely to immediately encounter different adhesion surfaces, supporting rapid decorrelation.

An important finding in this study is that serotonergic axons can travel adhered to available cellular surfaces, such as dendritic branches of other neurons. Some of the key axonal structures supporting this adhesion might have been observed in early studies but could not be accurately interpreted because of technical limitations (Azmitia and Whitaker-Azmitia, 1987; Aitken and Tork, 1988). In the densely packed neural tissue, dendrites and other cellular surfaces are readily available. This suggests that the strong stochasticity of serotonergic axon trajectories may not be a property of serotonergic fibers themselves but may instead reflect the stochastic geometry of the surrounding neural tissue (**Figure 21**). Given a specified stochastic process, computer simulations can predict the resultant axon densities, with no additional biological information (Janušonis and Detering, 2019; Janušonis et al., 2020). This leads to an intriguing conclusion that local serotonergic densities can directly reflect the local microarchitecture of a brain region. An abnormal local cytoarchitecture alone may generate an altered serotonergic density, with no other causal factors. It might be exemplified by the increased densities of serotonergic axons in some cortical regions of individuals with ASD (Azmitia et al., 2011), perhaps in association with the reported denser cell packing in cortical minicolumns (Casanova et al., 2006).

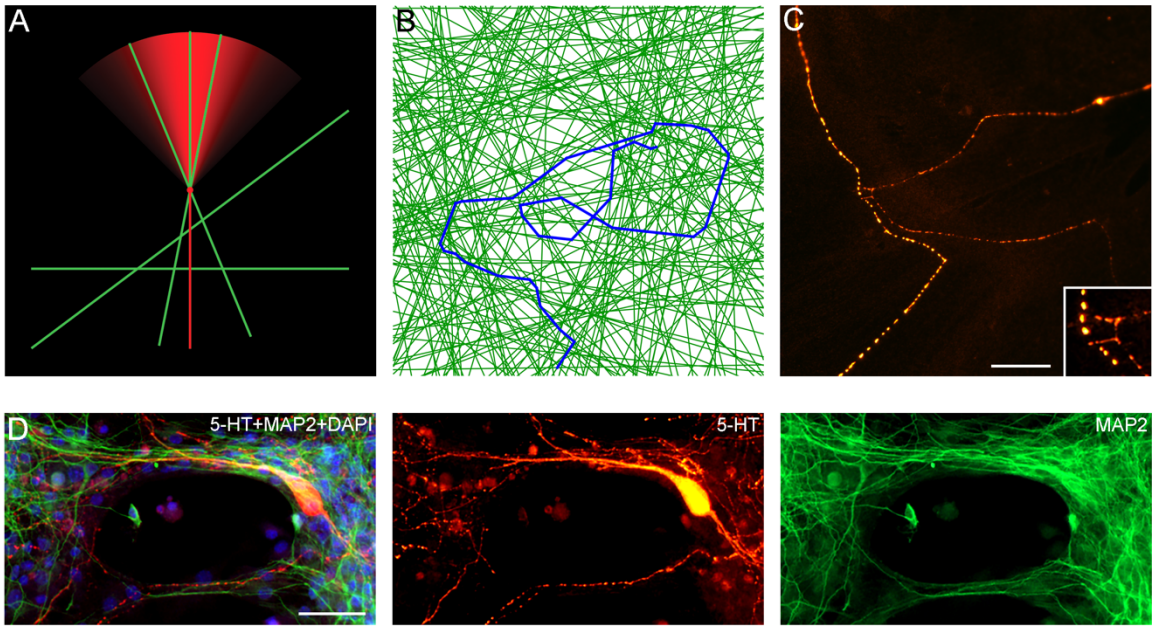

Figure 21 (A) A diagram showing the hypothetical choices available to an advancing serotonergic axon (red) that can choose any of the available neurites (green), provided they fall within its sector of possibilities. The cone is modeled with the von Mises distribution (here, the mean direction μ is aligned with the current direction of the fiber and the concentration parameter κ = 10. **(B)** A simulated walk of a fiber (blue) that can only advance only along available neurites (green). In the simulation, 200 randomly oriented lines were used, and the fiber advanced through 350 intersections. At each intersection, it could move in the current direction (a 0°-turn), turn "left" or "right" (at the available angles), or turn backward (a 180°-turn). The probabilities of the four events were calculated using the von-Mises distribution with μ = (0, 0) and κ = 5, and one event was drawn. The simulation was performed in Wolfram Mathematica 13.0. **(C)** A comparable configuration of 5-HT+ axons in a glia-neuron co-culture at DIV15, visualized with epifluorescence microscopy. The inset shows potential contact points. Scale bar = 20 μm. **(D)** Serotonergic axons (5-HT+/MAP2-, red) traveling along bridges of MAP2+ (green) neurites, visualized with epifluorescence microscopy. Scale bar = 50 μm. (From Hingorani et al., 2022).

VI. Chapter 5: Hydrogels

A. Hydrogel overview Hydrogels, crosslinked networks with tissue-like water content and easily tunable biochemical and mechanical properties, demonstrate a distinct efficacy as matrices for 3D cell culture (Duval et al., 2017). Here we will focus on transitioning from 2D to 3D systems (2.5D), natural hydrogels, and touch on synthetic hydrogels as these systems are the most relevant to the development of our platform.

2.5D: Transitioning from 2D to 3D

The ECM of the CNS is comprised of a complex 3D network of numerous macromolecules that are enmeshed together, with features as minute as 9 nm (Kim et al., 2018; Sharaf et al., 2022). In addition to being a structural scaffold for cells, the *ECM is an instructive entity*, responsible for regulating cellular behavior and affecting their proliferation, shape, function, migration, survival, and development (Adams & Watt, 1993; Bershadsky et al., 2003; Ingber, 1990; Jokhadar et al., 2007; Liberio et al., 2014). The ECM is comprised of polysaccharides and proteins (i.e., laminin, fibronectin, elastin, collagen) and their relative amount in tissue is temporally and regionally specific (Griffiths et al., 2020; Liberio et al., 2014). These proteins, many of which have essential adherence functions, are then embedded in a polysaccharide gel (Liberio et al., 2014).

Many cells are anchorage dependent and require ECM-attachment in order to proliferate and survive (Liberio et al., 2014). Integrins are transmembrane proteins in the form of αß heterodimers central to ECM protein-cell attachment (Liberio et al., 2014). This

interaction produces a cascade of intracellular signals that can also control differential gene expression (Damsky & Ilic, 2002; Liberio et al., 2014; Longhurst & Jennings, 1998). The signaling response is associated with the cell response to the micro-environment (Liberio et al., 2014). Consequently, the ECM is in a state of *constant flux* to support the cell requirements of developmental plasticity (Liberio et al., 2014; Miranti & Brugge, 2002). The cell response to the ECM components is flexible and contingent upon which integrin subunits are expressed by cells (Liberio et al., 2014).

A natural intermediate step between 2D and 3D models is a 2.5D model, often using a substance such as Matrigel, to replicate the ECM. Matrigel is a solubilized basement membrane preparation extracted from the Engelbreth-Holm-Swarm (EHS) mouse sarcoma, a tumor rich in ECM proteins such as laminin, collagen IV, heparan sulfate proteoglycans, entactin/nidogen, and a number of growth factors (Corning Matrigel Matrix). Cells seeded on Matrigel benefit not only from biochemical cues presented by the gel, but also from the mechanical arrangement of its molecules (Kaiser et al., 2020). Matrigel's *in vivo*-like structural organization is found to boost survival of the seeded cells, their morphological profiles, differentiation, and overall typical functions (Kaiser et al., 2020).

The success of Matrigel coating has been widely demonstrated. The major components of Matrigel (laminin and collagen Type IV) have been shown to promote neurite extension (Koh et al., 2008; Novikova et al., 2006; Tonge et al., 1997; Wu et al., 2018). In DRGs explanted on Polyvinylidene fluoride-trifluoroethylene (PVDF-TrFE) fiber scaffolds, Matrigel coating resulted in neurite extension 3-fold higher than DRGs on uncoated scaffolds (Wu et al., 2018). In addition, the longest neurite extension for DRGs on

Matrigel-coated scaffolds with SCs was roughly 5-fold higher than DRGs on uncoated scaffolds (Wu et al., 2018). Furthermore, the overall survival rate of human neural progenitor cells (HNPCs) on Matrigel-coated surfaces has been shown to be better than that on surfaces that were not coated with Matrigel (Kaiser et al., 2020).

Natural hydrogels

Natural hydrogels include collagen, silk fibroin, hyaluronic acid, chitosan, alginate and hydrogels derived from decellularized tissues (Catoira et al., 2019). The unique properties of natural hydrogels include: biocompatibility, biodegradability, low cytotoxicity, the possibility to tailor the hydrogel into an injectable gel and their similarity to physiological environment (Catoira et al., 2019). However, natural hydrogels typically do not have strong mechanical properties and are not easily controllable due to their batch-to-batch variation (Catoira et al., 2019). To enhance the mechanical strength and swelling responses of such hydrogels, multicomponent networks as interpenetrating polymer networks (IPNs) have been designed (Dragan, 2014). We tested the use of a hydrogel that combines the advantages of native ECM proteins and nonnative biopolymers in an IPN system consisting of rBM (reconstituted basement membrane) matrix and alginate (**Figure 11**). rBM (Matrigel) contains key proteins normally found in the basement membrane, including laminin-111 and collagen IV and forms a matrix at physiological temperatures due to bonding interactions between constituent proteins (Wisdom & Chaudhuri, 2017; Wisdom et al., 2018). Alginate, a polysaccharide derived from seaweed, is a non-repeating copolymer of β-D-mannuronic acid and α-L-guluronic acid and does not present cell adhesion ligands.

Therefore, it can be used as an inert, tunable, mechanical reinforcer of the rBM matrix (Wisdom & Chaudhuri, 2017). Alginate is ionically crosslinked, allowing cells to physically remodel the IPN network as they extend their processes or migrate.

Synthetic hydrogels

While natural hydrogels are those gels whose polymers have natural origins such as gelatin and collagen, synthetic hydrogels are synthesized using synthetic polymers such as polyamides and polyethene glycol (Gyles et al., 2017). Synthetic polymers are usually hydrophobic and are typically chemically and mechanically stronger in nature when compared with natural polymers (Gyles et al., 2017). The improved mechanical strength of synthetic hydrogels provides excellent durability of the biomaterial by reducing the rate of its degradation (Garnica-Palafox & Sanchez-Arevalo, 2016; Gyles et al., 2017). Hydrogels synthesized for biomedical use tend to incorporate synthetic polymers such as polyacrylamide and its derivatives (e.g., poly vinyl alcohol (PVA), polyethylene glycol (PEG)) (Gyles et al., 2017; Syed et al., 2011).

Polymers with long, densely grafted sidechains, commonly known as bottlebrush polymers, have attracted significant interest in a variety of fields due to their incredible softness and their lower propensity to entangle making them ideal biological tissue mimics (Sarapas et al., 2020). Bottlebrush polymers are one-to-two orders of magnitude softer than traditional polymeric materials due to molecular architecture effects (Daniel et al., 2016) (**Figure 22**). The large size of the sidechains (in comparison to the overall molecular dimensions) of each bottlebrush network strand suppresses backbone entanglements and

results in moduli that can approach several kPa, roughly 3 orders of magnitude lower than a typical entangled polymer network built from linear chains (≈1 MPa) (Mukherjee et al., 2020).

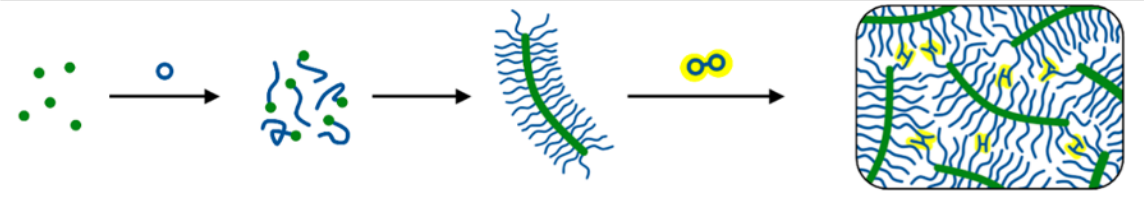

Figure 22 Schematic of the generation of dynamic bottlebrush polymer networks. (From Self et al., 2020.)

VitroGel®

VitroGel hydrogels are xeno-free (synthetic), commercially available, biocompatible hydrogel systems which contain proprietary formulations of various bio-functional ligands with tunable mechanical strengths to fulfill the needs of different culture conditions. The first commercially available hydrogel tested was VitroGel 3D-RGD, a xeno-free tunable hydrogel system modified with arginylglycylaspartic acid (RGD) cell adhesive peptide to promote the cell attachment and cell-matrix interactions. VitroGel 3D-RGD hydrogel

formation was produced by mixing the VitroGel 3D-RGD solution first with VitroGel Dilution Solution, and then adding the cell culture media (with or without cell suspension) to become a hydrogel matrix structure. The mechanical properties of the hydrogel are tunable as specialized soluble factors can be easily added, and the amount of culture media mixed with the diluted VitroGel 3D-RGD solution can be adjusted to regulate ion concentration within the hydrogel.

We also tested VitroGel Matrix, a xeno-free, functional hydrogel ready to use by mixing with cell solution. VitroGel Hydrogel Matrix closely mimics the natural ECM, is compatible with fresh bioprinting, is room temperature stable, has a neutral pH, is transparent, permeable, and compatible with different imaging systems (TheWell Bioscience, Inc.). VitroGel Hydrogel Matrix has most commonly been used with immortalized cell lines, particularly in cancer research.

B. ***Hydrogel methods*** *2.5D Methods*

Cell preparation was identical to monolayer method described previously (Chapter 3, Section C) apart from substrate coating and timing of media addition. 2.5D culturing was initially tested using Matrigel (Corning® Matrigel® Matrix). However, due to high batch-to-batch variability, ECM Gel from EHS murine sarcoma (Sigma E1270) was used as a Matrigel substitute. This ECM was prepared to a protein concentration of 8-12 mg/mL (in DMEM), containing laminin as a major component, collagen type IV, heparin sulfate proteoglycan, 50 mg/L gentamicin S=sulfate, entactin, and other minor components.

In the first method (*method 1*) ECM was incorporated by adding a thin layer to a well, allowing it to get to room temperature for ~20 minutes before adding cells, and then following a 2hr incubation period (5% CO_2 at 37°C), media was gently dripped into the dish until just covering the layer of ECM gel (**Figures 24B-I**). In the second method (*method 2*) the ECM gel was diluted with 1:2 with mNSM (**Figure 24A**). The latter method resulted in a less viscous substrate. Media was changed only, when necessary (where color change indicated pH unbalance), to avoid disturbing cells. Immunocytochemistry methods were identical to those described previously for 2D-conditions (Chapter 2, Section B), except for the thicker layer of substrate coating remaining on the glass coverslip.

Interpenetrating network hydrogels (IPN)

Serotonergic neurons were prepared using the same methods previously described and encapsulated in alginate-Matrigel IPNs using an established method (Wisdom & Chaudhuri, 2017) (**Figure 23**). Alginate was reconstituted in the neuronal culture-specific medium at 5 mg/mL (final concentration) and mixed with Matrigel (at the final concentration of 4.4 mg/mL) on ice. The serotonergic neurons were mixed with the alginate-Matrigel solution, deposited into a syringe, and mixed with a slurry of calcium sulfate through a syringe-coupler to initiate crosslinking. The solution was then deposited into standard culture dishes or chambered cover glasses and incubated for 30 minutes until gelation. The neuronal culture medium was added to the wells, and the neurons were maintained using the same methods described previously in the monolayer method.

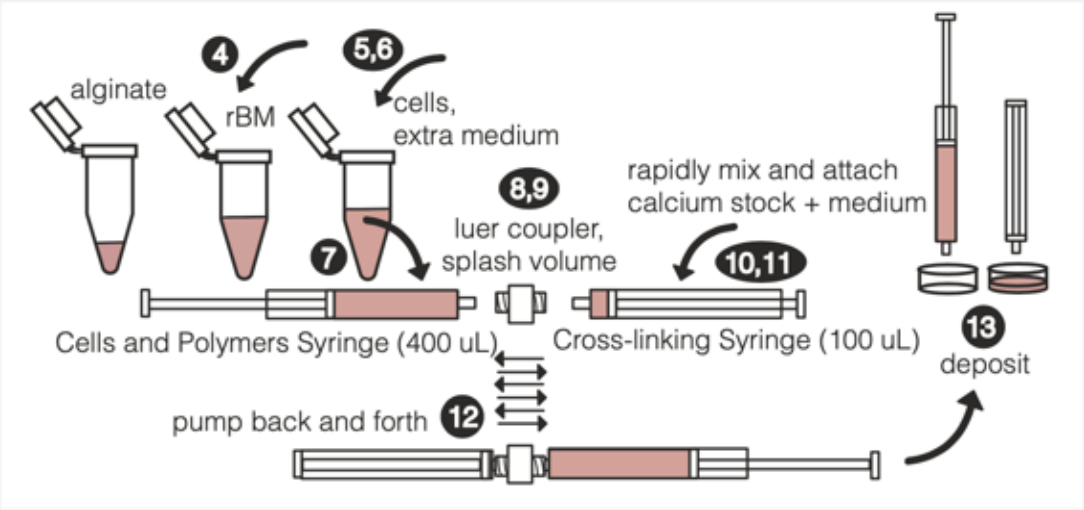

Figure 23 Overview of IPN method. (From Wisdom and Chaudhuri, 2017.)

Immunostaining the IPN hydrogel

The media was removed from hydrogels and the samples were warmed in DMEM + 4% PFA for 45 minutes at 37°C. PFA is aspirated out and samples are washed 2x in warmed calcium-PBS (15-30 min each wash). The samples were left overnight in a 30% sucrose in calcium-PBS solution to remove water and prevent ice crystal formation. In a traditional OCT freezing protocol, at this stage there would be a penetration step (50% OCT mixed solution for 4-6 hours). The hydrogels were embedded in freezing medium in cryomolds and allowed to freeze. The gel could be stored at -20°C at this stage.

Bottlebrush polymers

The cell culture protocol for initial bottlebrush polymer tests was identical to the monolayer method previously described (Chapter 3, Section C). Two media conditions were prepared for preliminary testing of the bottlebrush polymers in culture. Trituration media was cNSM and the feeding media consisted of mNSM (with 0.1% P/S). Bottlebrush polymer testing conditions comprised of feeding media with 5% bottlebrush polymer and feeding media with 25% bottlebrush polymer. The immunocytochemistry methods were identical to those in Chapter 2, Section B.

VitroGel® 3D-RGD

Following the manufacturer's instructions, varying ratios (1:1, 1:2, 1:3) of VitroGel 3D-RGD + VitroGel Dilution Solution were tested with feeding media of cNSM and mNSM to examine possible optimal hydrogel dilutions for 3D cell culture of primary brainstem neurons (TheWell Bioscience Inc., North Brunswick, NJ, USA). According to the manufacturer, the G' (the shear modulus) is about 4000 Pa at 1:0 dilution, 1200-2000 Pa at 1:1 dilution, 600-1000 Pa at 1:2 dilution, 200–500 Pa at 1:3 dilution, and < 500 Pa at dilution higher than 1:3 (TheWell Bioscience, Inc.). The final ratio of diluted VitroGel solution to cell medium with cells was 4:1. 0.1% P/S was used in simplified media due to contamination issues in prior cell platings due to shared facility challenges. VitroGel 3D-RGD + VitroGel Dilution Solution were combined, cells were added (100µl to all ratios), and the mixture was added to a 12-well plate. After a gelation period (10-15 min at room temperature) cNSM or the simplified mNSM media was added above well. The addition of

GDNF was identical to the 2D protocol. Roughly 60% of media was changed for the hydrogels every two days. The cNSM condition did not yield successful results.

VitroGel® Matrix

VitroGel Matrix solution was warmed to 37 °C (though manufacturer protocol says RT is also fine). Cells were triturated per the 2D protocol with simplified mNSM. VitroGel and cell suspension was kept at a 2:1 v/v mixing ratio and added to 12 well plates and/or standard cell culture dishes. After a 10–15-minute gelation period at room temperature (RT), mNSM media was added. GDNF addition was identical to 2D protocol. Partial media changes occurred every 2 days or as needed.

Immunostaining *VitroGel® Matrix*

Media was removed from the top of hydrogels and washed with PBS for 1 min, 3 times. Hydrogels were then fixed by adding PFA for 30 minutes. Hydrogels were washed 3x again with 0.1 M PBS and either processed immediately or stored for a few days at 4°C. Cultures were rinsed in PBS, and then incubated in 0.1% TX for a total of 5 minutes before being rinsed 3x with PBS (5 min each). They were then blocked for 30-60 minutes in 3% normal donkey serum (NDS) in PBS. They were incubated in goat anti-5-HT IgG (1:1000; ImmunoStar # 20079) and rabbit anti-MAP2 IgG (1:1000; Abcam #32454) with in the 3% NDS and PBS blocking solution overnight at 4°C on a shaker. They were rinsed 3 times in PBS (10 minutes each), incubated in Cy3-conjugated donkey anti-goat IgG (1:500; ImmunoResearch #705-165-147) and AlexaFluor 488-conjugated donkey anti-rabbit IgG

(1:1000; ThermoFisher #A-21206) with 3% NDS in PBS for 3 hours, and rinsed 3 times (10 minutes each) with PBS. For DAPI staining, NucBlue™ Fixed Cell ReadyProbes™ Reagent (Thermofisher #R37606) was added as described by the manufacturer (2 drops per 2ml solution). The cells were imaged at least 24 hours after DAPI addition.

Complications

Several yeast outbreaks in the shared cell culture facilities hindered our progress for several months. Working in shared facilities makes pinpointing and eradicating sources of contamination very difficult. In addition to extra sterilization steps, we attempted to combat the yeast problem by buying new reagents and when that did not eliminate the problem, we began incorporating fungicides (**Figure 28**).

The standard techniques for imaging and analyzing cell function and protein distribution are more involved in the 3D environment (Tibbitt & Anseth, 2009). When working in a 3D network, cells have limited accessibility for immunostaining or DNA/RNA extraction and secreted proteins can be difficult to extract from the gels (Tibbitt & Anseth, 2009). Cell imaging is often difficult as light scattering, refraction, and attenuation occur in a 3D composite, cell-laden gel. Imaging the various hydrogels was limited by the maximal depth of epiflorescent, confocal, and holotomographic microscopes (< 1 mm). We examined the compatibility of immunostained VitroGel hydrogels. One major challenge encountered when immunostaining the VitroGel hydrogels was the degradation of the gel in the dish, which led to a motile gel with uneven depth.

C. Main findings in hydrogel tests

2.5D

The Matrigel replacement ECM gel resulted in visibly healthy cultures (i.e., no signs of apoptosis/necrosis) (**Figure 24**). To our knowledge, this is the first demonstration of primary brainstem neurons cultured in this gel. Immunocytochemistry revealed the presence of 5HT positive axons, but the thicker substrate coating rendered them to be less visually identifiable compared to 2D-immunocytochemistry (**Figures 24G**, **J**). Importantly, in the 2.5D geometry (**Figures 24G**, **H**) we had comparable viability to our 2D (**Figures 24I**, **J**) model, with healthy cultures at DIV31.

IPNs

The first test of the IPN hydrogels involved plating onto Ibidi 4 well u-slides (Cat. # 80427). Cells were plated first on laminin coated glass bottom wells at ~80,000 cells/100 µL. IPN hydrogel was added on top following the protocol described by Wisdom and Chaudhuri (2017). Two trituration and feeding media conditions were initially tested: NBplus medium, 2% B27, 1% Culture-one supplement and pre-conditioned cNSM. The second IPN hydrogel test involved using a 12 well plate (Thermo Scientific™, 12-556-005). The plating and trituration medium were composed of: NBplus medium, 2% B27, 1% Culture One supplement, 1% l-glutamine (200mM), 1% P/S, and 5% HI-FBS. The feeding media that was added on top of the hydrogels consisted of Neurobasal Plus Medium, 2% B27, 1% l-glutamine (200mM), and 0.5% P/S. We tested three conditions: 3D-IPN Hydrogel (Matrigel (Corning Life Sciences, 354230) (**Figures 25A**, **B**) and alginate (FMC

Biopolymer, Protanal® LF 20/40) with cells mixed in Matrigel, control 3D hydrogel (Matrigel only) with cells mixed in (**Figures 25C**, **D**), and 2.5D hydrogel (Matrigel layer with cells added on top) (**Figures 25E**, **F**). Hydrogels were sectioned and immunostained, but they did not remain in the gelatin and appeared "lacey" (**Figure 25G**). The IPN hydrogel immunostaining was unsuccessful. This first test was performed right before the campus closed because of the COVID-19 pandemic.

Bottlebrush polymers

Preliminary tests of Bottlebrush polymers with 5% (**Figures 26A-F**) and 25% (**Figures 26G-L**) concentrations of the polymer mixed with cell culture media resulted in sparse, minimally viable cultures. However, this may have been due to the lack of sterility of the polymers. The viscosity made the polymer challenging to work with. Subsequently, creating a final solution (polymer + media) that had a homogenous viscosity was difficult, even with heating to 37°C. The 25% bottlebrush polymer 2D-culture system was tested with the Nanolive 3D Cell Explorer (**Figure 26N**, **O**) which showed the heterogeneity of the solution**.** Immunocytochemistry results demonstrated viability of many cells in the 25% concentration group, though MAP2 staining resulted in significant background staining, with dominating glia or fibroblast morphologies (**Figure 26M**).

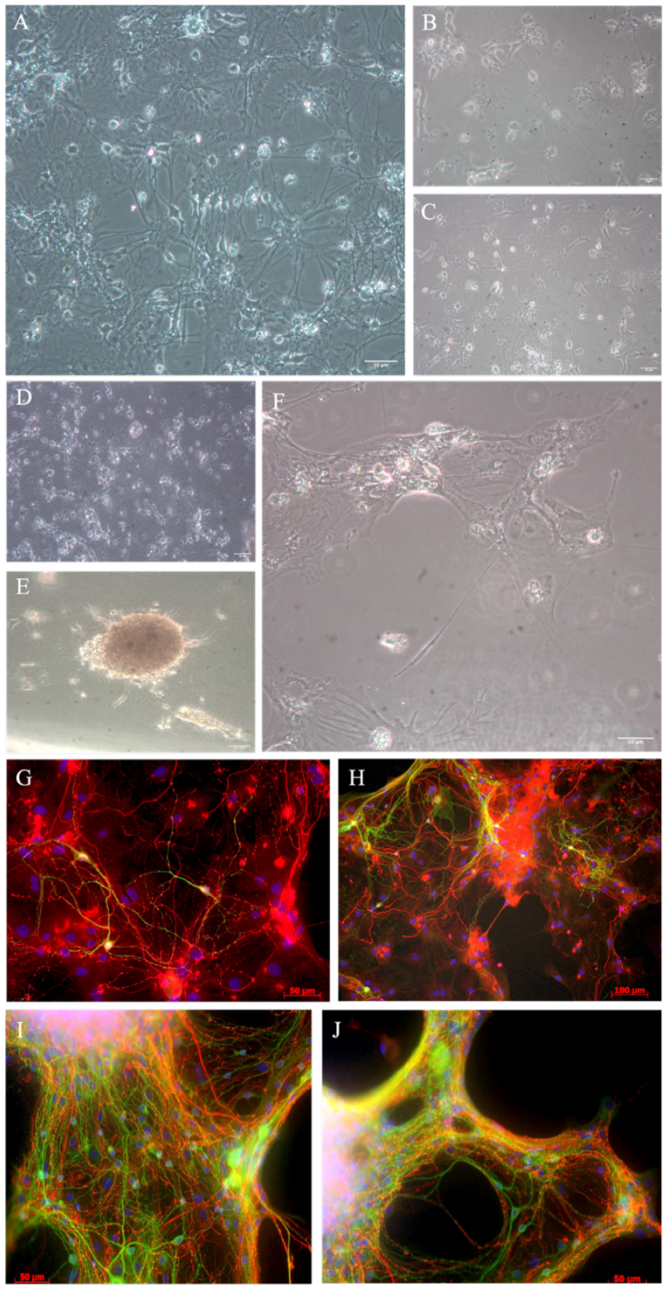

Figure 24 2.5D-Cell Culture **(A)** DIV7 primary brainstem neurons in a 2.5D system: ECM gel (Sigma, E1270-5ML) mixed with NB media before neurons are added (*method 2*). **(B-F)** 2.5D cell culture with primary brainstem neurons plated directly on top of ECM gel (*method 1*) **(B)** DIV1 **(C)** DIV2 **(D)** DIV3 **(E)** DIV4 **(F)** DIV31. Scale bar = 50 µm. **(G**, **H)** 2.5D cultures of primary brainstem neurons at DIV31. Scale bar = 50 µm **(G)**, 100 µm (**H**). **(I**, **J)** 2.D primary brainstem cultures at DIV31. 5-HT red, MAP2 green, DAPI blue. Scale bar = 50 µm. (Note: **(I**, **J)** were part of an experimental group ("scratch") to assess how slight variations in substrate topography may influence culture dynamics).

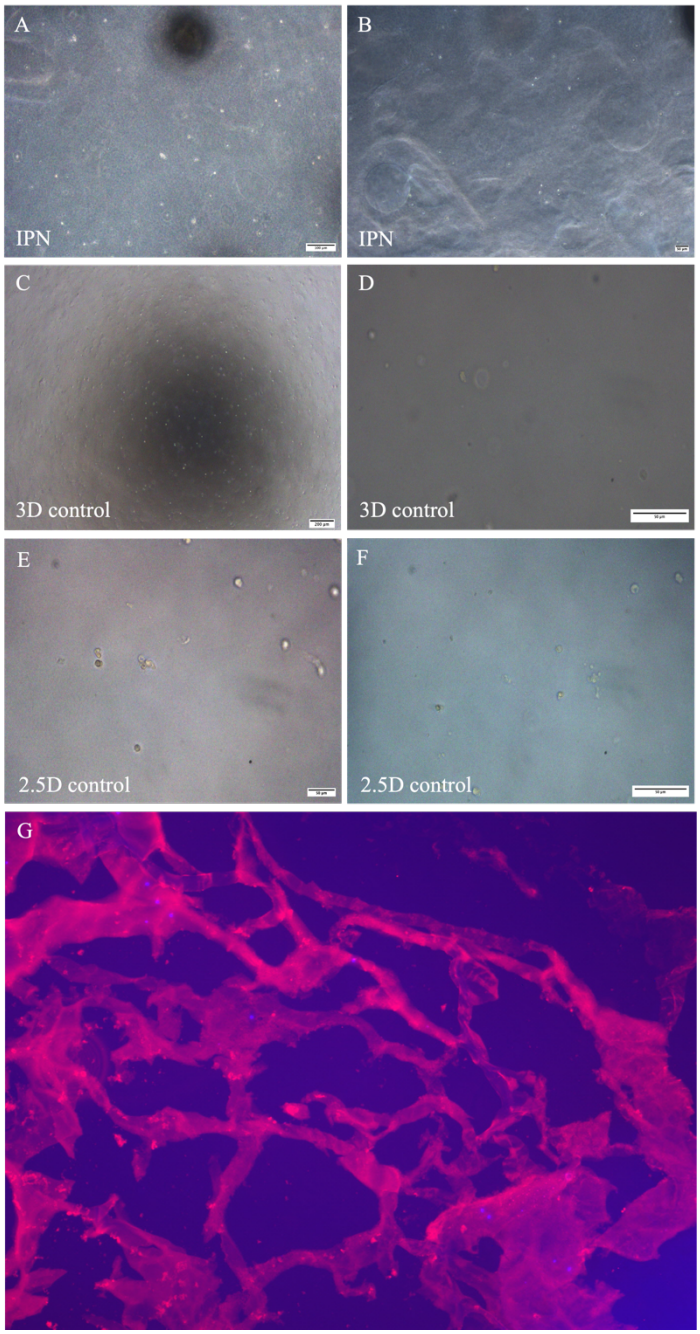

Figure 25 IPN hydrogel **(A)** and **(B)**: 3D-IPN Hydrogel: Matrigel (Corning Life Sciences, 354230) and alginate (FMC Biopolymer, Protanal® LF 20/40) with cells mixed in Matrigel. (**A**- DIV1; **B**- DIV4). (**C**) and **(D)**: 3D hydrogel control (Matrigel only) and cells mixed in Matrigel. (**C**- DIV2; **D**- DIV4). **(E)** and **(F)**: 2.5D control (Matrigel layer with cells added on top. (**E**- DIV2; **F**- DIV4). **(G)** Epifluorescent image of primary brainstem neurons in IPN hydrogel. DAPI (blue); 5-HT (red). (Scale bar = **(A)** 100 µm, **(B**, **D**, **E**, **F)** 50 µm, and **(C)** 200 µm.

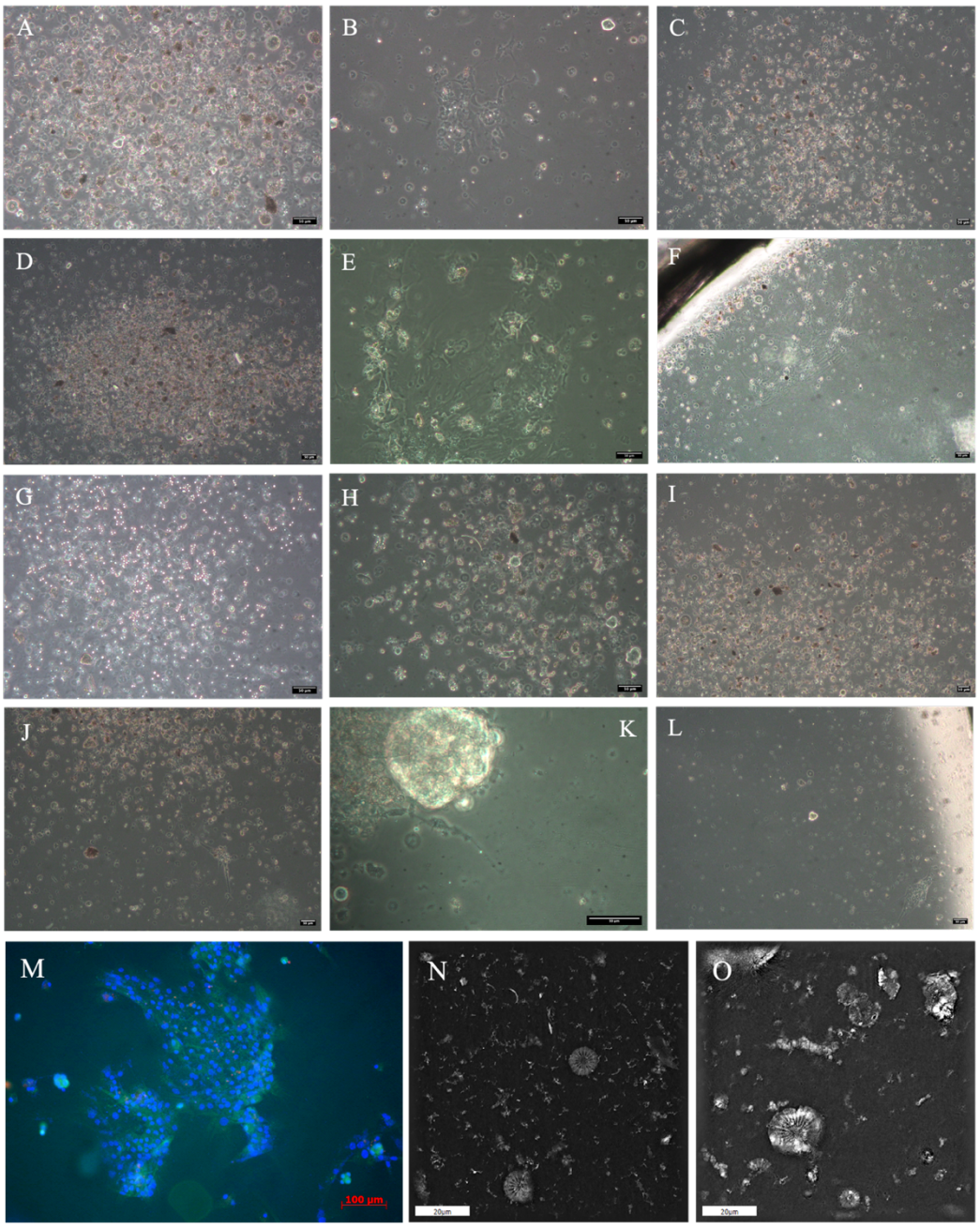

Figure 26 Bottlebrush polymers at 5% (BB 5%) and 25% (BB 25%). **(A-F)** 2D-cell cultures of primary brainstem neurons with media consisting of 5% bottlebrush polymer from the Bates Lab. **(A)** DIV1 **(B)** DIV1.5 **(C)** DIV3 (D) DIV5 **(E)** DIV7 **(F)** DIV8. Scale bar = 50µm. **(G-O)** 2D-cell cultures of primary brainstem neurons with media consisting of 25% bottlebrush polymer from the Bates Lab (UCSB Materials). **(G)** DIV1 **(H)** DIV1.5 **(I)** DIV3 **(J)** DIV5 **(K)** DIV7 **(L)** DIV8. Scale bar = 50µm. **(M)** Epifluorescent image of immunostained 25% bottlebrush polymer in 2D-*in vitro* system with primary brainstem neurons. 5-HT red, MAP2 green, DAPI blue. Scale bar = 100µm. **(N**, **O)** 2D-cell cultures of primary brainstem neurons with media consisting of 25% bottlebrush polymer, imaged with the Nanolive 3D-Cell Explorer Fluo. Scale bar = 20 µm.

VitroGel® 3D-RGD

Three ratios (1:1, 1:2, 1:3, with stiffnesses of 1200-2000 Pa, 600-1000 Pa, 200–500 Pa, respectively (TheWell Bioscience, Inc.) were tested using cNSM as the feeding medium. Despite cells being triturated in cNSM, when this medium was added on top of the hydrogels, there was minimal to no viability in all ratio conditions (**Figures 27A-C**). When cells were triturated with cNSM but mNSM was used as the feeding media, VitroGel-3D RGD hydrogels yielded significantly different results. At both 1:1 and 1:2 ratios, primary brainstem neurons differentiated and grew extensive processes (**Figures 27G-I**). Similarly, VitroGel-3D RGD hydrogels with a 1:3 ratio grew neurons with extensive processes (**Figures 27D-F**). However, viable cells were difficult to image after DIV 3.

VitroGel® Matrix

VitroGel Matrix hydrogel successfully worked as a scaffold conducive to growth for primary brainstem neurons (**Figures 28A-J**). Like VitroGel-3D RGD, health of cells deteriorated after DIV 3. Initial attempts at immunostaining the hydrogels were unsuccessful (**Figures 28K-N**).

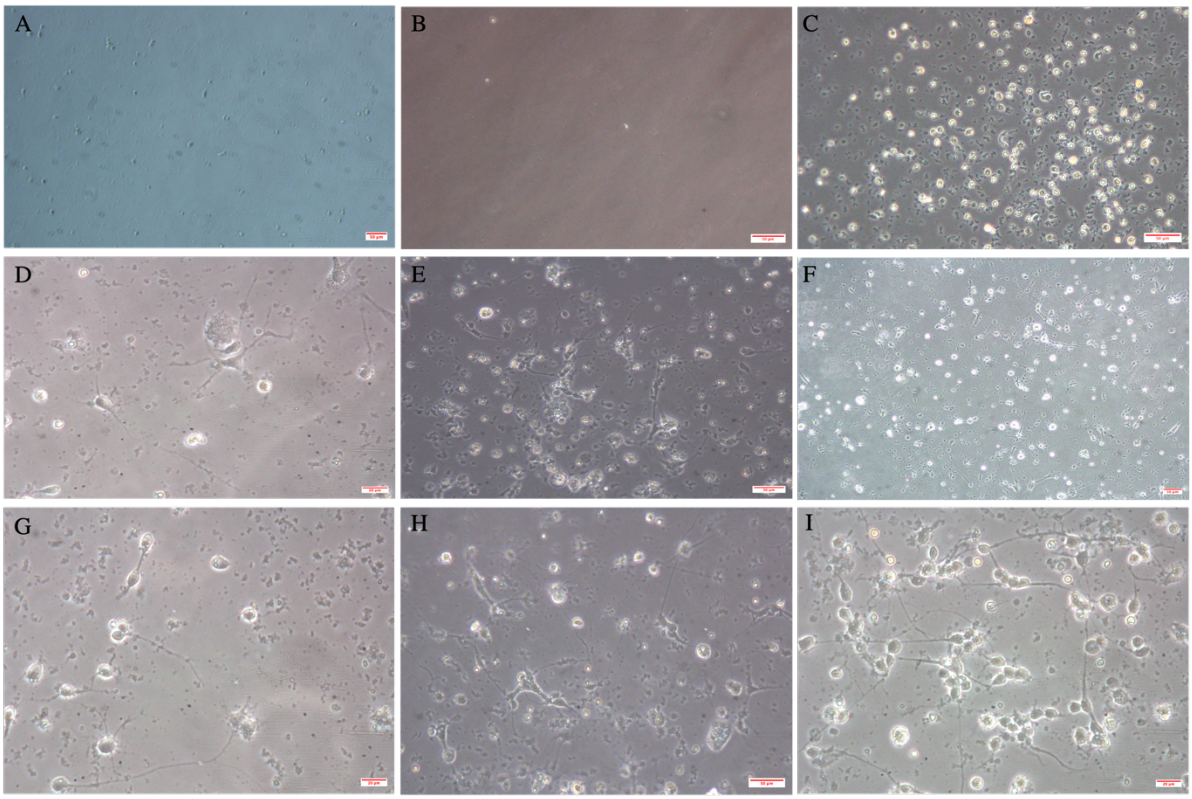

Figure 27 VitroGel-3D RGD **(A-C)** cNSM feeding media did not result in successful hydrogels across all ratio conditions. **(A)** DIV1 image of VitroGel RGD **(1:2)** hydrogel. **(B)** DIV2 image of VitroGel RGD (**1:1**) hydrogel. **(C)** DIV3 VitroGel RGD (**1:3**) hydrogel. Scale bar = 50 µm**. (D-F)** mNSM media was used as the feeding media for VitroGel RGD with a dilution solution ratio of 1:3. Cells quickly developed processes. **(D)** DIV1 image of VitroGel RGD (1:3) hydrogel. **(E)** DIV2 image of VitroGel RGD (1:3) hydrogel. **(F)** DIV3 image of VitroGel RGD (1:3) hydrogel. Scale bar = **(D)** 20 µm, **(E, F)** 50µm. **(G-I)** mNSM media was used as the feeding media at various ratios and cells quickly developed processes. **(G)** DIV1 image of VitroGel RGD (1:1) hydrogel. **(H)** DIV2 image of VitroGel RGD (1:1) hydrogel. **(I)** DIV1 image of VitroGel RGD (1:2) hydrogel. Scale bar = **(G**, **I)** 20 µm, **(H)** 50 µm.

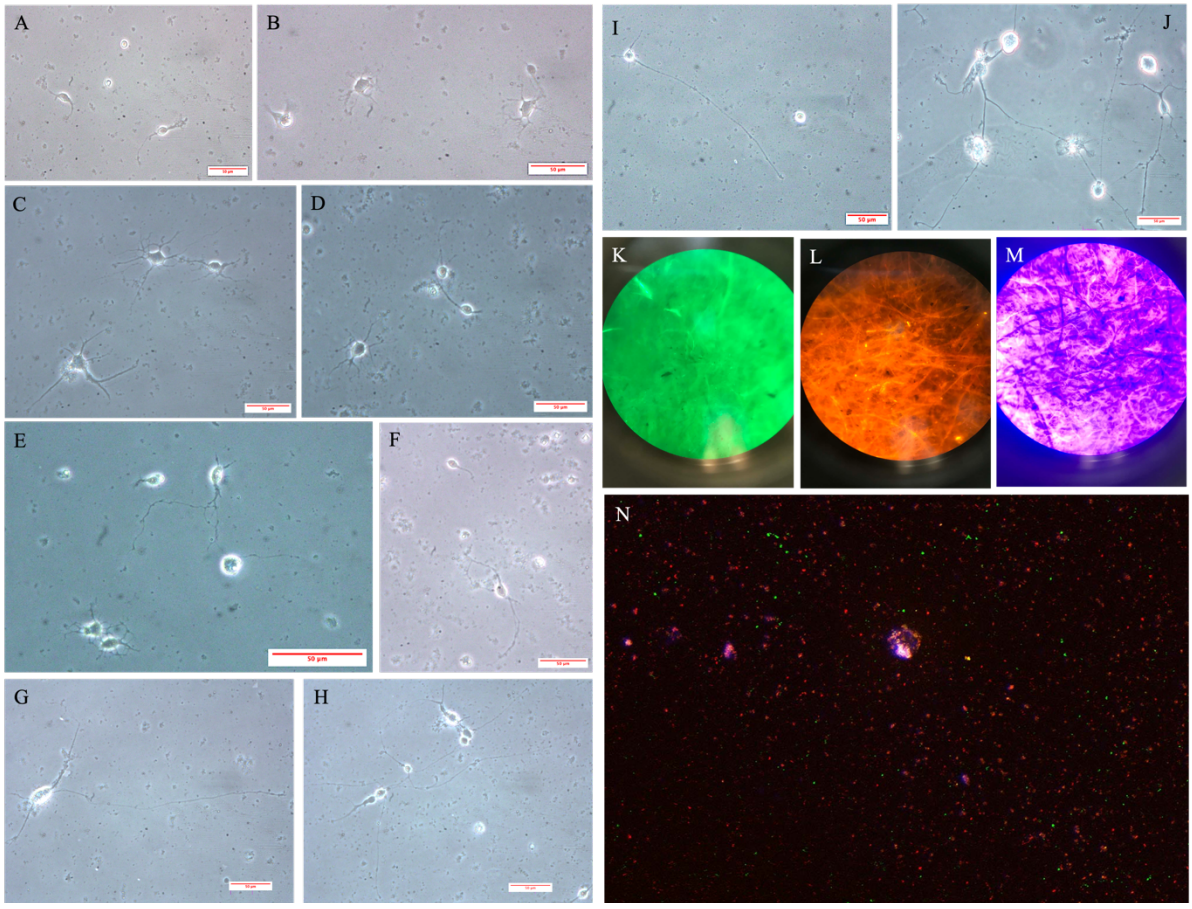

Figure 28 DIV1-DIV3 VitroGel Matrix hydrogels. mNSM media was used for both trituration and feeding media**. (A)** DIV1 VitroGel Matrix hydrogel with 0.001% primocin (Invivogen ant-pm-05) added for yeast. **(B)** DIV1 VitroGel Matrix hydrogel with 0.001%. **(C)** DIV2 VitroGel Matrix hydrogel with 0.001% primocin added as a yeast preventative. NB media was used for both trituration and feeding media. **(D)** DIV2 VitroGel Matrix hydrogel with 0.001% fungicin (Invivogen ant-fn-1) added as a yeast preventative. **(E**, **G**, **H**, **I)** DIV3 VitroGel Matrix hydrogel with 0.001% primocin added as a yeast preventative. **(F)** DIV3 VitroGel Matrix hydrogel with 0.001% fungicin added as a yeast preventative. **(J)** DIV3 2D mono-culture control group. Scale bar = 50 µm. **(K-N)** Epifluorescent images of VitroGel Matrix hydrogel. **(K)** MAP2; 5x magnification **(L)** Cy3; 5x magnification **(M)** DAPI; 5x magnification. **(N)** Confocal image of hydrogel (VitroGel Matrix).

D. Discussion of hydrogel tests

The “2.5D” ECM coating method often differs from methods used with VitroGel or other hydrogels in that the hydrogel solutions are premixed with the cell solution prior to plating and subsequent gelation, while with the ECM coating cells can be added on top or injected within. However, ECM gels can readily be mixed with cells prior to plating, thus rendering them a “3D” model. Therefore, future work can involve mixing the cell solution with the ECM gel prior to plating, like how hydrogel constructs (i.e., VitroGel) are prepared. Instead of simply providing a thicker substrate to resemble the ECM more closely, 2.5D models can also be constructed from micro-pillar and nano-pillar arrays (Sharaf et al., 2022). Such fabrications can result in a more biomimetic effective shear modulus and a greater resemblance to adhesion discrete sites in 3D environments (Sharaf et al., 2022).

Furthermore, future 2.5D work could implement nanofabricated scaffolds to adjust environmental stiffness to ideally provide a more biomimetic *in vitro* environment for modeling primary serotonergic neurons.

In addition to the 2.5D-culture system, we began preliminary testing of three distinct dynamic hydrogel systems with primary serotonergic neurons. We performed preliminary tests of serotonergic neurons in alginate-based IPNs. Alginate-based IPNs are biocompatible and have been used with great success for 3D cell culture and in tissue engineering (Wisdom & Chaudhuri, 2017). Alginate can be used as a tunable, mechanical framework in cell culture systems because it lacks adhesion ligands and is resistant to degradation by mammalian enzymes (Wisdom & Chaudhuri, 2017). Just as in our 2.5D-cultures, Matrigel is a component in the alginate based IPNs. As an IPN, Matrigel and alginate produce

hydrogels with variable stress relaxation rates, stiffness, and protein concentration (Wisdom & Chaudhuri, 2017). Varying the crosslinking density and the alginate chain length permits adjustment of the stiffness and stress relaxation rate across a range that is typical for soft tissue (elastic modulus: 100–20,000 Pa; $t1/2$: 100–10,000 s) (Chaudhuri et al., 2016). Dr. Stower's laboratory (UCSB Mechanical Engineering & Biological Engineering) has employed alginate-based hydrogels in 3D-cell cultures using a variety of cell types, including neural progenitor cells (Lee et al., 2019; Madl et al., 2017; Stowers et al., 2019). While we were unable to examine initial compatibility, these gels may be amenable to real-time cell tracking with confocal microscopy.

An additional variation of 2.5D culture involves cells being sandwiched between stiff tissue culture plastic and soft alginate hydrogel (Pebworth et al., 2014). In this setting, cells have been observed migrating from the underlying stiff substrate into the alginate matrix, effectively demonstrating the utility of the 2.5D culture platform to advance our understanding of the effects of stiffness gradients on adhesion-independent cell migration (Pebworth et al., 2014). The sandwich method can easily be tested by plating cells underneath a layer of ECM gel (Matrigel) and monitoring if primary brainstem neurons are migrating in an adhesion-independent manner similar to human HEK 293 and U87 glioblastoma cells (Pebworth et al., 2014). Furthermore, alginate is already a component of the 3D-IPN hydrogel that was tested with primary brainstem neurons. Since we have demonstrated the success of primary brainstem neurons with Matrigel (the other component of the IPN hydrogel), a possible intermediate step (2.5D) in forming a functional IPN hydrogel *or* a technique utilized with the IPN hydrogel could involve the sandwich method

performed again using the alginate-Matrigel hydrogel. While we did an initial test with the sandwich method and the IPN hydrogel, the results were inconclusive.

Bottlebrush polymers

We evaluated the general viability of primary serotonergic neurons in a second hydrogel platform that provides complementary functionality to the aforementioned alginate-based materials using new polymer building blocks that undergo a **self-assembly** mechanism of gelation (Self et al., 2020). The molecular design of these hydrogels supports a branched "bottlebrush" architecture that contains a long backbone and polymeric sidechains protruding from each repeat unit (Reynolds et al., 2020; Self et al., 2020). Bottlebrush polymers may be excellent 3D scaffolds for serotonergic neurons and axon growth because their softness closely approximates the mechanical properties of brain tissue than do traditional linear polymers (Self et al., 2020). The synthesis of novel bottlebrush copolymers (including statistical copolymers) has been pioneered using ring-opening metathesis polymerization for non-biological applications (Mukherjee et al., 2020; Reynolds et al., 2020; Self et al., 2020). Bottlebrush polymer hydrogels consist of (1) an *adhesion ligand* (e.g., an RGD-peptide) to promote **cell attachment and growth**, (2) *poly (ethylene oxide)* (PEO) for **water solubility**, and (3) *poly(dimethylsiloxane)* (PDMS) that forms **micelles** via the hydrophobic effect (which underlies self-assembly-induced gelation). Importantly, both PEO and PDMS are biocompatible and have been used extensively in cell culture applications (Lecault et al., 2011; Leivo et al., 2017; Naahidi et al., 2017). The

synthesized material for this hydrogel system is inherently tunable since the length of the backbone and the relative ratio of each sidechain can be controlled through synthesis.

Self-assembly is omnipresent in nature at both macro- and microscales; it describes the spontaneous association and organization of numerous individual units into rational and well-defined structures without external participation (Kopeček & Yang, 2012). Apart from environmental conditions (e.g., pH, temperature, ionic strength), surface characteristics influence intermolecular interactions and thus plays an important role in self-assembly (Kopeček & Yang, 2012). The assembly of copolymer micelles is a form of higher-level self-assembly occurring at the nanoscale level where the building blocks are preassembled micelles (Lu et al., 2020). Supported by preliminary data from Dr. Bates's laboratory (UCSB Materials), the bottlebrush copolymers may form micelles in culture media that undergo a liquid-solid phase transition via jamming, which can be exploited to encapsulate serotonergic neurons and their growing axons in three dimensions. Bottlebrush copolymers have a distinct yield stress that corresponds to a structural transition between an ordered solid arrangement and a disordered liquid state of micelles, induced by an applied force (Lu et al., 2020). Optimal compositions that balance solid-like properties and relaxation timescales will be used to incorporate serotonergic neurons by syringe-mixing. Neurons may be able to locally yield and remodel the bottlebrush scaffold as they grow, even if the macroscopic material retains its shape. Further examination of the use of primary serotonergic neurons is necessary including the assessment of 5-HT cell viability, general growth, and long-term survival in this novel bottlebrush hydrogel system. If this synthetic hydrogel system is found to be compatible with primary serotonergic neurons, future uses

may involve unprecedented control over the 3D spatial and temporal growth dynamics of serotonergic fibers via **3D-bioprinting** (Xie et al., 2020).

VitroGel

A study comparing VitroGel 3D-RGD with a competing commercially available ECM-hydrogel system found VitroGel 3D-RGD to be superior for promoting long-term neuronal maturation and survival reporting no significant loss of cell viability (Tomov, 2019). In addition, VitroGel 3D-RGD can be adjusted by seeding with soluble factors in a controlled, reproduceable, and defined manner to resemble the desired environment (Tomov, 2019). This offers the option to eventually enhance the VitroGel 3D-RGD system with soluble factors associated with serotonergic neuron development in the raphe nuclei.
To our knowledge, there are no known publications using VitroGel Matrix with primary neurons. VitroGel Matrix has recently been used in the bioprinting of a human skin substitute with a dermal layer containing xeno-free cultured human endothelial cells, fibroblasts (FBs), pericytes (PCs), in a bioink containing the VitroGel solution, human collagen type I and fibronectin layered in a biocompatible polyglycolic acid mesh and subsequently seeded with xeno-free human keratinocytes to form an epidermal layer (Baltazar et al., 2022). In addition, VitroGel Matrix has been used with *Dictyostelium discoideum* cells as a model for amoeboid movement in different 2D- and 3D-environments, with live-cell microscopy (Ishikawa-Ankerhold et al., 2022). VitroGel Matrix was successfully used in live-cell recordings using a confocal microscope and an inverted Leica DMi8 LED fluorescence microscope (Ishikawa-Ankerhold et al., 2022). Our early

examinations of primary brainstem neurons in various hydrogel models can support in the optimization of *ex vivo* models of the serotonergic matrix.

While advances in polymer chemistry are driving the evolution of sophisticated synthetic–biologic gels, 3D culture of mammalian cells in such microenvironments is not without challenges. For example, Matrigel is broadly used in 3D cell cultures but can show considerable batch-to-batch variability that can affect and its biochemical and mechanical properties. If necessary, cell adhesion peptides can be conjugated directly to the alginate chains (Stowers et al., 2019). In addition, calcium-crosslinking is used in the alginate-Matrigel hydrogels, but calcium signaling is also important in cell physiology. Calcium-crosslinked hydrogels have been successfully used in a variety of cell types, with minimal or undetectable interference with their functions (Chou & Nicoll, 2009; Im et al., 2017; Samorezov et al., 2015; Shoichet et al., 1996). In similar alginate-Matrigel IPNs, the addition of excess calcium in the millimolar range has not impacted cell signaling (Chaudhuri et al., 2014); this concentration is consistent with that of typical cell culture basal media. Furthermore, the bottlebrush copolymers have not yet been thoroughly tested in cell culture systems; regardless, the potential risks are outweighed by the unprecedented potential of these hydrogels to provide a means for *ex vivo* analysis of serotonergic fibers.

VII. Chapter 6: General Discussion

Given the fundamental importance of single fiber trajectories to the self-organization of the serotonergic matrix, further progress in modeling this system crucially depends on the experimental capability to track individual serotonergic axon dynamics in *time* and *space*. Accordingly, there is a high demand for *in vitro* and *ex vivo* models of the CNS that may allow to achieve this goal.

Mechanical properties of neurons

Variations in cell morphology and behavior *in vitro* vs *in vivo* emphasize the significance of developing biomimetic *in vitro* models to study cells in a physiologically relevant context, especially regarding the CNS (Sharaf et al., 2022). Primary brainstem neurons, particularly primary 5-HT neurons, are infrequently studied with few methodological consistencies in existing literature. Further modifications of this *in vitro* model must expand to include deeper considerations of the mechanical properties of these neurons. For example, investigating factors such as the axonal plasticity of 5-HT fibers and the effects of the growth substrate, or adhesion forces and traction stresses generated during axonal extensions, is necessary to further validate the platform.

Neurons and other constituents of nervous tissue (e.g., glial cells, ECM proteins) are heterogeneous, viscoelastic materials. Their mechanical response depends on the timescale, magnitude, and loading rates of the externally applied forces (Lu et al., 2006; O'Toole et al., 2008; Spedden et al., 2012). The outgrowth of neurites from the cell body of a neuron is an intricate process involving interactions with a nonuniform dynamic extracellular

environment (Lowery & Van Vactor, 2009; Wen & Zheng, 2006). Mechanical interactions and physical stimuli play a significant role in processes such as the rearrangements of the cytoskeleton and the generation of traction forces as a result of neurite growth, the adhesion of neurites to ECM proteins, the change in direction and velocity of the growth cone in response to guidance cues, or the axonal navigation through tissues of varying stiffness (Francisco et al., 2007; Franze et al., 2009; Lamoureux et al., 2002; O'Toole et al., 2008; Spedden et al., 2012). Brain tissue is among the softest tissues in the body with a Young's modulus ranging from 0.1 to 1 kPa (Lu et al., 2006; Taliban et al., 2019), whereas the Young's moduli of traditional Petri dishes made of polystyrene or glass are approximately 3 GPa or 70 GPa, respectively (Espinosa-Hoyos et al., 2018; Fekete et al., 2018; Sharaf et al., 2022). Future research should include measurements of stiffness of the presented platform in 2D, 2.5D, and 3D environments to elucidate how environmental geometry is affecting the trajectories and dynamics of primary 5-HT axons. Ultimately, optimal hydrogels will have viscoelastic properties comparable to that of actual neural tissue.

Parameter: substrate coating

It has been previously shown that different substrate conditions, such as surface charge, topography, hydrophobicity or hydrophilicity, surface chemistry, and surface energy may impact cell behavior (Harnett et al., 2007; Liberio et al., 2014). The features of the substrate can also influence the polymerization/conformation of the ECM protein that could present different binding sites to interact with integrins (Liberio et al., 2014). Consequently, the modified cell-substrate interaction can affect the initiation of intracellular signals

(Hocking et al., 1994; Liberio et al., 2014; Morla et al., 1994; Sottile et al., 1998). For example, prior research shows that poly-D-lysine substrates inhibit glial proliferation in chick embryo telencephalon cultures, whereas collagen substrate cultures have resulted in an overgrown glial cell population by DIV12-13 (Azmitia & Whitaker-Azmitia, 1987; Pettmann et al., 1979). Experiments with poly-D-lysine coated culture chambers with hippocampal and raphe co-cultures have shown that hippocampal cells strongly stimulate serotonergic uptake maturation (Azmitia & Whitaker-Azmitia, 1987). Rat hippocampal cells, plated on poly-D-lysine coverslips, show a marked suppression of non-neuronal cells (Banker & Cowan, 1977).

Substrate preference varies by research group, with literature rarely addressing how the choice has been made. However, this seemingly minute detail of cell culture can induce drastic changes in cell dynamics. This is particularly important when considering 5-HT axon dynamics, as primary cultures of midbrain neurons have been shown to have upregulated expression of genes associated with extracellular matrix and adhesion (Greco et al., 2009). Kivell et al. (2000) have reported the most successful and consistent cell attachment and neurite outgrowth of primary brainstem neurons by using poly-D-lysine compared to poly-L-lysine and polyethyleneimine (PEI). Ternaux and Portalier (1993) obtained poor results using poly-ornithine in primary brainstem cultures but found that substrates coated with laminin resulted in better growth of neurons compared to glial cells and a more rapid growth of neurites compared to dissociated cells plated on poly-L-lysine. In addition, the length of neurites was reported to be doubled when primary brainstem neurons were cultured on laminin (Ternaux & Portalier, 1993). Investigating axonal growth rate of 5-HT neurons in

2D-systems using different substrates would provide invaluable information about the influence of the physical environment on the mechanical properties of serotonergic axons. Physiologically relevant *in vitro* models would ideally not have more variation in neurite length and rate of growth than *in vivo* and those that do, should have defined metrics to account for these variations.

Axon extension

Axon extension is a fundamental process, but its interpretation in cell cultures requires caution. For example, in 2D-cell cultures axon growth is thought to strongly depend on adhesion, but adhesion may not be necessary for growth in 3D environments (Santos et al., 2020). Neurons grown with astrocytes in 3D-Matrigel scaffolds have been shown to have a 40-fold lower firing threshold compared to neurons grown in 2D cultures, due to differences in the expression of the voltage-gated sodium channel (Karahuseyinoglu et al., 2021). However, artificially grown axons may not automatically prefer 3D environments over 2D-environments and may incorporate other cues in their decisions (Li and Folch, 2005). The formation and dynamics of axon varicosities also remains poorly understood. Early studies in other systems have suggested that varicosities can form directly from "stopped" growth cones (Hatada et al., 1999), and that their distribution can be described by random point-processes such as the Poison process (Hellwig et al., 1994). More recent studies have shown that varicosities strongly respond to their mechanical and biological environment (Shepherd et al., 2002; Ma et al., 2022) and are generally plastic, including pathological states (Gu, 2021). In the mouse brain, serotonergic axons appear to undergo a

developmental transition from “dot-like” enlargements, with virtually undetectable connections, to a smooth morphology by the end of the first developmental month (Maddaloni et al., 2017). In our cultures derived from early postnatal brains, axons with a continuous smooth morphology typically showed no 5-HT-immunoreactivity or it barely exceeded the background level (e.g., **Figure 13B).** However, some serotonergic axons produced branches that reflected both morphologies, perhaps because of slightly different microenvironments they encountered in the same area (**Figure 20B**). Generally, neuronal cell cultures excel at revealing the entire “behavioral” repertoire of a particular class of neurons and their processes, especially if the neurons are tested in diverse artificial environments – but they do not imply that all of these “behaviors” are realized in the highly specialized environment of natural neural tissue.

Cells can sense the mechanical strength of their surrounding environment (Sharaf et al., 2022) which subsequently influences the discrepancies of morphology, behavior, and genotype observed *in vitro* vs *in vivo*. For example, cancer research has indicated that across various cell culture geometries, only 3D-cell culture with the same cell density as natural tissue shows a drug response analogous to that of a solid tumor (Hsieh et al., 2015; Kapałczyńska et al., 2018). Furthermore, 2D-cultures force cells to rely primarily on focal adhesions for forward traction. Migration in the absence of focal adhesions has recently been observed in 3D-cultures of primary neurons, where cells migrated via cytoskeletal rearrangements in an amoeba-like manner (Pebworth et al., 2014; Renkawitz et al., 2009; Santos et al., 2020). This amoeboid-like migration begins with the formation of sizeable blebs, or rounded membrane protrusions, which squeeze and flow through fibers and pores;

thus, allowing for cell migration via purely mechanical means (Guck et al., 2010; Pebworth et al., 2014). Developing a scaffold capable of allowing cells to receive stimuli from the local environment as it would happen *in vivo* is particularly important when studying the serotonergic matrix, a system crucial to neuroplasticity, that also exhibits inherent characteristics of axonal plasticity.

3D

Any specific changes in 5-HT fiber dynamics that may exist between 2D- vs 3D-systems is relatively unexplored. Only recently have 5-HT axons been explored in the context of hydrogel systems. Traumatic spinal cord injuries (SCI) frequently result in tissue defects, such as the formation of cystic spaces, which severely inhibits axonal regeneration due to a lack of the proteinaceous ECM (Park et al., 2022; Shechter & Schwartz, 2013; Spector & Lim, 2016). Outside of the CNS, wound healing is characterized by the neovascularization and the deposition of fibrotic matrix, which if unchecked, becomes scar tissue consisting of excessive fibrosis, ultimately hindering proper repair or regeneration (Eming et al., 2014; Park et al., 2022). Hong et al. (2017) developed a natural ECM biopolymer (chondroitin sulphate and gelatin)-based hydrogel containing polypyrrole, that showed mechanical (~928 Pa) and conductive properties (4.49 mS/cm) like natural spinal cord tissues. Furthermore, the hydrogels displayed shear-thinning and self-healing abilities, which allows it to be effectively injected into the injury site and to fill the lesion cavity to accelerate the tissue repair of traumatic SCI (Hong et al., 2017).

The hydrogel efficiently replaced cystic cavities with fibrotic matrix, which promoted functional recovery and attenuated degenerative pathology (Hong et al., 2017; Park et al., 2022). However, recent studies suggest that excessive fibrosis following SCI profoundly inhibits axonal regeneration (Park et al., 2022; Sofroniew, 2021; Zhu et al., 2015). To examine if the excessive accumulation of the fibrotic matrix in the developed hydrogel could hinder axonal growth from the brain into the hydrogel-created matrix, Park et al. (2022) augmented the hydrogel by modifying the fibrotic microenvironment with a chondroitin sulfate proteoglycan (CSPG)-degrading enzyme (CSPGs are produced by astrocytes and macrophages, and contribute to fibrotic scar formation). Indeed, such modifications rendered the hydrogel-created ECM inhospitable to regenerating 5-HT axons in contusion injury model rats injected with the hydrogel. Regenerating 5-HT axons rarely entered the central region within the fibrotic ECM and became confined to a region near the matrix border and spared spinal cord (Park et al., 2022).

Park et al. (2022) further modified the hydrogel by alleviating the fibrotic microenvironment with arylsulfatase B (ARSB). ARSB-modifications resulted in a hydrogel environment favorable to regenerating axons as 5-HT axons were able to grow deeper to the central areas of the matrix. In addition, animals injected with the ARSB-modified hydrogel demonstrated improved 5-HT axonal innervation in the ventral motor regions as well as the intermediate gray matter in the lumbar spinal cord, with this increase in innervation being correlated with locomotor recovery (Park et al., 2022).

In our preliminary IPN hydrogel test, it is possible that we did not see any axons due to the fibrotic appearance of the gel, rendering it inhospitable to growing axons. During the

formation of most IPN systems, a phase separation occurs, due to the chemically different structure of the components forming the IPNs (Zoratto & Matricardi, 2018). Unfortunately, this leads to the development of a heterogeneous structure, which was visible in our initial imaging test. However, the process of separation proceeds very slowly due to the high viscosity of the system and to entanglements between chains (Zoratto & Matricardi, 2018). Future work with the IPN system should incorporate the most powerful method in the investigation of viscoelastic properties of polymeric systems: dynamic mechanical spectroscopy (DMS), which enables the estimation of the elastic moduli, mechanical losses, glass transition temperature, and relaxation characteristics of IPN and semi-IPNs (Zoratto & Matricardi, 2018). Similarly, initial immunostaining of our VitroGel hydrogels emphasized the fibrotic nature of this system. Nevertheless, VitroGels® are becoming the preferred material for 3D-systems, compared to Matrigel, which not only has an animal origin but also significant batch-to-batch variability (Cherne et al., 2021; Hakuno et al., 2022). Future research should continue to explore the VitroGel hydrogel mixes, included the most recent, VitroGel® ORGANOID 1–4 (#VHM04-K, TheWell Bioscience, NJ), which has been found to support cultures of gastric organoids within an MPS (Cherne et al., 2021).

Future directions

Future applications of this platform are contingent upon identifying 5-HT neurons in living cell cultures. Once a reliable method of 5-HT neuron identification is available, the platform can be further expanded to include microphysiological systems (MPSs), and further validated by testing 5-HT axon behavior in response to various extracellular factors with

well-established effects on 5-HT axons (i.e., 5-HT, FLX, etc.). These devices have expanded experimental capabilities for studying axonal guidance through precise control of microenvironments and provide novel opportunities to create *in vitro* physiological and pathophysiologically relevant models (Holloway et al., 2021; Martins et al., 2017).

We have done preliminary testing to isolate serotonergic neurons from primary brainstem cultures in the XonaChips® (Xona Microfluidics) device. These devices typically consist of 4 wells, with 2 of the wells connected by a channel on each side of the device (Darbinyan et al., 2013). Channels are then connected by microgrooves, which are sized so that cell bodies cannot pass through, allowing only the passage of extending neurites (Darbinyan et al., 2013) (**Figure 29**).

A reliable method for 5-HT neuron identification *in vitro* will additionally assist in examining substrate influence on 5-HT axon dynamics and extend the applications of HTM. Live tracking in *in vitro* systems with controlled fiber densities can provide key insights into the formerly described dynamical characteristics of serotonergic axons, including their dependence on the physical properties of the environment. With HTM, we can also quantify subcellular dynamics in growth cones and along serotonergic axons. To date, there have been few prior observations of primary neurons using holotomography and no published data are available in serotonergic neurons. Only recently has HTM been successfully used to examine the timeline of fine-scale morphological changes in undifferentiated primary cortical neurons after exposure to neurite stimulation media (Nanolive, 2020). In a sample study of primary cortical neurons conducted by a company specializing in HTM imaging (Nanolive), researchers were able to quantify the dynamic behavior of individual growth

cones using digital staining that tracked the dry mass of neurites (Nanolive, 2020). Importantly, details such as fine protrusions, spines, and varicosities were captured with high accuracy, and changes in neurite volume and shape were detected with high precision (Nanolive, 2020). Thus, HTM provides a means to examine the biophysical components of how axonal growth cones detect and interpret extracellular signals in their environment.

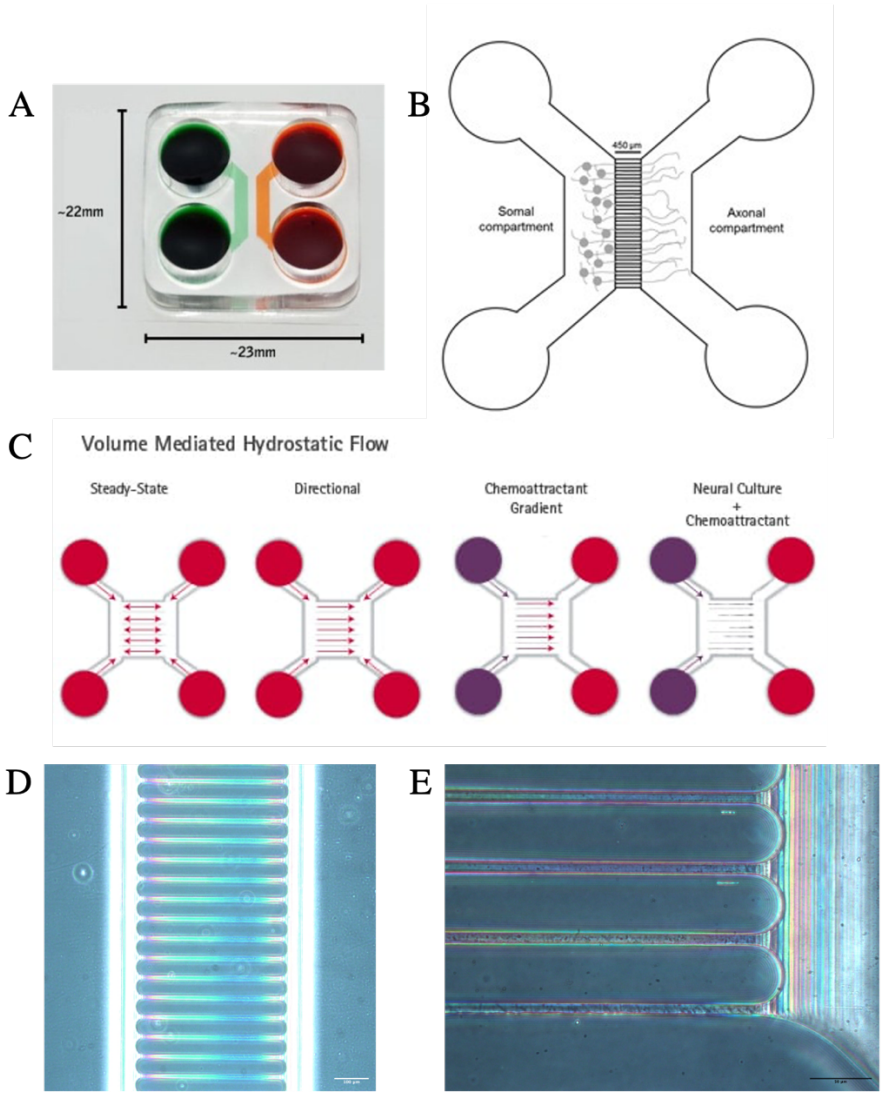

Figure 29 Overview of microfluidic devices used to isolate axons. **(A)** Microfluidic devices for axon isolation such as the Standard Neuron Device (XONA MICROFLUIDICS INC SND900) shown here are typically composed of two wells and an interconnected channel, separated by a set of microgrooves. From (*Fisher Scientific*). **(B)** Representative model of a microfluidic chamber. From (Martins et al., 2017). **(C)** Neuron filaments can grow outwards in response to axon guidance cues. Depending on the device used, hydrostatic pressure formed by volume differential between chambers induces fluidic isolation of the solution on the low volume side of the device. This can allow for development and maintenance of a fluidic gradient of chemoattractants, toxins or other molecules of interest, facilitating controlled exposure and differentiation of axons. (From *MilliporeSigma*). **(D**, **E)** Our first test of the XONA device 'XC450'. (E) The image shows the channels where axons get restricted to. In this particular example, remnants of debris are visible as image was taken immediately after cells were added to appropriate well. Scale bar is **(D)** 100 µm and **(E)** 50 µm.

Modeling the serotonergic system

The self-organization of serotonergic fibers depends in part on the spatiotemporal structure of their individual trajectories. The proposed platform can be used to obtain experimental data necessary to validate the mathematical models of these processes. Stochastic phenomena characterize many processes involved in neuronal growth, including neuron-neuron signaling, fluctuating weak environmental biochemical cues, biochemical reactions taking place in the growth cones, formation of lamellipodia and filopodia, and polymerization rates of microtubules and actin filaments (Yurchenko et al., 2019). Stochastic properties can be used to model both *single neuron* behavior involving the biophysical and biochemical mechanisms underlying synaptic neurotransmission and neuronal excitability (Saarinen et al., 2006), as well as *axon interactions within growing neuronal populations* (i.e., the serotonergic matrix) (Razetti et al., 2018). Our laboratory has recently introduced a novel mathematical framework to capture some of the essential properties of serotonergic axons (Janusonis et al., 2020; Janusonis et al., 2019; Vojta et al., 2020). Consistent with this framework, findings from the presented research of individual serotonergic fibers can be interpreted as paths of spatial stochastic processes.

A random walk based on the von Mises-Fisher distribution

The first model assumes that fibers perform a step-wise (discrete) random walk (Janusonis & Detering, 2019), where the direction of each step is described by a well-defined probability distribution. A fiber can be modeled as a random walk and represented as a sequence of points. Given the direction of the fiber, its extension is modeled by obtaining the next direction from the von Mises-Fisher probability distribution (on the unit

sphere) and calculating the next coordinates. The probability density is parametrized with the "concentration parameter" (Janusonis & Detering, 2019; Jupp & Mardia, 2009). Small values of this parameter reflect higher tortuosity, whereas large values reflect more rigid behavior. Computer simulations show that changes in the concentration parameter can ultimately result in significant differences in fiber density, demonstrating how the local behavior of an individual fiber can influence the overall fiber density in a particular brain region (Janusonis & Detering, 2019; Janusonis et al., 2019).

Fractional Brownian motion

The second model can also produce trajectories that closely resemble those of actual serotonergic fibers, but it assumes that fibers are sample paths of fractional Brownian motion (FBM) (Janusonis et al., 2020). This model is particularly suitable for analyses in which high-resolution temporal information is available, such as in the proposed project. It is likely to more accurately reflect the time-continuous but "jittery" dynamics of membrane extension during axon growth (Janušonis et al., 2020).

Theoretically, FBM is an extension of the normal Brownian motion (BM). The strength of the correlation between non-overlapping increments is determined by the Hurst index (H), which defines two different FBM regimes: subdiffusion ($0 < H < 1/2$, in which two neighboring increments are negatively correlated, producing "back-and-forth," "anti-persistent" trajectories) and superdiffusion (If $1/2 < H < 1$, in which two neighboring increments are positively correlated, which produces "persistent" trajectories that maintain their current direction) (Janušonis et al., 2020; Vojta et al., 2020). Serotonergic fibers are

considerably less “jittery” than BM and tend to maintain their current direction, so they can be modeled with superdiffusive FBM.

This model shows individual serotonergic fibers as paths of a stochastic process that reflects their physical properties and shows that regional arborization or other local control is not necessary to arrive at a good approximation of the observed fiber densities (Janusonis et al., 2020). Instead, these densities may strongly depend on the geometry of the brain. FBM has four fitting properties that make it a natural choice in this context (Janusonis et al., 2020). First, it is a continuous process, which is consistent with the time-continuity of axon growth. Second, it has stationary increments, meaning that its statistical properties do not change as the process evolves (this assumption is reasonable from the biological perspective). Third, it is a self-similar process, which ensures that the estimation of H does not depend on the discretization grid of experimental observations. Since time-dependent information is difficult to obtain in growing fibers (e.g., with time-lapse imaging in live animals; Jin et al., 2016), this property ensures robustness. Fourth, its increments are normally distributed. If randomness in the fiber trajectory arises from collision-like events in its microenvironment and each of these events has a small effect on the trajectory, the total effect of these collisions inevitably leads to a normal distribution (by the Central Limit Theorem) (Janusonis et al., 2020). Notably, FBM is the only stochastic process with all of these properties (assuming mean-zero increments) (Janusonis et al., 2020).

It is possible that varicosity behavior may impact the estimates of the Hurst index (H), as the emergence of varicosities may be associated with time periods in which the next

displacement of the advancing fiber happens to be small, due to the “jittery” and stochastic nature of the FBM process (Janusonis et al., 2020).

VIII. Chapter 7: Conclusion

The ability to produce *in vitro* 2D-cultures of neuronal cells has been fundamental in advancing understanding of *in vivo* cell behaviors, such as migration, growth, and mechanics (Duval et al., 2017). While serotonergic axons are typically studied regarding their collective and regionally specific densities, 2D-cell culture permits observation of single axon dynamics. However, visualizing this dynamic behavior *in vivo* is currently extremely difficult. Recent technological innovations (e.g., digital holotomography, 3D-cell culture systems, STED- super resolution microscopy) have changed the way complex neuronal systems can be studied and offer promising alternatives to *in vivo* approaches. We developed an *in vitro* model to study the dynamics of primary serotonergic axons and collected the first holotomographic images and recordings of primary brainstem neurons in culture at high spatial and temporal resolution. We additionally performed the first compatibility tests of FFNs (Henke et al., 2018) in dissociated cultures of primary brainstem neurons and began compatibility testing in both natural and synthetic hydrogel systems. The presented research introduced the development of an *ex vivo* platform to experimentally investigate serotonergic neurons and their axons with unprecedented spatiotemporal precision. These experimental data will provide crucial information for the current computational models that have the potential to predict regional fiber densities in the healthy and diseased brain. The rapid expansion of the currently available toolbox, including approaches developed in our research program (holotomography of primary brainstem cultures, advanced stochastic modeling, supercomputing simulations), promises to produce a radically new view of the serotonergic system, both at the structural and functional levels.

Adams, J. C., & Watt, F. M. (1993). Regulation of Development and Differentiation by the Extracellular-Matrix. *Development*, *117*(4), 1183-1198. <Go to ISI>://WOS:A1993LD08900001

Adell, A., Celada, P., Abellan, M. T., & Artigas, F. (2002). Origin and functional role of the extracellular serotonin in the midbrain raphe nuclei. *Brain Res Brain Res Rev*, *39*(2-3), 154-180. https://doi.org/10.1016/s0165-0173(02)00182-0

Adell, A., Sarna, G. S., Hutson, P. H., & Curzon, G. (1989). An *in vivo* dialysis and behavioural study of the release of 5-HT by p-chloroamphetamine in reserpine-treated rats. *Br J Pharmacol*, *97*(1), 206-212. https://doi.org/10.1111/j.1476-5381.1989.tb11943.x

Aggarwal, B. B., Danda, D., Gupta, S., & Gehlot, P. (2009). Models for prevention and treatment of cancer: problems vs promises. *Biochem Pharmacol*, *78*(9), 1083-1094. https://doi.org/10.1016/j.bcp.2009.05.027

Agnati, L. F., & Fuxe, K. (2014). Extracellular-vesicle type of volume transmission and tunnelling-nanotube type of wiring transmission add a new dimension to brain neuro-glial networks. *Philos Trans R Soc Lond B Biol Sci*, *369*(1652). https://doi.org/10.1098/rstb.2013.0505

Alonso, A., Merchán, P., Sandoval, J. E., Sánchez-Arrones, L., Garcia-Cazorla, A., Artuch, R., Ferrán, J. L., Martínez-de-la-Torre, M., & Puelles, L. (2013). Development of the serotonergic cells in murine raphe nuclei and their relations with rhombomeric domains. *Brain Struct Funct*, *218*(5), 1229-1277. https://doi.org/10.1007/s00429-012-0456-8

Arai, R., Karasawa, N., Kurokawa, K., Kanai, H., Horiike, K., & Ito, A. (2002). Differential subcellular location of mitochondria in rat serotonergic neurons depends on the presence and the absence of monoamine oxidase type B. *Neuroscience*, *114*(4), 825-835. https://doi.org/10.1016/s0306-4522(02)00351-2

Arigony, A. L. V., de Oliveira, I. M., Machado, M., Bordin, D. L., Bergter, L., Prá, D., & Pegas Henriques, J. A. (2013). The influence of micronutrients in cell culture: a reflection on viability and genomic stability. *BioMed research international*, *2013*.

Aswathy, S. H., Narendrakumar, U., & Manjubala, I. (2020). Commercial hydrogels for biomedical applications. *Heliyon*, *6*(4), e03719. https://doi.org/https://doi.org/10.1016/j.heliyon.2020.e03719

An award to oxygen sensing. (2019). *Nature Biomedical Engineering*, *3*(11), 843-844. https://doi.org/10.1038/s41551-019-0479-z

Awasthi, J. R., Tamada, K., Overton, E. T. N., & Takumi, T. (2021). Comprehensive topographical map of the serotonergic fibers in the male mouse brain. *J Comp Neurol*, *529*(7), 1391-1429. https://doi.org/10.1002/cne.25027

Azmitia, E. C. (1978). The Serotonin-Producing Neurons of the Midbrain Median and Dorsal Raphe Nuclei.

Azmitia, E. C. (2001). Neuronal instability: implications for Rett's syndrome. *Brain Dev*, *23 Suppl 1*, S1-S10. https://doi.org/10.1016/s0387-7604(01)00368-0

Azmitia, E. C., Dolan, K., & Whitaker-Azmitia, P. M. (1990). S-100B but not NGF, EGF, insulin or calmodulin is a CNS serotonergic growth factor. *Brain Res*, *516*(2), 354-356. https://doi.org/10.1016/0006-8993(90)90942-5

Azmitia, E. C., & Gannon, P. J. (1986). The primate serotonergic system: a review of human and animal studies and a report on Macaca fascicularis. *Adv Neurol*, *43*, 407-468.

Azmitia, E. C., Singh, J. S., & Whitaker-Azmitia, P. M. (2011). Increased serotonin axons (immunoreactive to 5-HT transporter) in postmortem brains from young autism donors. *Neuropharmacology*, *60*(7-8), 1347-1354. https://doi.org/10.1016/j.neuropharm.2011.02.002

Azmitia, E. C., & Whitaker-Azmitia, P. M. (1987). Target cell stimulation of dissociated serotonergic neurons in culture. *Neuroscience*, *20*(1), 47-63. https://doi.org/10.1016/0306-4522(87)90005-4

Baker, K. G., Halliday, G. M., Halasz, P., Hornung, J. P., Geffen, L. B., Cotton, R. G., & Törk, I. (1991). Cytoarchitecture of serotonin-synthesizing neurons in the pontine tegmentum of the human brain. *Synapse*, *7*(4), 301-320. https://doi.org/10.1002/syn.890070407

Baker, K. G., Halliday, G. M., & Törk, I. (1990). Cytoarchitecture of the human dorsal raphe nucleus. *J Comp Neurol*, *301*(2), 147-161. https://doi.org/10.1002/cne.903010202

Baltazar, T., Jiang, B., Moncayo, A., Merola, J., Albanna, M. Z., Saltzman, W. M., & Pober, J. S. (2022). 3D bioprinting of an implantable xeno-free vascularized human skin graft. *Bioengineering & Translational Medicine*. https://doi.org/ARTN e10324 10.1002/btm2.10324

Bang, S. J., Jensen, P., Dymecki, S. M., & Commons, K. G. (2012). Projections and interconnections of genetically defined serotonin neurons in mice. *European Journal of Neuroscience*, *35*(1), 85-96. https://doi.org/10.1111/j.1460-9568.2011.07936.x

Banker, G. A., & Cowan, W. M. (1977). Rat Hippocampal Neurons in Dispersed Cell-Culture. *Brain Research*, *126*(3), 397-425. https://doi.org/Doi 10.1016/0006-8993(77)90594-7

Barettino, C., Ballesteros-Gonzalez, A., Aylon, A., Soler-Sanchis, X., Orti, L., Diaz, S., Reillo, I., Garcia-Garcia, F., Iborra, F. J., Lai, C. R. Y., Dehorter, N., Leinekugel, X., Flames, N., & Del Pino, I. (2021). Developmental Disruption of Erbb4 in Pet1+ Neurons Impairs Serotonergic Sub-System Connectivity and Memory Formation. *Frontiers in Cell and Developmental Biology*, *9*. https://doi.org/ARTN 770458 10.3389/fcell.2021.770458

Bauman, M. D., & Amaral, D. G. (2005). The distribution of serotonergic fibers in the macaque monkey amygdala: An immunohistochemical study using antisera to 5-hydroxytryptamine. *Neuroscience*, *136*(1), 193-203. https://doi.org/https://doi.org/10.1016/j.neuroscience.2005.07.040

Baust, J. M., Buehring, G. C., Campbell, L., Elmore, E., Harbell, J. W., Nims, R. W., Price, P., Reid, Y. A., & Simione, F. (2017). Best practices in cell culture: an overview. *In Vitro Cellular & Developmental Biology - Animal*, *53*(8), 669-672. https://doi.org/10.1007/s11626-017-0177-7

Bellon, A., & Mann, F. (2018). Keeping up with advances in axon guidance. *Current opinion in neurobiology*, *53*, 183-191. https://doi.org/https://doi.org/10.1016/j.conb.2018.09.004

Belmer, A., Beecher, K., Jacques, A., Patkar, O. L., Sicherre, F., & Bartlett, S. E. (2019). Axonal Non-segregation of the Vesicular Glutamate Transporter VGLUT3 Within Serotonergic Projections in the Mouse Forebrain [Original Research]. *Frontiers in Cellular Neuroscience*, *13*(193). https://doi.org/10.3389/fncel.2019.00193

Benarroch, E. E. (2015). Brain-derived neurotrophic factor Regulation, effects, and potential clinical relevance. *Neurology*, *84*(16), 1693-1704. https://doi.org/10.1212/Wnl.0000000000001507

Benzekhroufa, K., Liu, B., Tang, F., Teschemacher, A. G., & Kasparov, S. (2009). Adenoviral vectors for highly selective gene expression in central serotonergic neurons reveal quantal characteristics of serotonin release in the rat brain. *Bmc Biotechnology*, *9*(1), 23. https://doi.org/10.1186/1472-6750-9-23

Berger, M., Gray, J. A., & Roth, B. L. (2009). The expanded biology of serotonin. *Annu Rev Med*, *60*, 355-366. https://doi.org/10.1146/annurev.med.60.042307.110802

Berthiaume, F., Moghe, P. V., Toner, M., & Yarmush, M. L. (1996). Effect of extracellular matrix topology on cell structure, function, and physiological responsiveness:

hepatocytes cultured in a sandwich configuration. *FASEB J*, *10*(13), 1471-1484. https://doi.org/10.1096/fasebj.10.13.8940293

Bershadsky, A. D., Balaban, N. Q., & Geiger, B. (2003). Adhesion-dependent cell mechanosensitivity. *Annual Review of Cell and Developmental Biology*, *19*, 677-695. https://doi.org/10.1146/annurev.cellbio.19.111301.153011

Birgersdotter, A., Sandberg, R., & Ernberg, I. (2005). Gene expression perturbation in vitro--a growing case for three-dimensional (3D) culture systems. *Semin Cancer Biol*, *15*(5), 405-412. https://doi.org/10.1016/j.semcancer.2005.06.009

Bissell, M. J., Rizki, A., & Mian, I. S. (2003). Tissue architecture: the ultimate regulator of breast epithelial function. *Current Opinion in Cell Biology*, *15*(6), 753-762. https://doi.org/10.1016/j.ceb.2003.10.016

Bomze, H. M., Bulsara, K. R., Iskandar, B. J., Caroni, P., & Skene, J. H. (2001). Spinal axon regeneration evoked by replacing two growth cone proteins in adult neurons. *Nat Neurosci*, *4*(1), 38-43. https://doi.org/10.1038/82881

Breslin, S., & O'Driscoll, L. (2013). Three-dimensional cell culture: the missing link in drug discovery. *Drug Discov Today*, *18*(5-6), 240-249. https://doi.org/10.1016/j.drudis.2012.10.003

Buchanan, J., Sun, Y. A., & Poo, M. M. (1989). Studies of nerve-muscle interactions in Xenopus cell culture: fine structure of early functional contacts. *J Neurosci*, *9*(5), 1540-1554. https://www.ncbi.nlm.nih.gov/pubmed/2723740

Bunin, M. A., Prioleau, C., Mailman, R. B., & Wightman, R. M. (1998). Release and uptake rates of 5-hydroxytryptamine in the dorsal raphe and substantia nigra reticulata of the rat brain. *J Neurochem*, *70*(3), 1077-1087. https://doi.org/10.1046/j.1471-4159.1998.70031077.x

Burry, R. W. (1986). Presynaptic elements on artificial surfaces. A model for the study of development and regeneration of synapses. *Neurochem Pathol*, *5*(3), 345-360. https://doi.org/10.1007/BF02842943

Busch, S. A., Horn, K. P., Silver, D. J., & Silver, J. (2009). Overcoming macrophage-mediated axonal dieback following CNS injury. *J Neurosci*, *29*(32), 9967-9976. https://doi.org/10.1523/jneurosci.1151-09.2009

Calizo, L. H., Akanwa, A., Ma, X., Pan, Y. Z., Lemos, J. C., Craige, C., Heemstra, L. A., & Beck, S. G. (2011). Raphe serotonin neurons are not homogenous: electrophysiological, morphological, and neurochemical evidence.

Neuropharmacology, *61*(3), 524-543. https://doi.org/10.1016/j.neuropharm.2011.04.008

Camand, E., Morel, M. P., Faissner, A., Sotelo, C., & Dusart, I. (2004). Long-term changes in the molecular composition of the glial scar and progressive increase of serotoninergic fibre sprouting after hemisection of the mouse spinal cord. *Eur J Neurosci*, *20*(5), 1161-1176. https://doi.org/10.1111/j.1460-9568.2004.03558.x

Cao, L., Hu, R., Xu, T., Zhang, Z. N., Li, W., & Lu, J. (2017). Characterization of Induced Pluripotent Stem Cell-derived Human Serotonergic Neurons. *Front Cell Neurosci*, *11*, 131. https://doi.org/10.3389/fncel.2017.00131

Carhart-Harris, R. L., & Nutt, D. J. (2017). Serotonin and brain function: a tale of two receptors. *Journal of psychopharmacology (Oxford, England)*, *31*(9), 1091-1120. https://doi.org/10.1177/0269881117725915

Carrera, I., Molist, P., Anadon, R., & Rodriguez-Moldes, I. (2008). Development of the serotoninergic system in the central nervous system of a shark, the lesser spotted dogfish Scyliorhinus canicula. *J Comp Neurol*, *511*(6), 804-831. https://doi.org/10.1002/cne.21857

Casanova, M. F., van Kooten, I. A., Switala, A. E., van Engeland, H., Heinsen, H., Steinbusch, H. W., Hof, P. R., Trippe, J., Stone, J., & Schmitz, C. (2006). Minicolumnar abnormalities in autism. *Acta Neuropathol*, *112*(3), 287-303. https://doi.org/10.1007/s00401-006-0085-5

Catoira, M. C., Fusaro, L., Di Francesco, D., Ramella, M., & Boccafoschi, F. (2019). Overview of natural hydrogels for regenerative medicine applications. *Journal of Materials Science: Materials in Medicine*, *30*(10), 115. https://doi.org/10.1007/s10856-019-6318-7

Cawkill, D., & Eaglestone, S. S. (2007). Evolution of cell-based reagent provision. *Drug Discov Today*, *12*(19-20), 820-825. https://doi.org/10.1016/j.drudis.2007.08.014

Celada, P., Siuciak, J. A., Tran, T. M., Altar, C. A., & Tepper, J. M. (1996). Local infusion of brain-derived neurotrophic factor modifies the firing pattern of dorsal raphe serotonergic neurons. *Brain Research*, *712*(2), 293-298. https://doi.org/Doi 10.1016/0006-8993(95)01469-1

Chaudhuri, O., Gu, L., Klumpers, D., Darnell, M., Bencherif, S. A., Weaver, J. C., Huebsch, N., Lee, H.-P., Lippens, E., Duda, G. N., & Mooney, D. J. (2016). Hydrogels with tunable stress relaxation regulate stem cell fate and activity. *Nature materials*, *15*(3), 326-334. https://doi.org/10.1038/nmat4489

Chaudhuri, O., Koshy, S. T., Branco da Cunha, C., Shin, J. W., Verbeke, C. S., Allison, K. H., & Mooney, D. J. (2014). Extracellular matrix stiffness and composition jointly regulate the induction of malignant phenotypes in mammary epithelium. *Nat Mater*, *13*(10), 970-978. https://doi.org/10.1038/nmat4009

Chazal, G., & Ralston, H. J., 3rd. (1987). Serotonin-containing structures in the nucleus raphe dorsalis of the cat: an ultrastructural analysis of dendrites, presynaptic dendrites, and axon terminals. *J Comp Neurol*, *259*(3), 317-329. https://doi.org/10.1002/cne.902590302

Chédotal, A., & Richards, L. J. (2010). Wiring the brain: the biology of neuronal guidance. *Cold Spring Harbor perspectives in biology*, *2*(6), a001917. https://doi.org/10.1101/cshperspect.a001917

Chen, W. S. V., Nwakeze, C. L., Denny, C. A., O'Keeffe, S., Rieger, M. A., Mountoufaris, G., Kirner, A., Dougherty, J. D., Hen, R., Wu, Q., & Maniatis, T. (2017). Pcdh alpha c2 is required for axonal tiling and assembly of serotonergic circuitries in mice. *Science*, *356*(6336), 406-410. https://doi.org/10.1126/science.aal3231

Chen, Y., Vartiainen, N. E., Ying, W., Chan, P. H., Koistinaho, J., & Swanson, R. A. (2001). Astrocytes protect neurons from nitric oxide toxicity by a glutathione-dependent mechanism. *J Neurochem*, *77*(6), 1601-1610. https://doi.org/10.1046/j.1471-4159.2001.00374.x

Cherne, M. D., Sidar, B., Sebrell, T. A., Sanchez, H. S., Heaton, K., Kassama, F. J., Roe, M. M., Gentry, A. B., Chang, C. B., Walk, S. T., Jutila, M., Wilking, J. N., & Bimczok, D. (2021). A Synthetic Hydrogel, VitroGel(®) ORGANOID-3, Improves Immune Cell-Epithelial Interactions in a Tissue Chip Co-Culture Model of Human Gastric Organoids and Dendritic Cells. *Front Pharmacol*, *12*, 707891. https://doi.org/10.3389/fphar.2021.707891

Chou, A. I., & Nicoll, S. B. (2009). Characterization of photocrosslinked alginate hydrogels for nucleus pulposus cell encapsulation. *J Biomed Mater Res A*, *91*(1), 187-194. https://doi.org/10.1002/jbm.a.32191

Cooke, P., Janowitz, H., & Dougherty, S. E. (2022). Neuronal Redevelopment and the Regeneration of Neuromodulatory Axons in the Adult Mammalian Central Nervous System. *Frontiers in Cellular Neuroscience*, *16*. https://doi.org/ARTN 872501 10.3389/fncel.2022.872501

Corning Matrigel Matrix. https://www.corning.com/in/en/products/life-sciences/products/surfaces/matrigel-matrix.html

Couch, J. A., Chen, J., Rieff, H. I., Uri, E. M., & Condron, B. G. (2004). robo2 and robo3 interact with eagle to regulate serotonergic neuron differentiation. *Development*, *131*(5), 997-1006. https://doi.org/10.1242/dev.00962

Cumming, P., Gryglewski, G., Kranz, G. S., & Lanzenberger, R. (2016). Commentary: The serotonin transporter in depression: Meta-analysis of *in vivo* and postmortem findings and implications for understanding and treating depression. *Journal of Affective Disorders*, *199*, 21-22. https://doi.org/10.1016/j.jad.2016.03.058

D. B, D. (1930). Degeneration and Regeneration of the Nervous System. *Nature*, *125*(3146), 230-231. https://doi.org/10.1038/125230a0

Dahlstrom, A., & Fuxe, K. (1964). Localization of monoamines in the lower brain stem. *Experientia*, *20*(7), 398-399. https://doi.org/10.1007/BF02147990

Damato, R. J., Blue, M. E., Largent, B. L., Lynch, D. R., Ledbetter, D. J., Molliver, M. E., & Snyder, S. H. (1987). Ontogeny of the Serotonergic Projection to Rat Neocortex - Transient Expression of a Dense Innervation to Primary Sensory Areas. *Proceedings of the National Academy of Sciences of the United States of America*, *84*(12), 4322-4326. https://doi.org/DOI 10.1073/pnas.84.12.4322

Damsky, C. H., & Ilic, D. (2002). Integrin signaling it's where the action is. *Current Opinion in Cell Biology*, *14*(5), 594-602. https://doi.org/10.1016/S0955-0674(02)00368-X

Daniel, W. F., Burdynska, J., Vatankhah-Varnoosfaderani, M., Matyjaszewski, K., Paturej, J., Rubinstein, M., Dobrynin, A. V., & Sheiko, S. S. (2016). Solvent-free, supersoft and superelastic bottlebrush melts and networks. *Nat Mater*, *15*(2), 183-189. https://doi.org/10.1038/nmat4508

Darbinyan, A., Pozniak, P., Darbinian, N., White, M. K., & Khalili, K. (2013). Compartmentalized neuronal cultures. *Methods in molecular biology (Clifton, N.J.)*, *1078*, 147-152. https://doi.org/10.1007/978-1-62703-640-5_13

Daub, A., Sharma, P., & Finkbeiner, S. (2009). High-content screening of primary neurons: ready for prime time. *Current opinion in neurobiology*, *19*(5), 537-543. https://doi.org/10.1016/j.conb.2009.10.002

Deligianni, D. D., Katsala, N., Ladas, S., Sotiropoulou, D., Amedee, J., & Missirlis, Y. F. (2001). Effect of surface roughness of the titanium alloy Ti-6Al-4V on human bone marrow cell response and on protein adsorption. *Biomaterials*, *22*(11), 1241-1251. https://doi.org/10.1016/s0142-9612(00)00274-x

Desagher, S., Glowinski, J., & Premont, J. (1996). Astrocytes protect neurons from hydrogen peroxide toxicity. *J Neurosci*, *16*(8), 2553-2562. https://doi.org/10.1523/jneurosci.16-08-02553.1996

Descarries, L., Watkins, K. C., Garcia, S., & Beaudet, A. (1982). The serotonin neurons in nucleus raphe dorsalis of adult rat: a light and electron microscope radioautographic study. *J Comp Neurol*, *207*(3), 239-254. https://doi.org/10.1002/cne.902070305

Dichter, M. A. (1978). Rat Cortical-Neurons in Cell-Culture - Culture Methods, Cell Morphology, Electrophysiology, and Synapse Formation. *Brain Research*, *149*(2), 279-293. https://doi.org/Doi 10.1016/0006-8993(78)90476-6

Donovan, L. J., Spencer, W. C., Kitt, M. M., Eastman, B. A., Lobur, K. J., Jiao, K., Silver, J., & Deneris, E. S. (2019). Lmx1b is required at multiple stages to build expansive serotonergic axon architectures. *Elife*, *8*, e48788. https://doi.org/10.7554/eLife.48788

Donovan, S. L., Mamounas, L. A., Andrews, A. M., Blue, M. E., & McCasland, J. S. (2002). GAP-43 is critical for normal development of the serotonergic innervation in forebrain. *Journal of Neuroscience*, *22*(9), 3543-3552. <Go to ISI>://WOS:000175296200032

Dragan, E. S. (2014). Design and applications of interpenetrating polymer network hydrogels. A review. *Chemical Engineering Journal*, *243*, 572-590. https://doi.org/https://doi.org/10.1016/j.cej.2014.01.065

Dreyfus, C. F., Gershon, M. D., & Crain, S. M. (1979). Innervation of Hippocampal Explants by Central Catecholaminergic Neurons in Co-Cultured Fetal Mouse-Brain Stem Explants. *Brain Research*, *161*(3), 431-445. https://doi.org/Doi 10.1016/0006-8993(79)90673-5

Ducray, A., Krebs, S. H., Schaller, B., Seiler, R. W., Meyer, M., & Widmer, H. R. (2006). GDNF family ligands display distinct action profiles on cultured GABAergic and serotonergic neurons of rat ventral mesencephalon. *Brain Research*, *1069*(1), 104-112. https://doi.org/10.1016/j.brainres.2005.11.056

Dudok, J. J., Groffen, A. J. A., Witter, M. P., Voorn, P., & Verhage, M. (2009). Chronic activation of the 5-HT2 receptor reduces 5-HT neurite density as studied in organotypic slice cultures. *Brain Research*, *1302*, 1-9. https://doi.org/https://doi.org/10.1016/j.brainres.2009.08.071

Duval, K., Grover, H., Han, L. H., Mou, Y., Pegoraro, A. F., Fredberg, J., & Chen, Z. (2017). Modeling Physiological Events in 2D vs. 3D Cell Culture. *Physiology (Bethesda)*, *32*(4), 266-277. https://doi.org/10.1152/physiol.00036.2016

El-Merahbi, R., Löffler, M., Mayer, A., & Sumara, G. (2015). The roles of peripheral serotonin in metabolic homeostasis. *FEBS Lett*, *589*(15), 1728-1734. https://doi.org/10.1016/j.febslet.2015.05.054

Eming, S. A., Martin, P., & Tomic-Canic, M. (2014). Wound repair and regeneration: Mechanisms, signaling, and translation. *Science Translational Medicine*, *6*(265). https://doi.org/ARTN 265sr610.1126/scitranslmed.3009337

Engler, A. J., Sen, S., Sweeney, H. L., & Discher, D. E. (2006). Matrix elasticity directs stem cell lineage specification. *Cell*, *126*(4), 677-689. https://doi.org/10.1016/j.cell.2006.06.044

Eriksen, J. L., & Druse, M. J. (2001). Astrocyte-mediated trophic support of developing serotonin neurons: effects of ethanol, buspirone, and S100B. *Developmental Brain Research*, *131*(1), 9-15. https://doi.org/https://doi.org/10.1016/S0165-3806(01)00240-1

Fanibunda, S. E., Deb, S., Maniyadath, B., Tiwari, P., Ghai, U., Gupta, S., Figueiredo, D., Weisstaub, N., Gingrich, J. A., Vaidya, A. D. B., Kolthur-Seetharam, U., & Vaidya, V. A. (2019). Serotonin regulates mitochondrial biogenesis and function in rodent cortical neurons via the 5-HT_{2A} receptor and SIRT1–PGC-1α axis. *Proceedings of the National Academy of Sciences*, *116*(22), 11028-11037. https://doi.org/10.1073/pnas.1821332116

Feng, Y., & Walsh, C. A. (2001). Protein-protein interactions, cytoskeletal regulation, and neuronal migration. *Nat Rev Neurosci*, *2*(6), 408-416. https://doi.org/10.1038/35077559

Fernandez, S. P., Cauli, B., Cabezas, C., Muzerelle, A., Poncer, J. C., & Gaspar, P. (2016). Multiscale single-cell analysis reveals unique phenotypes of raphe 5-HT neurons projecting to the forebrain. *Brain Struct Funct*, *221*(8), 4007-4025. https://doi.org/10.1007/s00429-015-1142-4

Flippo, K. H., & Strack, S. (2017). Mitochondrial dynamics in neuronal injury, development, and plasticity. *Journal of Cell Science*, *130*(4), 671-681. https://doi.org/10.1242/jcs.171017

Fournet, V., Jany, M., Fabre, V., Chali, F., Orsal, D., Schweitzer, A., Andrieux, A., Messanvi, F., Giros, B., Hamon, M., Lanfumey, L., Deloulme, J. C., & Martres, M. P. (2010). The deletion of the microtubule-associated STOP protein affects the serotonergic mouse brain network. *Journal of Neurochemistry*, *115*(6), 1579-1594. https://doi.org/10.1111/j.1471-4159.2010.07064.x

Francisco, H., Yellen, B. B., Halverson, D. S., Friedman, G., & Gallo, G. (2007). Regulation of axon guidance and extension by three-dimensional constraints. *Biomaterials*, *28*(23), 3398-3407. https://doi.org/10.1016/j.biomaterials.2007.04.015

Franze, K., Gerdelmann, J., Weick, M., Betz, T., Pawlizak, S., Lakadamyali, M., Bayer, J., Rillich, K., Gögler, M., Lu, Y. B., Reichenbach, A., Janmey, P., & Käs, J. (2009). Neurite branch retraction is caused by a threshold-dependent mechanical impact. *Biophysical Journal*, *97*(7), 1883-1890. https://doi.org/10.1016/j.bpj.2009.07.033

Freedman, L. P., Cockburn, I. M., & Simcoe, T. S. (2015). The Economics of Reproducibility in Preclinical Research. *Plos Biology*, *13*(6). https://doi.org/ARTN e1002165 10.1371/journal.pbio.1002165

Freedman, L. P., Gibson, M. C., Ethier, S. P., Soule, H. R., Neve, R. M., & Reid, Y. A. (2015). Reproducibility: changing the policies and culture of cell line authentication. *Nat Methods*, *12*(6), 493-497. https://doi.org/10.1038/nmeth.3403

Frieboes, H. B., Zheng, X., Sun, C. H., Tromberg, B., Gatenby, R., & Cristini, V. (2006). An integrated computational/experimental model of tumor invasion. *Cancer Res*, *66*(3), 1597-1604. https://doi.org/10.1158/0008-5472.CAN-05-3166

Fuchs, E., Tumbar, T., & Guasch, G. (2004). Socializing with the Neighbors: Stem Cells and Their Niche. *Cell*, *116*(6), 769-778. https://doi.org/https://doi.org/10.1016/S0092-8674(04)00255-7

Fujimiya, M., Kimura, H., & Maeda, T. (1986). Postnatal-Development of Serotonin Nerve-Fibers in the Somatosensory Cortex of Mice Studied by Immunohistochemistry. *Journal of Comparative Neurology*, *246*(2), 191-201. https://doi.org/DOI 10.1002/cne.902460205

Gagnon, D., & Parent, M. (2014). Distribution of VGLUT3 in highly collateralized axons from the rat dorsal raphe nucleus as revealed by single-neuron reconstructions. *PLOS ONE*, *9*(2), e87709. https://doi.org/10.1371/journal.pone.0087709

Gallo, G., & Letourneau, P. C. (2004). Regulation of growth cone actin filaments by guidance cues. *J Neurobiol*, *58*(1), 92-102. https://doi.org/10.1002/neu.10282

Galter, D., & Unsicker, K. (1999). Regulation of the transmitter phenotype of rostral and caudal groups of cultured serotonergic raphe neurons. *Neuroscience*, *88*(2), 549-559. https://doi.org/https://doi.org/10.1016/S0306-4522(98)00224-3

Galter, D., & Unsicker, K. (2000). Sequential activation of the 5-HT1(A) serotonin receptor and TrkB induces the serotonergic neuronal phenotype. *Molecular and Cellular Neuroscience*, *15*(5), 446-455. https://doi.org/DOI 10.1006/mcne.2000.0841

Garnica-Palafox, I. M., & Sanchez-Arevalo, F. M. (2016). Influence of natural and synthetic crosslinking reagents on the structural and mechanical properties of chitosan-based hybrid hydrogels. *Carbohydr Polym*, *151*, 1073-1081. https://doi.org/10.1016/j.carbpol.2016.06.036

Gaspar, P., & Lillesaar, C. (2012). Probing the diversity of serotonin neurons. *Philos Trans R Soc Lond B Biol Sci*, *367*(1601), 2382-2394. https://doi.org/10.1098/rstb.2011.0378

Gershon, M. D., & Tack, J. (2007). The serotonin signaling system: from basic understanding to drug development for functional GI disorders. *Gastroenterology*, *132*(1), 397-414. https://doi.org/10.1053/j.gastro.2006.11.002

Ghaffari Darab, M., Hedayati, A., Khorasani, E., Bayati, M., & Keshavarz, K. (2020). Selective serotonin reuptake inhibitors in major depression disorder treatment: an umbrella review on systematic reviews. *Int J Psychiatry Clin Pract*, *24*(4), 357-370. https://doi.org/10.1080/13651501.2020.1782433

Giachello, C. N. G., Montarolo, P. G., & Ghirardi, M. (2012). Synaptic Functions of Invertebrate Varicosities: What Molecular Mechanisms Lie Beneath. *Neural Plasticity*, *2012*, 670821. https://doi.org/10.1155/2012/670821

Gibson, D. A., & Ma, L. (2011). Developmental regulation of axon branching in the vertebrate nervous system. *Development*, *138*(2), 183-195. https://doi.org/10.1242/dev.046441

Gilbert, P. M., Havenstrite, K. L., Magnusson, K. E., Sacco, A., Leonardi, N. A., Kraft, P., Nguyen, N. K., Thrun, S., Lutolf, M. P., & Blau, H. M. (2010). Substrate elasticity regulates skeletal muscle stem cell self-renewal in culture. *Science*, *329*(5995), 1078-1081. https://doi.org/10.1126/science.1191035

Golan, M., Schreiber, G., & Avissar, S. (2011). Antidepressants elevate GDNF expression and release from C6 glioma cells in a beta-arrestin1-dependent, CREB interactive pathway. *Journal of Molecular Neuroscience*, *45*(Suppl 1), S45-S45. <Go to ISI>://WOS:000520322000110

Gomez-Lechon, M. J., Jover, R., Donato, T., Ponsoda, X., Rodriguez, C., Stenzel, K. G., Klocke, R., Paul, D., Guillen, I., Bort, R., & Castell, J. V. (1998). Long-term expression of differentiated functions in hepatocytes cultured in three-dimensional collagen matrix. *J Cell Physiol*, *177*(4), 553-562. https://doi.org/10.1002/(SICI)1097-4652(199812)177:4<553::AID-JCP6>3.0.CO;2-F

Goodman, C. S., & Shatz, C. J. (1993). Developmental mechanisms that generate precise patterns of neuronal connectivity. *Cell*, *72*, 77-98. https://doi.org/https://doi.org/10.1016/S0092-8674(05)80030-3

Grabham, P. W., Wu, F., Schacher, S., & Goldberg, D. J. (2005). Initiating morphological changes associated with long-term facilitation in Aplysia is independent of transcription or translation in the cell body. *J Neurobiol*, *64*(2), 202-212. https://doi.org/10.1002/neu.20133

Gras, C., Herzog, E., Bellenchi, G. C., Bernard, V., Ravassard, P., Pohl, M., Gasnier, B., Giros, B., & El Mestikawy, S. (2002). A third vesicular glutamate transporter expressed by cholinergic and serotoninergic neurons. *J Neurosci*, *22*(13), 5442-5451. https://doi.org/10.1523/jneurosci.22-13-05442.2002

Griffiths, D. R., Jenkins, T. M., Addington, C. P., Stabenfeldt, S. E., & Lifshitz, J. (2020). Extracellular matrix proteins are time-dependent and regional-specific markers in experimental diffuse brain injury. *Brain Behav*, *10*(9), e01767. https://doi.org/10.1002/brb3.1767

Griffith, L. G., & Swartz, M. A. (2006). Capturing complex 3D tissue physiology in vitro. *Nat Rev Mol Cell Biol*, *7*(3), 211-224. https://doi.org/10.1038/nrm1858

Gryglewski, G., Lanzenberger, R., Kranz, G. S., & Cumming, P. (2014). Meta-analysis of molecular imaging of serotonin transporters in major depression. *Journal of Cerebral Blood Flow and Metabolism*, *34*(7), 1096-1103. https://doi.org/10.1038/jcbfm.2014.82

Guck, J., Lautenschlager, F., Paschke, S., & Beil, M. (2010). Critical review: cellular mechanobiology and amoeboid migration. *Integrative Biology*, *2*(11-12), 575-583. https://doi.org/10.1039/c0ib00050g

Gyles, D. A., Castro, L. D., Silva, J. O. C., & Ribeiro-Costa, R. M. (2017). A review of the designs and prominent biomedical advances of natural and synthetic hydrogel formulations. *European Polymer Journal*, *88*, 373-392. https://doi.org/https://doi.org/10.1016/j.eurpolymj.2017.01.027

Hagmeyer, S., Romão, M. A., Cristóvão, J. S., Vilella, A., Zoli, M., Gomes, C. M., & Grabrucker, A. M. (2019). Distribution and Relative Abundance of S100 Proteins in the Brain of the APP23 Alzheimer's Disease Model Mice [Original Research]. *Frontiers in Neuroscience*, *13*(640). https://doi.org/10.3389/fnins.2019.00640

Hakuno, S. K., Michiels, E., Kuhlemaijer, E. B., Rooman, I., Hawinkels, L. J. A. C., & Slingerland, M. (2022). Multicellular Modelling of Difficult-to-Treat

Gastrointestinal Cancers: Current Possibilities and Challenges. *International Journal of Molecular Sciences*, *23*(6), 3147. https://www.mdpi.com/1422-0067/23/6/3147

Hale, M. W., & Lowry, C. A. (2011). Functional topography of midbrain and pontine serotonergic systems: implications for synaptic regulation of serotonergic circuits. *Psychopharmacology (Berl)*, *213*(2-3), 243-264. https://doi.org/10.1007/s00213-010-2089-z

Halgren, E., & Varon, S. (1972). Serotonin Turnover in Cultured Raphe Nuclei from New Born Rat - in-Vitro Development and Drug Effects. *Brain Research*, *48*(Dec24), 438-442. https://doi.org/Doi 10.1016/0006-8993(72)90207-7

Harnett, E. M., Alderman, J., & Wood, T. (2007). The surface energy of various biomaterials coated with adhesion molecules used in cell culture. *Colloids and Surfaces B-Biointerfaces*, *55*(1), 90-97. https://doi.org/10.1016/j.colsurfb.2006.11.021

Hatada, Y., Wu, F., Silverman, R., Schacher, S., & Goldberg, D. J. (1999). En passant synaptic varicosities form directly from growth cones by transient cessation of growth cone advance but not of actin-based motility. *Journal of Neurobiology*, *41*(2), 242-251. https://doi.org/https://doi.org/10.1002/(SICI)1097-4695(19991105)41:2

Hatada, Y., Wu, F., Sun, Z. Y., Schacher, S., & Goldberg, D. J. (2000). Presynaptic morphological changes associated with long-term synaptic facilitation are triggered by actin polymerization at preexisting varicositis. *J Neurosci*, *20*(13), RC82. https://www.ncbi.nlm.nih.gov/pubmed/10864976

Hawthorne, A. L., Hu, H., Kundu, B., Steinmetz, M. P., Wylie, C. J., Deneris, E. S., & Silver, J. (2011). The unusual response of serotonergic neurons after CNS Injury: lack of axonal dieback and enhanced sprouting within the inhibitory environment of the glial scar. *J Neurosci*, *31*(15), 5605-5616. https://doi.org/10.1523/JNEUROSCI.6663-10.2011

Hawthorne, A. L., Wylie, C. J., Landmesser, L. T., Deneris, E. S., & Silver, J. (2010). Serotonergic neurons migrate radially through the neuroepithelium by dynamin-mediated somal translocation. *J Neurosci*, *30*(2), 420-430. https://doi.org/10.1523/JNEUROSCI.2333-09.2010

Hayashi, Y., Jacob-Vadakot, S., Dugan, E. A., McBride, S., Olexa, R., Simansky, K., Murray, M., & Shumsky, J. S. (2010). 5-HT precursor loading, but not 5-HT receptor agonists, increases motor function after spinal cord contusion in adult rats. *Experimental Neurology*, *221*(1), 68-78. https://doi.org/10.1016/j.expneurol.2009.10.003

Henke, A., Kovalyova, Y., Dunn, M., Dreier, D., Gubernator, N. G., Dincheva, I., Hwu, C., Sebej, P., Ansorge, M. S., Sulzer, D., & Sames, D. (2018). Toward Serotonin Fluorescent False Neurotransmitters: Development of Fluorescent Dual Serotonin and Vesicular Monoamine Transporter Substrates for Visualizing Serotonin Neurons. *ACS Chem Neurosci*, *9*(5), 925-934. https://doi.org/10.1021/acschemneuro.7b00320

Hickman, J. A., Graeser, R., de Hoogt, R., Vidic, S., Brito, C., Gutekunst, M., van der Kuip, H., & Consortium, I. P. (2014). Three-dimensional models of cancer for pharmacology and cancer cell biology: capturing tumor complexity in vitro/ex vivo. *Biotechnol J*, *9*(9), 1115-1128. https://doi.org/10.1002/biot.201300492

Hingorani, M., Viviani, A. M. L., Sanfilippo, J. E., & Janušonis, S. (2022). High-Resolution Spatiotemporal Analysis of Single Serotonergic Axons in an In Vitro System. *bioRxiv*, 2022.2007.2016.500161. https://doi.org/10.1101/2022.07.16.500161

Hisaoka, K., Nishida, A., Koda, T., Miyata, M., Zensho, H., Morinobu, S., Ohta, M., & Yamawaki, S. (2001). Antidepressant drug treatments induce glial cell line-derived neurotrophic factor (GDNF) synthesis and release in rat C6 glioblastoma cells. *Journal of Neurochemistry*, *79*(1), 25-34. https://doi.org/DOI 10.1046/j.1471-4159.2001.00531.x

Hocking, D. C., Sottile, J., & McKeown-Longo, P. J. (1994). Fibronectin's III-1 module contains a conformation-dependent binding site for the amino-terminal region of fibronectin. *J Biol Chem*, *269*(29), 19183-19187.

Holloway, P. M., Willaime-Morawek, S., Siow, R., Barber, M., Owens, R. M., Sharma, A. D., Rowan, W., Hill, E., & Zagnoni, M. (2021). Advances in microfluidic *in vitro* systems for neurological disease modeling. *Journal of Neuroscience Research*, *n/a*(n/a). https://doi.org/https://doi.org/10.1002/jnr.24794

Holmes, G. M., Van Meter, M. J., Beattie, M. S., & Bresnahan, J. C. (2005). Serotonergic fiber sprouting to external anal sphincter motoneurons after spinal cord contusion. *Experimental Neurology*, *193*(1), 29-42. https://doi.org/10.1016/j.expneurol.2005.01.002

Homberg, J. R., Molteni, R., Calabrese, F., & Riva, M. A. (2014). The serotonin-BDNF duo: Developmental implications for the vulnerability to psychopathology. *Neuroscience and Biobehavioral Reviews*, *43*, 35-47. https://doi.org/10.1016/j.neubiorev.2014.03.012

Hong, L. T. A., Kim, Y. M., Park, H. H., Hwang, D. H., Cui, Y., Lee, E. M., Yahn, S., Lee, J. K., Song, S. C., & Kim, B. G. (2017). An injectable hydrogel enhances tissue

repair after spinal cord injury by promoting extracellular matrix remodeling. *Nature Communications*, *8*. https://doi.org/ARTN 53310.1038/s41467-017-00583-8

Hornung, J. P. (2003). The human raphe nuclei and the serotonergic system. *Journal of Chemical Neuroanatomy*, *26*(4), 331-343. https://doi.org/10.1016/j.jchemneu.2003.10.002

Hrdina, P. D., Foy, B., Hepner, A., & Summers, R. J. (1990). Antidepressant binding sites in brain: autoradiographic comparison of [3H]paroxetine and [3H]imipramine localization and relationship to serotonin transporter. *J Pharmacol Exp Ther*, *252*(1), 410-418. https://www.ncbi.nlm.nih.gov/pubmed/2137177

Hsieh, C. H., Chen, Y. D., Huang, S. F., Wang, H. M., & Wu, M. H. (2015). The effect of primary cancer cell culture models on the results of drug chemosensitivity assays: the application of perfusion microbioreactor system as cell culture vessel. *Biomed Res Int*, *2015*, 470283. https://doi.org/10.1155/2015/470283

Hyung, S., Yoon Lee, B., Park, J. C., Kim, J., Hur, E. M., & Francis Suh, J. K. (2015). Coculture of Primary Motor Neurons and Schwann Cells as a Model for *In Vitro* Myelination. *Sci Rep*, *5*, 15122. https://doi.org/10.1038/srep15122

Im, P., Ji, D. H., Kim, M. K., & Kim, J. (2017). Fabrication of cell-benign inverse opal hydrogels for three-dimensional cell culture. *J Colloid Interface Sci*, *494*, 389-396. https://doi.org/10.1016/j.jcis.2017.01.108

Ingber, D. E. (1990). Fibronectin Controls Capillary Endothelial-Cell Growth by Modulating Cell-Shape. *Proceedings of the National Academy of Sciences of the United States of America*, *87*(9), 3579-3583. https://doi.org/DOI 10.1073/pnas.87.9.3579

Inman, D. M., & Steward, O. (2003). Ascending sensory, but not other long-tract axons, regenerate into the connective tissue matrix that forms at the site of a spinal cord injury in mice. *J Comp Neurol*, *462*(4), 431-449. https://doi.org/10.1002/cne.10768

Ishikawa-Ankerhold, H., Kroll, J., Heuvel, D. v. d., Renkawitz, J., & Müller-Taubenberger, A. (2022). Centrosome Positioning in Migrating Dictyostelium Cells. *Cells*, *11*(11), 1776. https://www.mdpi.com/2073-4409/11/11/1776

Ishimura, K., Takeuchi, Y., Fujiwara, K., Tominaga, M., Yoshioka, H., & Sawada, T. (1988). Quantitative analysis of the distribution of serotonin-immunoreactive cell bodies in the mouse brain. *Neurosci Lett*, *91*(3), 265-270. https://doi.org/10.1016/0304-3940(88)90691-x

Ivenshitz, M., & Segal, M. (2010). Neuronal Density Determines Network Connectivity and Spontaneous Activity in Cultured Hippocampus. *Journal of Neurophysiology*, *104*(2), 1052-1060. https://doi.org/10.1152/jn.00914.2009

Ivgy-May, N., Tamir, H., & Gershon, M. D. (1994). Synaptic properties of serotonergic growth cones in developing rat brain. *J Neurosci*, *14*(3 Pt 1), 1011-1029. https://www.ncbi.nlm.nih.gov/pubmed/7509861

Jacobs, B. L., & Azmitia, E. C. (1992). Structure and function of the brain serotonin system. *Physiol Rev*, *72*(1), 165-229. https://doi.org/10.1152/physrev.1992.72.1.165

Jacobson, R. D., Virág, I., & Skene, J. H. (1986). A protein associated with axon growth, GAP-43, is widely distributed and developmentally regulated in rat CNS. *J Neurosci*, *6*(6), 1843-1855. https://doi.org/10.1523/jneurosci.06-06-01843.1986

Janusonis, S. (2014). Serotonin dynamics in and around the central nervous system: Is autism solvable without fundamental insights? *International Journal of Developmental Neuroscience*, *39*, 9-15. https://doi.org/10.1016/j.ijdevneu.2014.05.009

Janusonis, S., & Detering, N. (2019). A stochastic approach to serotonergic fibers in mental disorders. *Biochimie*, *161*, 15-22. https://doi.org/10.1016/j.biochi.2018.07.014

Janusonis, S., Detering, N., Metzler, R., & Vojta, T. (2020). Serotonergic Axons as Fractional Brownian Motion Paths: Insights Into the Self-Organization of Regional Densities. *Front Comput Neurosci*, *14*, 56. https://doi.org/10.3389/fncom.2020.00056

Janusonis, S., Detering, N., Metzler, R., & Vojta, T. (2020). Serotonergic Axons as Fractional Brownian Motion Paths: Insights Into the Self-Organization of Regional Densities. *Front Comput Neurosci*, *14*, 56. https://doi.org/10.3389/fncom.2020.00056

Janusonis, S., Mays, K. C., & Hingorani, M. T. (2019). Serotonergic Axons as 3D-Walks. *ACS Chem Neurosci*, *10*(7), 3064-3067. https://doi.org/10.1021/acschemneuro.8b00667

Jensen, P., Farago, A. F., Awatramani, R. B., Scott, M. M., Deneris, E. S., & Dymecki, S. M. (2008). Redefining the serotonergic system by genetic lineage. *Nature Neuroscience*, *11*(4), 417-419. https://doi.org/10.1038/nn2050

Jin, Y., Dougherty, S. E., Wood, K., Sun, L., Cudmore, R. H., Abdalla, A., Kannan, G., Pletnikov, M., Hashemi, P., & Linden, D. J. (2016). Regrowth of Serotonin Axons in the Adult Mouse Brain Following Injury. *Neuron*, *91*(4), 748-762. https://doi.org/10.1016/j.neuron.2016.07.024

Jokhadar, S. Z., Znidarcic, T., Svetina, S., & Batista, U. (2007). The effect of substrate and adsorbed proteins on adhesion, growth, and shape of CaCo-2 cells. *Cell Biology International*, *31*(10), 1097-1108. https://doi.org/10.1016/j.cellbi.2007.03.019

Kaech, S., & Banker, G. (2006). Culturing hippocampal neurons. *Nature Protocols*, *1*(5), 2406-2415. https://doi.org/10.1038/nprot.2006.356

Kaiser, A., Kale, A., Novozhilova, E., & Olivius, P. (2020). The Effects of Matrigel® on the Survival and Differentiation of a Human Neural Progenitor Dissociated Sphere Culture. *The Anatomical Record*, *303*(3), 441-450. https://doi.org/https://doi.org/10.1002/ar.24131

Kajstura, T. J., Dougherty, S. E., & Linden, D. J. (2018). Serotonin axons in the neocortex of the adult female mouse regrow after traumatic brain injury. *Journal of Neuroscience Research*, *96*(4), 512-526. https://doi.org/10.1002/jnr.24059

Kapałczyńska, M., Kolenda, T., Przybyła, W., Zajączkowska, M., Teresiak, A., Filas, V., Ibbs, M., Bliźniak, R., Łuczewski, Ł., & Lamperska, K. (2018). 2D and 3D cell cultures - a comparison of different types of cancer cell cultures. *Arch Med Sci*, *14*(4), 910-919. https://doi.org/10.5114/aoms.2016.63743

Katori, S., Noguchi-Katori, Y., Okayama, A., Kawamura, Y., Luo, W., Sakimura, K., Hirabayashi, T., Iwasato, T., & Yagi, T. (2017). Protocadherin-αC2 is required for diffuse projections of serotonergic axons. *Scientific Reports*, *7*(1), 15908. https://doi.org/10.1038/s41598-017-16120-y

Keesom, S. M., Morningstar, M. D., Sandlain, R., Wise, B. M., & Hurley, L. M. (2018). Social isolation reduces serotonergic fiber density in the inferior colliculus of female, but not male, mice. *Brain Res*, *1694*, 94-103. https://doi.org/10.1016/j.brainres.2018.05.010

Kidambi, S., Lee, I., & Chan, C. (2008). Primary Neuron/Astrocyte Co-Culture on Polyelectrolyte Multilayer Films: A Template for Studying Astrocyte-Mediated Oxidative Stress in Neurons. *Adv Funct Mater*, *18*(2), 294-301. https://doi.org/10.1002/adfm.200601237

Kilian, K. A., Bugarija, B., Lahn, B. T., & Mrksich, M. (2010). Geometric cues for directing the differentiation of mesenchymal stem cells. *Proc Natl Acad Sci U S A*, *107*(11), 4872-4877. https://doi.org/10.1073/pnas.0903269107

Kim, Meade, S. M., Chen, K., Feng, H., Rayyan, J., Hess-Dunning, A., & Ereifej, E. S. (2018). Nano-Architectural Approaches for Improved Intracortical Interface Technologies. *Front Neurosci*, *12*, 456. https://doi.org/10.3389/fnins.2018.00456

Kim, D., Lee, S., Lee, M., Oh, J., Yang, S.-A., & Park, Y. (2018). Holotomography: refractive index as an intrinsic imaging contrast for 3-D label-free live cell imaging. *bioRxiv*, 106328. https://doi.org/10.1101/106328

Kim, D., Oh, N., Kim, K., Lee, S., Pack, C. G., Park, J. H., & Park, Y. (2018). Label-free high-resolution 3-D imaging of gold nanoparticles inside live cells using optical diffraction tomography. *Methods*, *136*, 160-167. https://doi.org/10.1016/j.ymeth.2017.07.008

Kim, K., Lee, S., Yoon, J., Heo, J., Choi, C., & Park, Y. (2016). Three-dimensional label-free imaging and quantification of lipid droplets in live hepatocytes. *Sci Rep*, *6*, 36815. https://doi.org/10.1038/srep36815

Kivell, B. M., McDonald, F. J., & Miller, J. H. (2000). Serum-free culture of rat post-natal and fetal brainstem neurons. *Developmental Brain Research*, *120*(2), 199-210.

Kiyasova, V., Fernandez, S. P., Laine, J., Stankovski, L., Muzerelle, A., Doly, S., & Gaspar, P. (2011). A genetically defined morphologically and functionally unique subset of 5-HT neurons in the mouse raphe nuclei. *J Neurosci*, *31*(8), 2756-2768. https://doi.org/10.1523/JNEUROSCI.4080-10.2011

Kiyasova, V., & Gaspar, P. (2011). Development of raphe serotonin neurons from specification to guidance. *Eur J Neurosci*, *34*(10), 1553-1562. https://doi.org/10.1111/j.1460-9568.2011.07910.x

Koh, H. S., Yong, T., Chan, C. K., & Ramakrishna, S. (2008). Enhancement of neurite outgrowth using nano-structured scaffolds coupled with laminin. *Biomaterials*, *29*(26), 3574-3582. https://doi.org/10.1016/j.biomaterials.2008.05.014

Kondoh, M., Shiga, T., & Okado, N. (2004). Regulation of dendrite formation of Purkinje cells by serotonin through serotonin(1A) and serotonin(2A) receptors in culture. *Neuroscience Research*, *48*(1), 101-109. https://doi.org/10.1016/j.neures.2003.10.001

Kopeček, J., & Yang, J. (2012). Smart self-assembled hybrid hydrogel biomaterials. *Angewandte Chemie (International ed. in English)*, *51*(30), 7396-7417. https://doi.org/10.1002/anie.201201040

Kosofsky, B. E., & Molliver, M. E. (1987). The serotoninergic innervation of cerebral cortex: Different classes of axon terminals arise from dorsal and median raphe nuclei. *Synapse*, *1*(2), 153-168. https://doi.org/https://doi.org/10.1002/syn.890010204

Krishnamurthy, S., & Nor, J. E. (2013). Orosphere assay: a method for propagation of head and neck cancer stem cells. *Head Neck*, *35*(7), 1015-1021. https://doi.org/10.1002/hed.23076

Kuhn, D. M., Wolf, W. A., & Youdim, M. B. (1985). 5-Hydroxytryptamine release *in vivo* from a cytoplasmic pool: studies on the 5-HT behavioural syndrome in reserpinized rats. *Br J Pharmacol*, *84*(1), 121-129. https://www.ncbi.nlm.nih.gov/pubmed/2579697

KV Mardia, P. J. (2000). *Directional Statistics*.

Lamoureux, P., Ruthel, G., Buxbaum, R. E., & Heidemann, S. R. (2002). Mechanical tension can specify axonal fate in hippocampal neurons. *Journal of Cell Biology*, *159*(3), 499-508. https://doi.org/10.1083/jcb.200207174

Lazarevic, V., Mantas, I., Flais, I., & Svenningsson, P. (2019). Fluoxetine Suppresses Glutamate- and GABA-Mediated Neurotransmission by Altering SNARE Complex. *Int J Mol Sci*, *20*(17). https://doi.org/10.3390/ijms20174247

Lecault, V., VanInsberghe, M., Sekulovic, S., Knapp, D. J. H. F., Wohrer, S., Bowden, W., Viel, F., McLaughlin, T., Jarandehei, A., Miller, M., Falconnet, D., White, A. K., Kent, D. G., Copley, M. R., Taghipour, F., Eaves, C. J., Humphries, R. K., Piret, J. M., & Hansen, C. L. (2011). High-throughput analysis of single hematopoietic stem cell proliferation in microfluidic cell culture arrays. *Nature Methods*, *8*(7), 581-586. https://doi.org/10.1038/nmeth.1614

Lee, J., Cuddihy, M. J., & Kotov, N. A. (2008). Three-dimensional cell culture matrices: state of the art. *Tissue Eng Part B Rev*, *14*(1), 61-86. https://doi.org/10.1089/teb.2007.0150

Lee, H. P., Stowers, R., & Chaudhuri, O. (2019). Volume expansion and TRPV4 activation regulate stem cell fate in three-dimensional microenvironments. *Nat Commun*, *10*(1), 529. https://doi.org/10.1038/s41467-019-08465-x

Lee, J.-H., & Kim, H.-W. (2018). Emerging properties of hydrogels in tissue engineering. *Journal of tissue engineering*, *9*, 2041731418768285.

Leivo, J., Virjula, S., Vanhatupa, S., Kartasalo, K., Kreutzer, J., Miettinen, S., & Kallio, P. (2017). A durable and biocompatible ascorbic acid-based covalent coating method of polydimethylsiloxane for dynamic cell culture. *Journal of the Royal Society, Interface*, *14*(132), 20170318. https://doi.org/10.1098/rsif.2017.0318

Letourneau, P. C. (1982). Nerve Fiber Growth and Its Regulation by Extrinsic Factors. In N. C. Spitzer (Ed.), *Neuronal Development* (pp. 213-254). Springer US. https://doi.org/10.1007/978-1-4684-1131-7_6

Levi, G., & Raiteri, M. (1993). Carrier-mediated release of neurotransmitters. *Trends in Neurosciences*, *16*(10), 415-419. https://doi.org/10.1016/0166-2236(93)90010-j

Levitt, P., Moore, R. Y., & Garber, B. B. (1976). Selective Cell Association of Catecholamine Neurons in Brain Aggregates Invitro. *Brain Research*, *111*(2), 311-320. https://doi.org/Doi 10.1016/0006-8993(76)90776-9

Li, C., Kato, M., Shiue, L., Shively, J. E., Ares, M., Jr., & Lin, R. J. (2006). Cell type and culture condition-dependent alternative splicing in human breast cancer cells revealed by splicing-sensitive microarrays. *Cancer Res*, *66*(4), 1990-1999. https://doi.org/10.1158/0008-5472.CAN-05-2593

Li, Y. Q., Li, H., Kaneko, T., & Mizuno, N. (2001). Morphological features and electrophysiological properties of serotonergic and non-serotonergic projection neurons in the dorsal raphe nucleus. An intracellular recording and labeling study in rat brain slices. *Brain Res*, *900*(1), 110-118. https://doi.org/10.1016/s0006-8993(01)02272-7

Liberio, M. S., Sadowski, M. C., Soekmadji, C., Davis, R. A., & Nelson, C. C. (2014). Differential Effects of Tissue Culture Coating Substrates on Prostate Cancer Cell Adherence, Morphology and Behavior. *PLOS ONE*, *9*(11). https://doi.org/ARTN e112122 10.1371/journal.pone.0112122

Lidov, H. G., & Molliver, M. E. (1982). An immunohistochemical study of serotonin neuron development in the rat: ascending pathways and terminal fields. *Brain Research Bulletin*, *8*(4), 389-430. https://doi.org/10.1016/0361-9230(82)90077-6

Liu, C., Maejima, T., Wyler, S. C., Casadesus, G., Herlitze, S., & Deneris, E. S. (2010). Pet-1 is required across different stages of life to regulate serotonergic function. *Nat Neurosci*, *13*(10), 1190-1198. https://doi.org/10.1038/nn.2623

Liu, J. P., & Lauder, J. M. (1992). S-100 beta and insulin-like growth factor-II differentially regulate growth of developing serotonin and dopamine neurons *in vitro*. *J Neurosci Res*, *33*(2), 248-256. https://doi.org/10.1002/jnr.490330208

Liu, P. Y., Chin, L. K., Ser, W., Chen, H. F., Hsieh, C. M., Lee, C. H., Sung, K. B., Ayi, T. C., Yap, P. H., Liedberg, B., Wang, K., Bourouina, T., & Leprince-Wang, Y. (2016). Cell refractive index for cell biology and disease diagnosis: past, present, and future. *Lab Chip*, *16*(4), 634-644. https://doi.org/10.1039/c5lc01445j

Liu, Y., Bhowmick, T., Liu, Y., Gao, X., Mertens, H. D. T., Svergun, D. I., Xiao, J., Zhang, Y., Wang, J.-h., & Meijers, R. (2018). Structural Basis for Draxin-Modulated Axon

Guidance and Fasciculation by Netrin-1 through DCC. *Neuron*, *97*(6), 1261-1267.e1264. https://doi.org/https://doi.org/10.1016/j.neuron.2018.02.010

Longhurst, C. M., & Jennings, L. K. (1998). Integrin-mediated signal transduction. *Cellular and Molecular Life Sciences*, *54*(6), 514-526. https://doi.org/DOI 10.1007/s000180050180

Lowery, L. A., & Van Vactor, D. (2009). The trip of the tip: understanding the growth cone machinery. *Nat Rev Mol Cell Biol*, *10*(5), 332-343. https://doi.org/10.1038/nrm2679

Lu, J., Zhong, X., Liu, H., Hao, L., Huang, C. T., Sherafat, M. A., Jones, J., Ayala, M., Li, L., & Zhang, S. C. (2016). Generation of serotonin neurons from human pluripotent stem cells. *Nat Biotechnol*, *34*(1), 89-94. https://doi.org/10.1038/nbt.3435

Lu, Y., Lin, J., Wang, L., Zhang, L., & Cai, C. (2020). Self-Assembly of Copolymer Micelles: Higher-Level Assembly for Constructing Hierarchical Structure. *Chemical Reviews*, *120*(9), 4111-4140. https://doi.org/10.1021/acs.chemrev.9b00774

Lu, Y. B., Franze, K., Seifert, G., Steinhäuser, C., Kirchhoff, F., Wolburg, H., Guck, J., Janmey, P., Wei, E. Q., Käs, J., & Reichenbach, A. (2006). Viscoelastic properties of individual glial cells and neurons in the CNS. *Proc Natl Acad Sci U S A*, *103*(47), 17759-17764. https://doi.org/10.1073/pnas.0606150103

Maddaloni, G., Bertero, A., Pratelli, M., Barsotti, N., Boonstra, A., Giorgi, A., Migliarini, S., & Pasqualetti, M. (2017). Development of Serotonergic Fibers in the Post-Natal Mouse Brain. *Front Cell Neurosci*, *11*, 202. https://doi.org/10.3389/fncel.2017.00202

Madl, C. M., LeSavage, B. L., Dewi, R. E., Dinh, C. B., Stowers, R. S., Khariton, M., Lampe, K. J., Nguyen, D., Chaudhuri, O., Enejder, A., & Heilshorn, S. C. (2017). Maintenance of neural progenitor cell stemness in 3D hydrogels requires matrix remodelling. *Nat Mater*, *16*(12), 1233-1242. https://doi.org/10.1038/nmat5020

Mai JK, A. K. (2004). Fetal Development of the Central Nervous System. In M. J. Edited by Paxinos G (Ed.), *The Human Nervous System. edn.* (pp. 49-94.). Elsevier.

Malkinson, G., Fridman, Z. M., Kamber, D., Dormann, A., Shapira, E., & Spira, M. E. (2006). Calcium-induced exocytosis from actomyosin-driven, motile varicosities formed by dynamic clusters of organelles. *Brain Cell Biol*, *35*(1), 57-73. https://doi.org/10.1007/s11068-006-9007-7

Malkinson, G., & Spira, M. E. (2010). Clustering of excess growth resources within leading growth cones underlies the recurrent “deposition” of varicosities along developing neurites. *Experimental Neurology*, *225*(1), 140-153. https://doi.org/https://doi.org/10.1016/j.expneurol.2010.06.005

Mamounas, L. A., Altar, C. A., Blue, M. E., Kaplan, D. R., Tessarollo, L., & Lyons, W. E. (2000). BDNF promotes the regenerative sprouting, but not survival, of injured serotonergic axons in the adult rat brain. *Journal of Neuroscience*, *20*(2), 771-782. https://doi.org/Doi 10.1523/Jneurosci.20-02-00771.2000

Mamounas, L. A., & Molliver, M. E. (1988). Evidence for Dual Serotonergic Projections to Neocortex - Axons from the Dorsal and Median Raphe Nuclei Are Differentially Vulnerable to the Neurotoxin Para-Chloroamphetamine (Pca). *Experimental Neurology*, *102*(1), 23-36. https://doi.org/Doi 10.1016/0014-4886(88)90075-1

Jupp, P. E. and K. V. Mardia (2009). Directional Statistics, Wiley.

Martins, L. F., Costa, R. O., Pedro, J. R., Aguiar, P., Serra, S. C., Teixeira, F. G., Sousa, N., Salgado, A. J., & Almeida, R. D. (2017). Mesenchymal stem cells secretome-induced axonal outgrowth is mediated by BDNF. *Scientific Reports*, *7*(1), 4153. https://doi.org/10.1038/s41598-017-03592-1

Masuko, S., Nakajima, Y., Nakajima, S., & Yamaguchi, K. (1986). Noradrenergic neurons from the locus ceruleus in dissociated cell culture: culture methods, morphology, and electrophysiology. *The Journal of Neuroscience*, *6*(11), 3229-3241. https://doi.org/10.1523/jneurosci.06-11-03229.1986

Mattson, M. P., Gleichmann, M., & Cheng, A. (2008). Mitochondria in neuroplasticity and neurological disorders. *Neuron*, *60*(5), 748-766. https://doi.org/10.1016/j.neuron.2008.10.010

Mercier, G., Lennon, A. M., Renouf, B., Dessouroux, A., Ramauge, M., Courtin, F., & Pierre, M. (2004). MAP kinase activation by fluoxetine and its relation to gene expression in cultured rat astrocytes. *Journal of Molecular Neuroscience*, *24*(2), 207-216. https://doi.org/Doi 10.1385/Jmn:24:2:207

Michelsen, K. A., Prickaerts, J., & Steinbusch, H. W. M. (2008). The dorsal raphe nucleus and serotonin: implications for neuroplasticity linked to major depression and Alzheimer's disease. *Serotonin-Dopamine Interaction: Experimental Evidence and Therapeutic Relevance*, *172*, 233-264. https://doi.org/10.1016/S0079-6123(08)00912-6

Michelsen, K. A., Schmitz, C., & Steinbusch, H. W. M. (2007). The dorsal raphe nucleus - From silver stainings to a role in depression. *Brain Research Reviews*, *55*(2), 329-342. https://doi.org/10.1016/j.brainresrev.2007.01.002

Michetti, F., D'Ambrosi, N., Toesca, A., Puglisi, M. A., Serrano, A., Marchese, E., Corvino, V., & Geloso, M. C. (2019). The S100B story: from biomarker to active factor in neural injury. *J Neurochem*, *148*(2), 168-187. https://doi.org/10.1111/jnc.14574

Minocha, S., Valloton, D., Ypsilanti, A. R., Fiumelli, H., Allen, E. A., Yanagawa, Y., Marin, O., Chédotal, A., Hornung, J.-P., & Lebrand, C. (2015). Nkx2. 1-derived astrocytes and neurons together with Slit2 are indispensable for anterior commissure formation. *Nature Communications*, *6*(1), 1-15.

Miranti, C. K., & Brugge, J. S. (2002). Sensing the environment: a historical perspective on integrin signal transduction. *Nature Cell Biology*, *4*(4), E83-E90. https://doi.org/DOI 10.1038/ncb0402-e83

Molliver, M. E., Berger, U. V., Mamounas, L. A., Molliver, D. C., Ohearn, E., & Wilson, M. A. (1990). Neurotoxicity of Mdma and Related-Compounds - Anatomic Studies. *Annals of the New York Academy of Sciences*, *600*, 640-664. https://doi.org/DOI 10.1111/j.1749-6632.1990.tb16916.x

Montgomery, D. L. (1994). Astrocytes - Form, Functions, and Roles in Disease. *Veterinary Pathology*, *31*(2), 145-167. https://doi.org/Doi 10.1177/030098589403100201

Morla, A., Zhang, Z., & Ruoslahti, E. (1994). Superfibronectin is a functionally distinct form of fibronectin. *Nature*, *367*(6459), 193-196. https://doi.org/10.1038/367193a0

Motti, D., Blackmore, M., Bixby, J. L., & Lemmon, V. P. (2018). High Content Screening of Mammalian Primary Cortical Neurons. *3d Cell Culture: Methods and Protocols*, *1683*, 293-304. https://doi.org/10.1007/978-1-4939-7357-6_17

Mseka, T., Bamburg, J. R., & Cramer, L. P. (2007). ADF/cofilin family proteins control formation of oriented actin-filament bundles in the cell body to trigger fibroblast polarization. *Journal of Cell Science*, *120*(Pt 24), 4332-4344. https://doi.org/10.1242/jcs.017640

Mukherjee, S., Xie, R., Reynolds, V. G., Uchiyama, T., Levi, A. E., Valois, E., Wang, H., Chabinyc, M. L., & Bates, C. M. (2020). Universal Approach to Photo-Crosslink Bottlebrush Polymers. *Macromolecules*, *53*(3), 1090-1097. https://doi.org/10.1021/acs.macromol.9b02210

Naahidi, S., Jafari, M., Logan, M., Wang, Y., Yuan, Y., Bae, H., Dixon, B., & Chen, P. (2017). Biocompatibility of hydrogel-based scaffolds for tissue engineering applications. *Biotechnology Advances*, *35*(5), 530-544. https://doi.org/https://doi.org/10.1016/j.biotechadv.2017.05.006

Nanolive. https://www.nanolive.ch

Nanolive. (2020, October 2020). *Characterization of neurons*. Nanolive SA. nanolive_application_note_neurons_web.pdf

Naumenko, V. S., Popova, N. K., Lacivita, E., Leopoldo, M., & Ponimaskin, E. G. (2014). Interplay between Serotonin 5-HT1A and 5-HT7 Receptors in Depressive Disorders. *Cns Neuroscience & Therapeutics*, *20*(7), 582-590. https://doi.org/10.1111/cns.12247

Nazzi, S., Maddaloni, G., Pratelli, M., & Pasqualetti, M. (2019). Fluoxetine Induces Morphological Rearrangements of Serotonergic Fibers in the Hippocampus. *ACS Chem Neurosci*, *10*(7), 3218-3224. https://doi.org/10.1021/acschemneuro.8b00655

Nishiyama, H., Takemura, M., Takeda, T., & Itohara, S. (2002). Normal development of serotonergic neurons in mice lacking S100B. *Neuroscience Letters*, *321*(1), 49-52. https://doi.org/https://doi.org/10.1016/S0304-3940(01)02549-6

Noble, M., Fok-Seang, J., & Cohen, J. (1984). Glia are a unique substrate for the *in vitro* growth of central nervous system neurons. *J Neurosci*, *4*(7), 1892-1903. https://www.ncbi.nlm.nih.gov/pubmed/6737045

Nolan, G. P. (2007). What's wrong with drug screening today. *Nat Chem Biol*, *3*(4), 187-191. https://doi.org/10.1038/nchembio0407-187

Novikova, L. N., Mosahebi, A., Wiberg, M., Terenghi, G., Kellerth, J. O., & Novikov, L. N. (2006). Alginate hydrogel and matrigel as potential cell carriers for neurotransplantation. *J Biomed Mater Res A*, *77*(2), 242-252. https://doi.org/10.1002/jbm.a.30603

Numasawa, Y., Hattori, T., Ishiai, S., Kobayashi, Z., Kamata, T., Kotera, M., Ishibashi, S., Sanjo, N., Mizusawa, H., & Yokota, T. (2017). Depressive disorder may be associated with raphe nuclei lesions in patients with brainstem infarction. *J Affect Disord*, *213*, 191-198. https://doi.org/10.1016/j.jad.2017.02.005

O'Toole, M., Lamoureux, P., & Miller, K. E. (2008). A physical model of axonal elongation: force, viscosity, and adhesions govern the mode of outgrowth. *Biophysical Journal*, *94*(7), 2610-2620. https://doi.org/10.1529/biophysj.107.117424

Ohearn, E., Battaglia, G., Desouza, E. B., Kuhar, M. J., & Molliver, M. E. (1988). Methylenedioxyamphetamine (Mda) and Methylenedioxymethamphetamine (Mdma) Cause Selective Ablation of Serotonergic Axon Terminals in Forebrain - Immunocytochemical Evidence for Neurotoxicity. *Journal of Neuroscience*, *8*(8), 2788-2803. <Go to ISI>://WOS:A1988P831400011

Okaty, B. W., Commons, K. G., & Dymecki, S. M. (2019). Embracing diversity in the 5-HT neuronal system. *Nat Rev Neurosci*, *20*(7), 397-424. https://doi.org/10.1038/s41583-019-0151-3

Okaty, B. W., Sturrockt, N., Lozoya, Y. E., Chang, Y., Senft, R. A., Lyon, K. A., Alekseyenko, O. V., & Dymecki, S. M. (2020). A single-cell transcriptomic and anatomic atlas of mouse dorsal raphe Pet1 neurons. *Elife*, *9*. https://doi.org/ARTN e55523 10.7554/eLife.55523

Okay, O. (2010). General Properties of Hydrogels. In G. Gerlach & K.-F. Arndt (Eds.), *Hydrogel Sensors and Actuators: Engineering and Technology* (pp. 1-14). Springer Berlin Heidelberg. https://doi.org/10.1007/978-3-540-75645-3_1

Oleskevich, S., & Descarries, L. (1990). Quantified Distribution of the Serotonin Innervation in Adult-Rat Hippocampus. *Neuroscience*, *34*(1), 19-33. https://doi.org/Doi 10.1016/0306-4522(90)90301-J

Olson, L., & Seiger, A. (1972). Early Prenatal Ontogeny of Central Monoamine Neurons in Rat - Fluorescence Histochemical Observations. *Zeitschrift Fur Anatomie Und Entwicklungsgeschichte*, *137*(3), 301-+. https://doi.org/Doi 10.1007/Bf00519099

Onishi, K., Hollis, E., & Zou, Y. (2014). Axon guidance and injury-lessons from Wnts and Wnt signaling. *Current opinion in neurobiology*, *27*, 232-240. https://doi.org/10.1016/j.conb.2014.05.005

Palin, E., Liu, H., & Webster, T. J. (2005). Mimicking the nanofeatures of bone increases bone-forming cell adhesion and proliferation. *Nanotechnology*, *16*(9), 1828.

Papadopoulos, G. C., Parnavelas, J. G., & Buijs, R. (1987). Monoaminergic fibers form conventional synapses in the cerebral cortex. *Neurosci Lett*, *76*(3), 275-279. https://doi.org/10.1016/0304-3940(87)90414-9

Papesh, M. A., & Hurley, L. M. (2016). Modulation of auditory brainstem responses by serotonin and specific serotonin receptors. *Hearing Research*, *332*, 121-136. https://doi.org/https://doi.org/10.1016/j.heares.2015.11.014

Papp, E. C., Heimrich, B., & Freund, T. F. (1995). Development of the raphe-hippocampal projection *in vitro*. *Neuroscience*, *69*(1), 99-105. https://doi.org/https://doi.org/10.1016/0306-4522(95)00240-J

Park, H. H., Kim, Y.-M., Anh Hong, L. T., Kim, H. S., Kim, S. H., Jin, X., Hwang, D. H., Kwon, M. J., Song, S.-C., & Kim, B. G. (2022). Dual-functional hydrogel system for spinal cord regeneration with sustained release of arylsulfatase B alleviates fibrotic microenvironment and promotes axonal regeneration. *Biomaterials*, *284*, 121526. https://doi.org/https://doi.org/10.1016/j.biomaterials.2022.121526

Park, L. C., Zhang, H., & Gibson, G. E. (2001). Co-culture with astrocytes or microglia protects metabolically impaired neurons. *Mech Ageing Dev*, *123*(1), 21-27. https://doi.org/10.1016/s0047-6374(01)00336-0

Pebworth, M.-P., Cismas, S. A., & Asuri, P. (2014). A Novel 2.5D Culture Platform to Investigate the Role of Stiffness Gradients on Adhesion-Independent Cell Migration. *PLOS ONE*, *9*(10), e110453. https://doi.org/10.1371/journal.pone.0110453

Petersen, O. W., Ronnov-Jessen, L., Howlett, A. R., & Bissell, M. J. (1992). Interaction with basement membrane serves to rapidly distinguish growth and differentiation pattern of normal and malignant human breast epithelial cells. *Proc Natl Acad Sci U S A*, *89*(19), 9064-9068. https://doi.org/10.1073/pnas.89.19.9064

Pettmann, B., Louis, J. C., & Sensenbrenner, M. (1979). Morphological and Biochemical Maturation of Neurons Cultured in the Absence of Glial-Cells. *Nature*, *281*(5730), 378-380. https://doi.org/DOI 10.1038/281378a0

Popova, N. K., Ilchibaeva, T. V., & Naumenko, V. S. (2017). Neurotrophic Factors (BDNF and GDNF) and the Serotonergic System of the Brain. *Biochemistry (Mosc)*, *82*(3), 308-317. https://doi.org/10.1134/s0006297917030099

Pozzi, D., Ban, J., Iseppon, F., & Torre, V. (2017). An improved method for growing neurons: Comparison with standard protocols. *Journal of Neuroscience Methods*, *280*, 1-10. https://doi.org/https://doi.org/10.1016/j.jneumeth.2017.01.013

Pratelli, M., Migliarini, S., Pelosi, B., Napolitano, F., Usiello, A., & Pasqualetti, M. (2017). Perturbation of Serotonin Homeostasis during Adulthood Affects Serotonergic Neuronal Circuitry. *eneuro*, ENEURO.0376-0316.2017. https://doi.org/10.1523/eneuro.0376-16.2017

Prochiantz, A., di Porzio, U., Kato, A., Berger, B., & Glowinski, J. (1979). *In vitro* maturation of mesencephalic dopaminergic neurons from mouse embryos is enhanced in presence of their striatal target cells. *Proc Natl Acad Sci U S A*, *76*(10), 5387-5391. https://doi.org/10.1073/pnas.76.10.5387

Quentin, E., Belmer, A., & Maroteaux, L. (2018). Somato-Dendritic Regulation of Raphe Serotonin Neurons; A Key to Antidepressant Action [Review]. *Frontiers in Neuroscience*, *12*(982). https://doi.org/10.3389/fnins.2018.00982

Rafa-Zablocka, K., Kreiner, G., Baginska, M., & Nalepa, I. (2018). Selective Depletion of CREB in Serotonergic Neurons Affects the Upregulation of Brain-Derived Neurotrophic Factor Evoked by Chronic Fluoxetine Treatment. *Frontiers in Neuroscience*, *12*. https://doi.org/ARTN 637 10.3389/fnins.2018.00637

Rajkowska, G., Mahajan, G., Legutko, B., Challagundla, L., Griswold, M., Albert, P. R., Daigle, M., Miguel-Hidalgo, J. J., Austin, M. C., Blakely, R. D., Steffens, D. C., & Stockmeier, C. A. (2017). Length of Axons Expressing the Serotonin Transporter in

Orbitofrontal Cortex Is Lower with Age in Depression. *Neuroscience*, *359*, 30-39. https://doi.org/10.1016/j.neuroscience.2017.07.006

Rangaraju, V., Lewis, T. L., Hirabayashi, Y., Bergami, M., Motori, E., Cartoni, R., Kwon, S.-K., & Courchet, J. (2019). Pleiotropic Mitochondria: The Influence of Mitochondria on Neuronal Development and Disease. *The Journal of Neuroscience*, *39*(42), 8200-8208. https://doi.org/10.1523/jneurosci.1157-19.2019

Razetti, A., Medioni, C., Malandain, G., Besse, F., & Descombes, X. (2018). A stochastic framework to model axon interactions within growing neuronal populations. *Plos Computational Biology*, *14*(12). https://doi.org/ARTN e1006627 10.1371/journal.pcbi.1006627

Rees, R. P., Bunge, M. B., & Bunge, R. P. (1976). Morphological changes in the neuritic growth cone and target neuron during synaptic junction development in culture. *Journal of Cell Biology*, *68*(2), 240-263. https://doi.org/10.1083/jcb.68.2.240

Refresh cell culture. (2021). *Nature Biomedical Engineering*, *5*(8), 783-784. https://doi.org/10.1038/s41551-021-00790-1

Reid, Y. A. (2011). Characterization and Authentication of Cancer Cell Lines: An Overview. *Cancer Cell Culture: Methods and Protocols, Second Edition*, *731*, 35-43. https://doi.org/10.1007/978-1-61779-080-5_4

Ren, J., Friedmann, D., Xiong, J., Liu, C. D., Ferguson, B. R., Weerakkody, T., DeLoach, K. E., Ran, C., Pun, A., Sun, Y. W., Weissbourd, B., Neve, R. L., Huguenard, J., Horowitz, M. A., & Luo, L. Q. (2018). Anatomically Defined and Functionally Distinct Dorsal Raphe Serotonin Sub-systems. *Cell*, *175*(2), 472-+. https://doi.org/10.1016/j.cell.2018.07.043

Renkawitz, J., Schumann, K., Weber, M., Lammermann, T., Pflicke, H., Piel, M., Polleux, J., Spatz, J. P., & Sixt, M. (2009). Adaptive force transmission in amoeboid cell migration. *Nature Cell Biology*, *11*(12), 1438-U1121. https://doi.org/10.1038/ncb1992

Reynolds, V. G., Mukherjee, S., Xie, R., Levi, A. E., Atassi, A., Uchiyama, T., Wang, H., Chabinyc, M. L., & Bates, C. M. (2020). Super-soft solvent-free bottlebrush elastomers for touch sensing [10.1039/C9MH00951E]. *Materials Horizons*, *7*(1), 181-187. https://doi.org/10.1039/C9MH00951E

Rodemer, W., Gallo, G., & Selzer, M. E. (2020). Mechanisms of Axon Elongation Following CNS Injury: What Is Happening at the Axon Tip? *Front Cell Neurosci*, *14*, 177. https://doi.org/10.3389/fncel.2020.00177

Rodríguez, J. J., Noristani, H. N., & Verkhratsky, A. (2012). The serotonergic system in ageing and Alzheimer's disease. *Progress in Neurobiology*, *99*(1), 15-41. https://doi.org/https://doi.org/10.1016/j.pneurobio.2012.06.010

Rumajogee, P., Madeira, A., Verge, D., Hamon, M., & Miquel, M. C. (2002). Up-regulation of the neuronal serotoninergic phenotype *in vitro*: BDNF and cAMP share Trk B-dependent mechanisms. *Journal of Neurochemistry*, *83*(6), 1525-1528. https://doi.org/DOI 10.1046/j.1471-4159.2002.01264.x

Saarinen, A., Linne, M.-L., & Yli-Harja, O. (2006). Modeling single neuron behavior using stochastic differential equations. *Neurocomputing*, *69*(10), 1091-1096. https://doi.org/https://doi.org/10.1016/j.neucom.2005.12.052

Saha, K., Pollock, J. F., Schaffer, D. V., & Healy, K. E. (2007). Designing synthetic materials to control stem cell phenotype. *Current opinion in chemical biology*, *11*(4), 381-387. https://doi.org/10.1016/j.cbpa.2007.05.030

Sahu, A., Gopalakrishnan, L., Gaur, N., Chatterjee, O., Mol, P., Modi, P. K., Dagamajalu, S., Advani, J., Jain, S., & Keshava Prasad, T. S. (2018). The 5-Hydroxytryptamine signaling map: an overview of serotonin-serotonin receptor mediated signaling network. *Journal of cell communication and signaling*, *12*(4), 731-735. https://doi.org/10.1007/s12079-018-0482-2

Saltzman, W. M. (2000). CHAPTER 19 – CELL INTERACTIONS WITH POLYMERS.

Samorezov, J. E., Morlock, C. M., & Alsberg, E. (2015). Dual Ionic and Photo-Crosslinked Alginate Hydrogels for Micropatterned Spatial Control of Material Properties and Cell Behavior. *Bioconjug Chem*, *26*(7), 1339-1347. https://doi.org/10.1021/acs.bioconjchem.5b00117

Sandoz, P. A., Tremblay, C., van der Goot, F. G., & Frechin, M. (2019). Image-based analysis of living mammalian cells using label-free 3D refractive index maps reveals new organelle dynamics and dry mass flux. *Plos Biology*, *17*(12), e3000553. https://doi.org/10.1371/journal.pbio.3000553

Santos, T. E., Schaffran, B., Broguière, N., Meyn, L., Zenobi-Wong, M., & Bradke, F. (2020). Axon Growth of CNS Neurons in Three Dimensions Is Amoeboid and Independent of Adhesions. *Cell Reports*, *32*(3), 107907. https://doi.org/https://doi.org/10.1016/j.celrep.2020.107907

Sarapas, J. M., Martin, T. B., Chremos, A., Douglas, J. F., & Beers, K. L. (2020). Bottlebrush polymers in the melt and polyelectrolytes in solution share common structural features. *Proceedings of the National Academy of Sciences*, *117*(10), 5168-5175. https://doi.org/10.1073/pnas.1916362117

Schlumpf, M., Shoemaker, W. J., & Bloom, F. E. (1977). Explant Cultures of Catecholamine-Containing Neurons from Rat-Brain - Biochemical, Histofluorescence, and Electron-Microscopic Studies. *Proceedings of the National Academy of Sciences of the United States of America*, *74*(10), 4471-4475. https://doi.org/DOI 10.1073/pnas.74.10.4471

Scholpa, N. E., Lynn, M. K., Corum, D., Boger, H. A., & Schnellmann, R. G. (2018). 5-HT1F receptor-mediated mitochondrial biogenesis for the treatment of Parkinson's disease. *British Journal of Pharmacology*, *175*(2), 348-358. https://doi.org/https://doi.org/10.1111/bph.14076

Schürmann, M., Scholze, J., Müller, P., Guck, J., & Chan, C. J. (2016). Cell nuclei have lower refractive index and mass density than cytoplasm. *Journal of Biophotonics*, *9*(10), 1068-1076. https://doi.org/https://doi.org/10.1002/jbio.201500273

Self, J. L., Sample, C. S., Levi, A. E., Li, K., Xie, R., de Alaniz, J. R., & Bates, C. M. (2020). Dynamic Bottlebrush Polymer Networks: Self-Healing in Super-Soft Materials. *J Am Chem Soc*, *142*(16), 7567-7573. https://doi.org/10.1021/jacs.0c01467

Shapiro, L. A., Bialowas-McGoey, L. A., & Whitaker-Azmitia, P. M. (2010). Effects of S100B on Serotonergic Plasticity and Neuroinflammation in the Hippocampus in Down Syndrome and Alzheimer's Disease: Studies in an S100B Overexpressing Mouse Model. *Cardiovascular psychiatry and neurology*, *2010*, 153657. https://doi.org/10.1155/2010/153657

Sharaf, A., Roos, B., Timmerman, R., Kremers, G. J., Bajramovic, J. J., & Accardo, A. (2022). Two-Photon Polymerization of 2.5D and 3D Microstructures Fostering a Ramified Resting Phenotype in Primary Microglia. *Frontiers in Bioengineering and Biotechnology*, *10*. https://doi.org/ARTN 926642 10.3389/fbioe.2022.926642

Shechter, R., & Schwartz, M. (2013). CNS sterile injury: just another wound healing? *Trends in molecular medicine*, *19*(3), 135-143.

Sheu, S.-H., Upadhyayula, S., Dupuy, V., Pang, S., Deng, F., Wan, J., Walpita, D., Pasolli, H. A., Houser, J., Sanchez-Martinez, S., Brauchi, S. E., Banala, S., Freeman, M., Xu, C. S., Kirchhausen, T., Hess, H. F., Lavis, L., Li, Y., Chaumont-Dubel, S., & Clapham, D. E. (2022). A serotonergic axon-cilium synapse drives nuclear signaling to alter chromatin accessibility. *Cell*, *185*(18), 3390-3407.e3318. https://doi.org/https://doi.org/10.1016/j.cell.2022.07.026

Shoichet, M. S., Li, R. H., White, M. L., & Winn, S. R. (1996). Stability of hydrogels used in cell encapsulation: An *in vitro* comparison of alginate and agarose. *Biotechnol Bioeng*, *50*(4), 374-381. https://doi.org/10.1002/(sici)1097-0290(19960520)50:4

Siuciak, J. A., Boylan, C., Fritsche, M., Altar, C. A., & Lindsay, R. M. (1996). BDNF increases monoaminergic activity in rat brain following intracerebroventricular or intraparenchymal administration. *Brain Res*, *710*(1-2), 11-20. https://doi.org/10.1016/0006-8993(95)01289-3

Šmít, D., Fouquet, C., Pincet, F., Zapotocky, M., & Trembleau, A. (2017). Axon tension regulates fasciculation/defasciculation through the control of axon shaft zippering. *Elife*, *6*. https://doi.org/10.7554/eLife.19907

Smith, G. M., & Gallo, G. (2018). The role of mitochondria in axon development and regeneration. *Developmental neurobiology*, *78*(3), 221-237. https://doi.org/10.1002/dneu.22546

Smith, G. M., & Onifer, S. M. (2011). Construction of pathways to promote axon growth within the adult central nervous system. *Brain Research Bulletin*, *84*(4-5), 300-305. https://doi.org/10.1016/j.brainresbull.2010.05.013

Smithmyer, M. E., Cassel, S. E., & Kloxin, A. M. (2019). Bridging 2D and 3D culture: Probing impact of extracellular environment on fibroblast activation in layered hydrogels. *AIChE Journal*, *65*(12), e16837. https://doi.org/https://doi.org/10.1002/aic.16837

Sodunke, T. R., Turner, K. K., Caldwell, S. A., McBride, K. W., Reginato, M. J., & Noh, H. M. (2007). Micropatterns of Matrigel for three-dimensional epithelial cultures. *Biomaterials*, *28*(27), 4006-4016. https://doi.org/10.1016/j.biomaterials.2007.05.021

Sofroniew, M. V. (2021). Inflammation drives fibrotic scars in the CNS. *Nature Neuroscience*, *24*(2), 157-159. https://doi.org/10.1038/s41593-020-00777-2

Sottile, J., Hocking, D. C., & Swiatek, P. J. (1998). Fibronectin matrix assembly enhances adhesion-dependent cell growth. *Journal of Cell Science*, *111*, 2933-2943.

Spector, M., & Lim, T. C. (2016). Injectable biomaterials: a perspective on the next wave of injectable therapeutics. *Biomedical Materials*, *11*(1). https://doi.org/Artn 014110 10.1088/1748-6041/11/1/014110

Spedden, E., White, J. D., Naumova, E. N., Kaplan, D. L., & Staii, C. (2012). Elasticity maps of living neurons measured by combined fluorescence and atomic force microscopy. *Biophysical Journal*, *103*(5), 868-877. https://doi.org/10.1016/j.bpj.2012.08.005

Spillane, M., Ketschek, A., Merianda, Tanuja T., Twiss, Jeffery L., & Gallo, G. (2013). Mitochondria Coordinate Sites of Axon Branching through Localized Intra-axonal Protein Synthesis. *Cell Reports*, *5*(6), 1564-1575. https://doi.org/https://doi.org/10.1016/j.celrep.2013.11.022

Staal, R. G. W., Rayport, S., & Sulzer, D. (2007). Amperometric Detection of Dopamine Exocytosis from Synaptic Terminals. *Electrochemical Methods for Neuroscience*, *1*, 337-352. <Go to ISI>://WOS:000269356600018

Stamp, J. A., & Semba, K. (1995). Extent of colocalization of serotonin and GABA in the neurons of the rat raphe nuclei. *Brain Res*, *677*(1), 39-49. https://doi.org/10.1016/0006-8993(95)00119-b

Steinbusch, H. W. M., Nieuwenhuys, R., Verhofstad, A. A. J., & Vanderkooy, D. (1981). The Nucleus Raphe Dorsalis of the Rat and Its Projection Upon the Caudatoputamen - a Combined Cytoarchitectonic, Immunohistochemical and Retrograde Transport Study. *Journal De Physiologie*, *77*(2-3), 157-174.

Stowers, R. S., Shcherbina, A., Israeli, J., Gruber, J. J., Chang, J., Nam, S., Rabiee, A., Teruel, M. N., Snyder, M. P., Kundaje, A., & Chaudhuri, O. (2019). Matrix stiffness induces a tumorigenic phenotype in mammary epithelium through changes in chromatin accessibility. *Nat Biomed Eng*, *3*(12), 1009-1019. https://doi.org/10.1038/s41551-019-0420-5

Strauss, S., Neumeister, A., Barcikowski, S., Kracht, D., Kuhbier, J. W., Radtke, C., Reimers, K., & Vogt, P. M. (2013). Adhesion, vitality, and osteogenic differentiation capacity of adipose derived stem cells seeded on nitinol nanoparticle coatings. *PLOS ONE*, *8*(1), e53309. https://doi.org/10.1371/journal.pone.0053309

Sundstrom, E., Kolare, S., Souverbie, F., Samuelsson, E. B., Pschera, H., Lunell, N. O., & Seiger, A. (1993). Neurochemical differentiation of human bulbospinal monoaminergic neurons during the first trimester. *Brain Res Dev Brain Res*, *75*(1), 1-12. https://doi.org/10.1016/0165-3806(93)90059-j

Sung, W., Jeong, Y., Kim, H., Jeong, H., Grassberger, C., Jung, S., Ahn, G. O., Kim, I. H., Schuemann, J., Lee, K., & Ye, S. J. (2018). Computational Modeling and Clonogenic Assay for Radioenhancement of Gold Nanoparticles Using 3D Live Cell Images. *Radiat Res*, *190*(5), 558-564. https://doi.org/10.1667/RR15134.1

Syed K. H. Gulrez, Saphwan Al-Assaf, & Glyn O Phillips (2011). Hydrogels: Methods of Preparation, Characterisation and Applications. In *InTech, Progress in Molecular and Environmental Bioengineering – From Analysis and Modeling to Technology Applications*. https://doi.org/10.5772/24553

Talebian, S., Mehrali, M., Taebnia, N., Pennisi, C. P., Kadumudi, F. B., Foroughi, J., Hasany, M., Nikkhah, M., Akbari, M., Orive, G., & Dolatshahi-Pirouz, A. (2019). Self-Healing Hydrogels: The Next Paradigm Shift in Tissue Engineering? *Adv Sci (Weinh)*, *6*(16), 1801664. https://doi.org/10.1002/advs.201801664

Tao-Cheng, J. H., & Zhou, F. C. (1999). Differential polarization of serotonin transporters in axons versus soma-dendrites: an immunogold electron microscopy study. *Neuroscience*, *94*(3), 821-830. https://doi.org/10.1016/s0306-4522(99)00373-5

Teissier, A., Soiza-Reilly, M., & Gaspar, P. (2017). Refining the Role of 5-HT in Postnatal Development of Brain Circuits. *Frontiers in Cellular Neuroscience*, *11*. https://doi.org/ARTN 139 10.3389/fncel.2017.00139

Tempio, A., Niso, M., Laera, L., Trisolini, L., Favia, M., Ciranna, L., Marzulli, D., Petrosillo, G., Pierri, C. L., Lacivita, E., & Leopoldo, M. (2020). Mitochondrial Membranes of Human SH-SY5Y Neuroblastoma Cells Express Serotonin 5-HT7 Receptor. *International Journal of Molecular Sciences*, *21*(24), 9629. https://www.mdpi.com/1422-0067/21/24/9629

Ternaux, J.-P., & Portalier, P. (1993). Culture of hypoglossal cells, dissociated from foetal and new-born rats. *Journal of Neuroscience Methods*, *49*(1), 33-47. https://doi.org/https://doi.org/10.1016/0165-0270(93)90107-3

Tibbitt, M. W., & Anseth, K. S. (2009). Hydrogels as extracellular matrix mimics for 3D cell culture. *Biotechnology and bioengineering*, *103*(4), 655-663. https://doi.org/10.1002/bit.22361

Tomov, M. L. (2019). Long-Term Neuron Culture Maturation in 3D Hydrogel Constructs. A comparison study of VitroGel™ and Matrigel® for long-term neuron maturation and survival *in vitro*. *Stanley Center; Broad Institute of MIT and Harvard.* https://www.thewellbio.com/wp-content/uploads/2019/05/Long-Term-Neuron-Culture-Maturation-in-3D-Hydrogel-Constructs.pdf

Tonge, D. A., Golding, J. P., Edbladh, M., Kroon, M., Ekstrom, P. E., & Edstrom, A. (1997). Effects of extracellular matrix components on axonal outgrowth from peripheral nerves of adult animals *in vitro*. *Exp Neurol*, *146*(1), 81-90. https://doi.org/10.1006/exnr.1997.6498

Tork, I. (1990). Anatomy of the serotonergic system. *Ann N Y Acad Sci*, *600*, 9-34; discussion 34-35. https://doi.org/10.1111/j.1749-6632.1990.tb16870.x

Vadodaria, K. C., Mertens, J., Paquola, A., Bardy, C., Li, X., Jappelli, R., Fung, L., Marchetto, M. C., Hamm, M., Gorris, M., Koch, P., & Gage, F. H. (2016).

Generation of functional human serotonergic neurons from fibroblasts. *Molecular Psychiatry*, *21*(1), 49-61. https://doi.org/10.1038/mp.2015.161

Vadodaria, K. C., Stern, S., Marchetto, M. C., & Gage, F. H. (2018). Serotonin in psychiatry: *in vitro* disease modeling using patient-derived neurons. *Cell and Tissue Research*, *371*(1), 161-170. https://doi.org/10.1007/s00441-017-2670-4

Valenti, D., de Bari, L., Vigli, D., Lacivita, E., Leopoldo, M., Laviola, G., Vacca, R. A., & De Filippis, B. (2017). Stimulation of the brain serotonin receptor 7 rescues mitochondrial dysfunction in female mice from two models of Rett syndrome. *Neuropharmacology*, *121*, 79-88. https://doi.org/https://doi.org/10.1016/j.neuropharm.2017.04.024

Vojta, T., Halladay, S., Skinner, S., Janusonis, S., Guggenberger, T., & Metzler, R. (2020). Reflected fractional Brownian motion in one and higher dimensions. *Phys Rev E*, *102*(3-1), 032108. https://doi.org/10.1103/PhysRevE.102.032108

Voyiadjis, A. G., Doumi, M., Curcio, E., & Shinbrot, T. (2011). Fasciculation and Defasciculation of Neurite Bundles on Micropatterned Substrates. *Annals of Biomedical Engineering*, *39*(1), 559-569. https://doi.org/10.1007/s10439-010-0168-2

Wang, Q., Zhang, H., Xu, H., Guo, D., Shi, H., Li, Y., Zhang, W., & Gu, Y. (2016). 5-HTR3 and 5-HTR4 located on the mitochondrial membrane and functionally regulated mitochondrial functions. *Sci Rep*, *6*, 37336. https://doi.org/10.1038/srep37336

Weiswald, L. B., Bellet, D., & Dangles-Marie, V. (2015). Spherical cancer models in tumor biology. *Neoplasia*, *17*(1), 1-15. https://doi.org/10.1016/j.neo.2014.12.004

Wen, Z., & Zheng, J. Q. (2006). Directional guidance of nerve growth cones. *Current opinion in neurobiology*, *16*(1), 52-58. https://doi.org/10.1016/j.conb.2005.12.005

Wilson, M. A., & Molliver, M. E. (1994). Microglial Response to Degeneration of Serotonergic Axon Terminals. *Glia*, *11*(1), 18-34. https://doi.org/DOI 10.1002/glia.440110105

Wilson, M. A., Ricaurte, G. A., & Molliver, M. E. (1989). Distinct Morphologic Classes of Serotonergic Axons in Primates Exhibit Differential Vulnerability to the Psychotropic-Drug 3,4-Methylenedioxymethamphetamine. *Neuroscience*, *28*(1), 121-137. https://doi.org/Doi 10.1016/0306-4522(89)90237-6

Wisdom, K., & Chaudhuri, O. (2017). 3D Cell Culture in Interpenetrating Networks of Alginate and rBM Matrix. *3d Cell Culture: Methods and Protocols*, *1612*, 29-37. https://doi.org/10.1007/978-1-4939-7021-6_3

Wisdom, K. M., Adebowale, K., Chang, J., Lee, J. Y., Nam, S., Desai, R., Rossen, N. S., Rafat, M., West, R. B., Hodgson, L., & Chaudhuri, O. (2018). Matrix mechanical plasticity regulates cancer cell migration through confining microenvironments. *Nat Commun*, *9*(1), 4144. https://doi.org/10.1038/s41467-018-06641-z

Wu, S., Chen, M.-S., Maurel, P., Lee, Y.-S., Bunge, M. B., & Arinzeh, T. L. (2018). Aligned fibrous PVDF-TrFE scaffolds with Schwann cells support neurite extension and myelination *in vitro*. *Journal of neural engineering*, *15*(5), 056010-056010. https://doi.org/10.1088/1741-2552/aac77f

Xie, R., Mukherjee, S., Levi, A. E., Reynolds, V. G., Wang, H., Chabinyc, M. L., & Bates, C. M. (2020). Room temperature 3D printing of super-soft and solvent-free elastomers. *Science Advances*, *6*(46), eabc6900. https://doi.org/10.1126/sciadv.abc6900

Yakimovich, A., Witte, R., Andriasyan, V., Georgi, F., & Greber, U. F. (2018). Label-Free Digital Holo-tomographic Microscopy Reveals Virus-Induced Cytopathic Effects in Live Cells. *mSphere*, *3*(6). https://doi.org/10.1128/mSphereDirect.00599-18

Yamada, K. M., & Cukierman, E. (2007). Modeling tissue morphogenesis and cancer in 3D. *Cell*, *130*(4), 601-610. https://doi.org/10.1016/j.cell.2007.08.006

Yavin, E., & Yavin, Z. (1974). Attachment and Culture of Dissociated Cells from Rat Embryo Cerebral Hemispheres on Polylysine-Coated Surface. *Journal of Cell Biology*, *62*(2), 540-546. https://doi.org/DOI 10.1083/jcb.62.2.540

Yoon, Y., McKenna, M. C., Rollins, D. A., Song, M., Nuriel, T., Gross, S. S., Xu, G., & Glatt, C. E. (2013). Anxiety-associated alternative polyadenylation of the serotonin transporter mRNA confers translational regulation by hnRNPK. *Proc Natl Acad Sci U S A*, *110*(28), 11624-11629. https://doi.org/10.1073/pnas.1301485110

Yurchenko, I., Vensi Basso, J. M., Syrotenko, V. S., & Staii, C. (2019). Anomalous diffusion for neuronal growth on surfaces with controlled geometries. *PLOS ONE*, *14*(5), e0216181. https://doi.org/10.1371/journal.pone.0216181

Zahrai, A., Vahid-Ansari, F., Daigle, M., & Albert, P. R. (2020). Fluoxetine-induced recovery of serotonin and norepinephrine projections in a mouse model of post-stroke depression. *Translational Psychiatry*, *10*(1), 334. https://doi.org/10.1038/s41398-020-01008-9

Zhang, J., Hernandez-Gordillo, V., Trapecar, M., Wright, C., Taketani, M., Schneider, K., Chen, W. L. K., Stas, E., Breault, D. T., Carrier, R. L., Voigt, C. A., & Griffith, L. G. (2021). Coculture of primary human colon monolayer with human gut bacteria. *Nat Protoc*, *16*(8), 3874-3900. https://doi.org/10.1038/s41596-021-00562-w

Zhang, X. B., Zhang, Z. J., Xie, C. M., Xi, G. J., Zhou, H. H., Zhang, Y. M., & Sha, W. W. (2008). Effect of treatment on serum glial cell line-derived neurotrophic factor in depressed patients. *Progress in Neuro-Psychopharmacology & Biological Psychiatry*, *32*(3), 886-890. https://doi.org/10.1016/j.pnpbp.2008.01.004

Zhang, X. F., Hyland, C., Van Goor, D., & Forscher, P. (2012). Calcineurin-dependent cofilin activation and increased retrograde actin flow drive 5-HT-dependent neurite outgrowth in Aplysia bag cell neurons. *Mol Biol Cell*, *23*(24), 4833-4848. https://doi.org/10.1091/mbc.E12-10-0715

Zheng, X., Baker, H., Hancock, W. S., Fawaz, F., McCaman, M., & Pungor Jr, E. (2006). Proteomic analysis for the assessment of different lots of fetal bovine serum as a raw material for cell culture. Part IV. Application of proteomics to the manufacture of biological drugs. *Biotechnology progress*, *22*(5), 1294-1300.

Zhou, L., Huang, K. X., Kecojevic, A., Welsh, A. M., & Koliatsos, V. E. (2006). Evidence that serotonin reuptake modulators increase the density of serotonin innervation in the forebrain. *Journal of Neurochemistry*, *96*(2), 396-406. https://doi.org/10.1111/j.1471-4159.2005.03562.x

Zhu, Y., Soderblom, C., Krishnan, V., Ashbaugh, J., Bethea, J. R., & Lee, J. K. (2015). Hematogenous macrophage depletion reduces the fibrotic scar and increases axonal growth after spinal cord injury. *Neurobiology of Disease*, *74*, 114-125. https://doi.org/10.1016/j.nbd.2014.10.024

Zoratto, N., & Matricardi, P. (2018). Semi-IPN- and IPN-Based Hydrogels. In J. M. Oliveira, S. Pina, R. L. Reis, & J. San Roman (Eds.), *Osteochondral Tissue Engineering: Challenges, Current Strategies, and Technological Advances* (pp. 155-188). Springer International Publishing. https://doi.org/10.1007/978-3-319-76735-2_7